The TITAN cooler Penning trap for short-lived highly charged ions; investigations for nested trap applications and fast electrode switching

Diplomarbeit

by
Benjamin Eberhardt

Johannes Gutenberg-Universität
Institut für Physik
Mainz, Germany

JOHANNES
GUTENBERG
UNIVERSITÄT
MAINZ

TRIUMF
Canada's National Laboratory
for Particle and Nuclear Physics
Vancouver, Canada

TRIUMF

Vancouver, Sunday 1st May, 2011

The TITAN cooler Penning trap for short-lived highly charged ions; investigations for nested trap applications and fast electrode switching

Diplomarbeit by Benjamin Eberhardt
  eberhab@students.uni-mainz.de
  eberhab@triumf.ca

Referees: Prof. Dr. J. Dilling, TRIUMF/ University of British Columbia
             Prof. Dr. J. Walz, Universität Mainz

Abstract

TRIUMF's Ion Trap for Atomic and Nuclear science (TITAN, located at the ISAC radioactive beam facility at TRIUMF, Vancouver, Canada) is dedicated to high precision mass measurements on short lived radioactive isotopes. The science program at TITAN included the 2 and 4 neutron halo nuclei of ^{6}He, ^{8}He, ^{11}Li, and ^{11}Be with ^{11}Li the shortest lived nucleus ($t_{1/2} = 8.5$ ms) ever measured in a trap. The isotope ^{74}Rb was recently investigated, as the q-value of this super allowed β-decay contributes to CKM unitarity tests. In general atomic masses are a key to various fields of sub-atomic research which require specific precision. This precision can be raised by increasing the ion's charge state. TITAN implements a unique combination of an electron beam ion trap charge breeder process with a mass spectrometer for studies on short lived isotopes.

The charge breeding is coupled to an increased energy spread of the ions which counteracts the precision gain. To mitigate that effect a cooler Penning trap (CPET) is developed. CPET implements sympathetic cooling of highly charged radioactive ions, where the ions undergo energy exchanging collisions with electrons or protons used as a coolant.

This thesis is concerned with investigating the effect of the switching of the trap electrode's potentials on trapped particles. In particular possible heating effects during fast switching processes are studied. Modifying the electrode potentials is essential to trap and eject particles. This potentially counteracts the cooling process and needs to be understood and minimized.

The first part of the thesis describes the setup and the results of two different single particle simulations. Furthermore, an arbitrarily programmable multi channel power supply was attached to the CPET electrodes to study the characteristics of the supply and the impact of potential switching on the trap.

Contents

List of Tables

List of Figures

Acknowledgements

I would like to thank Prof. Dr. Jens Dilling for providing me with the opportunity to perform research and write this diploma thesis at TRIUMF in Vancouver. I am very grateful for all of the support throughout the year, and the many encouraging ideas. This also goes to Prof. Dr. Gerald Gwinner from the University of Manitoba.

I would like to give a special thanks to Prof. Dr. J. Walz who agreed to evaluate this thesis for the University of Mainz, to Prof. Dr. L. Köpke of the University of Mainz who enabled me to write this thesis abroad and put the project into practice, and to Prof. Dr. Klaus Blaum for establishing the first contact with Vancouver.

Many thanks to Vanessa Simon, Aaron Gallant, Brad Schultz, Mel Good, Matthew Pearson, Daryl Bishop, Usman Chowdhury, Martin Simon, Stephan Ettenauer, Hicham Al Falou and the whole TITAN group. They all gave me a lot of support and valuable input, and introduced me into the versatile research performed at TITAN.

It has been an instructive and eventful time in many respects. Not only did I learn about ion traps and the theory and practice of precision mass measurements, but also about the many aspects of the nuclear and particle physics research laboratory that is TRIUMF.

Having said this, I would like to mention Ken Lukas and Matthew Pearson for two fascinating tours they gave us through the entire facility, and especially to the cyclotron vault, the target station and the mass separator.

To Maya and James, the people who introduced them to me and many new friends in Vancouver who made my stay as a whole a unique and memorable experience, and are a source of many new ideas goes a big thanks as well.

x

Chapter 1

Introduction and Theory

1.1 Motivation

TRIUMF's Ion Trap for Atomic and Nuclear science (TITAN [1]) is dedicated to high precision mass measurements ($\delta m/m \approx 10^{-9}$) of short lived radioactive isotopes (the shortest lifetime measured so far in an ion trap was $t_{1/2} \approx 8.6$ ms of ^{11}Li [2]).

Atomic masses are a key to various fields of study ([3] Chapter 9), such as nuclear astrophysical processes (e.g. [4]) which is concerned with the creation of heavier elements in exploding stellar objects. Moreover, tests of the conserved vector current hypothesis (CVC[1]) and tests of the unitarity of the Cabbibo-Kobayashi-Maskawa (CKM[2]) quark mixing matrix (e.g. [7]) help to explore the limitations of the Standard Model of Particle Physics. Also, proton or neutron binding energies[3] can be obtained by measuring the difference in mass of neighbouring nuclei. These energies are a key to understand the forces inside the atomic nucleus (e.g. [9]).

It depends on the field of study which isotopes' masses have to be measured and with what precision ([3] Table 1). As an example, the test of unitarity of the fundamental Cabbibo–Kobayashi–Maskawa (CKM) quark mixing matrix is taken. One of the necessary experimental quantities is the q-value of the nuclear beta decay[4]. The q-value is the mass difference of the initial and the final isotope of the decay. In this case, the q-value of the β^+-decay of ^{74}Rb ($t_{1/2} \approx 64.78$ ms) to ^{74}Kr ($t_{1/2} \approx 4.5$ m) is taken, which can be obtained by measuring both masses. The required precision for this purpose is $\delta m/m \approx 10^{-8}$ [11].

In order for the isotopes to measured, they need to be trapped electromagnetically ([3] Chapter 3) and transported along the experimental setup and are therefore ionized, typically to A^{1+}.

---

[1][Particles and Nuclei, Chapter 15.5 of 5, p. 217]
[2][Particles and Nuclei, Chapter 10.4 of 6, p. 139]
[3][Particles and Nuclei, Chapter 2 of 8, p. 11]
[4][Particles and Nuclei, Chapter 3.1 of 10, p. 26]

One option to achieve the required precision of the mass measurement is to further increase the charge state of the ions [12]. This task is accomplished by an electron beam ion trap (EBIT [13]), which can produce highly charged ions (HCI). In an EBIT electrons from a high energy electron beam (E_{kin} = 20–40 keV) remove electrons of the ion via collisions. This procedure introduces energy into the system of trapped ions and increases their energy spread. However, this effect counteracts the precision gain of the mass measurement and should ideally be eliminated by cooling the ions after charge breading. A cooler Penning trap (CPET) is developed [14–18] to serve this purpose and is currently being assembled.

CPET will implement sympathetic cooling, where the ions undergo energy exchanging collisions with a charged coolant e.g. electrons, protons or other ions. A first test setup adjacent to the TITAN system is planned, which will initially implement electron cooling [18].

The cooler Penning trap is an ion trap which uses electric fields to trap, confine and eject the ions axially. Modifying the trap electrode potentials is therefore essential but also introduces potential energy into the system of trapped particles. As the particles oscillate in the electric trapping potential, this energy gain is converted into kinetic energy gain. This counteracts the cooling process and can even lead to loss of coolant and ions of interest. This thesis focuses on the effect that the switching of the trap electrode potentials has on the energy of trapped electrons. The Ph.D. thesis of Dr. Ke [15] provides values for initial energy requirements of the coolant.

The first chapter will give an introduction to Penning traps and ion cooling techniques. An overview of the TITAN setup at TRIUMF will show how these traps and techniques are implemented.

Simulations of the cooler Penning trap are performed in the second chapter. The energy of single trapped electrons is investigated while the potential of trap electrodes is changed (e.g. switched from one value to another). The aim of the simulations is to investigate the effect of the switching with respect to kinetic energy spread of the electrons.

Furthermore, an arbitrarily programmable multi channel power supply was attached to the CPET electrodes in order to study the characteristics of the supply and the impact of electrode potential switching on the trap structure (e.g. induced potential on other electrodes).

1.2 Penning traps

1.2.1 Types of Penning traps

A Penning trap[5][20, 21] is a particle trap able to confine charged particles in all three spatial dimensions using a constant strong magnetic dipole field and a constant weak electric field. The typically electric quadrupole field is produced by at least three electrodes which are placed in the homogeneous field region of a magnet. A sketch of an ideal Penning trap, also called precision trap, is
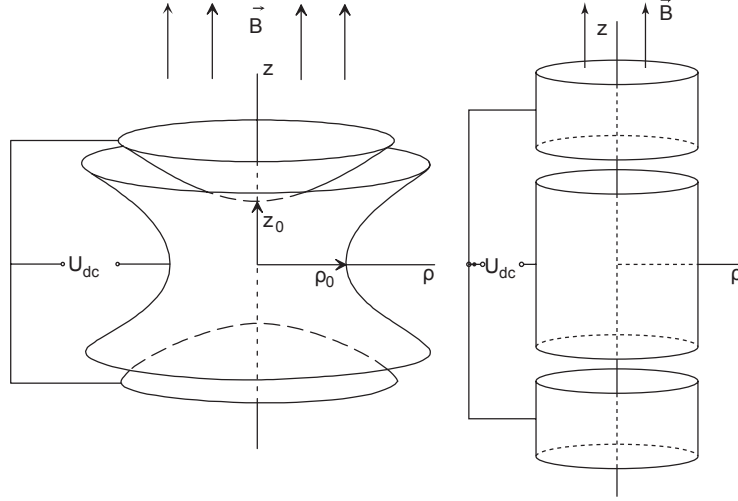
Figure 1.1: Sketch of an ideal hyperbolic (left) and cylindrical (right) Penning trap with with indicated applied trapping potential U_{dc} and magnetic field $\vec{B}$ [19]. The magnetic field lines run along the trap centre axis z. The radial cylindrical coordinate is ρ.

shown in Fig. 1.1 (left) which is a hyperbolical Penning trap consisting of three electrodes and a magnet. The magnetic dipole field forces the charged particles to a circular motion around the magnetic field lines, thus confining them radially in two dimensions based on the Lorentz force law $\vec{F} = q(\vec{E} + \vec{v} \times \vec{B})$.

Axial confinement is provided by a quadrupolar electric field. In an ideal Penning trap, the electric quadrupole potential is [21]

$$U(\rho, z) = \frac{U_0}{4d^2}(\rho^2 - 2z^2) \tag{1.1}$$

with $U_0 = U_{\mathrm{dc}}$ being the potential difference between the trapping electrodes. In the ideal case the electrodes are hyperbola of revolution[6] with the geometry $\rho^2 - 2z^2 = \rho_0^2$ of the centre or ring electrode and $\rho^2 - 2z^2 = -2z_0^2$ of the outer electrodes or end caps. The value of

$$d = \sqrt{\frac{z_0^2}{2} + \frac{\rho_0^2}{4}} \tag{1.2}$$

is a measure for the characteristic trap dimension. In order to trap positively charged particles the end caps are set to a positive potential relative to the ring,

---

[5]Named after F. M. Penning (1894–1953). The first Penning trap was built in 1959 by Hans Georg Dehmelt who shared the 1989 Nobel Prize in Physics for the development of the ion trap technique.

[6]A hyperboloid which is symmetric around the centre axis z. The ring electrode is a hyperboloid of one sheet. The end caps are a hyperboloid of two sheets. A more detailed description about deriving the hyperbola equations and 3D confinement in general is given on [Ph.D. Thesis of Brodeur, M. 22, p. 46].
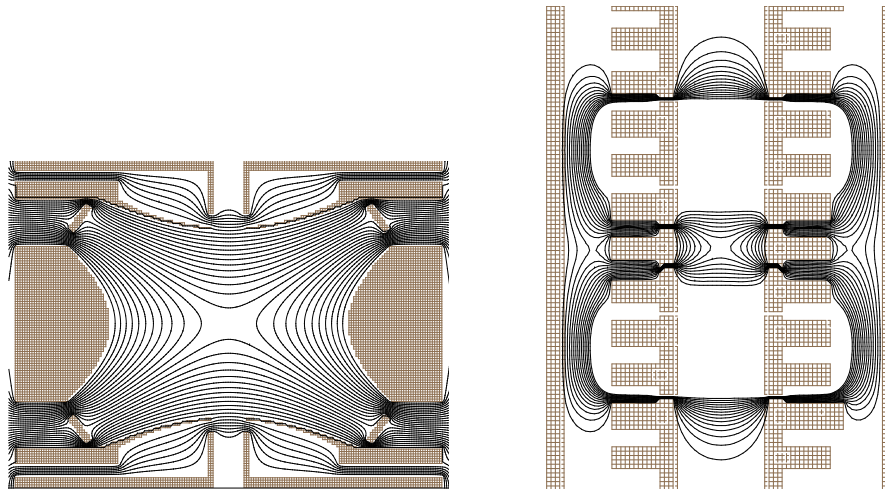
Figure 1.2: Simulation screenshot of a hyperbolic Penning trap (left) and a cylindrical Penning trap (right) with lines of equal potential. The trap axis, as well as the magnetic field lines run from the bottom centre to the top centre of the figures. The particles also enter and leave the trap this way. These sketches are taken from simulations of the TITAN mass spectrometer MPET (left) and the cooler Penning trap CPET (right).

which forces the charged particles towards the axial centre of the trap. As the real trap electrodes are not ideal (e.g. hyperbola of revolution are ideally infinite in size), correction electrodes are implemented to generate a trapping potential U as close to Eq. (1.1) as possible.

The cylindrical Penning trap (Fig. 1.1, right) is constructed of at least three electrodes of cylindrical shape. In order to confine positively charged particles the outer electrodes are set to a positive potential relative to inner electrodes. Due to the cylindrical shape, the trapping potential U contains higher-order electric multipoles, which can be suppressed by applying correction potentials to additional electrodes. The magnetic field again provides radial confinement perpendicular to the centre axis z. The length of a cylindrical Penning trap is limited by the length of the homogeneous region of the magnet. It allows a larger storage volume and can be used to set up multiple trapping regions depending on the number of trap electrodes. The outer electrodes of a trapping region are in the following referred to as trap walls, gate electrodes or trap gates. A sketch of a hyperbolical and cylindrical Penning trap including lines of equal potential U is shown in Fig. 1.2.

Based on Laplace's equation $\vec{\nabla}^2 U = 0$ it is not possible to confine particles in more than one dimension with a constant electric field, because of the global minimum at the potential source. Charged particles are pushed away from the outer towards the centre electrode. To prevent the particle from hitting the centre electrode and thus leaving the trap, radial confinement is provided by

the magnetic field. An alternative approach is to apply an alternating potential

$$U_0 = \frac{1}{2}(U_{\mathrm{dc}} + U_{\mathrm{rf}} \cos \omega_{\mathrm{rf}} t) \tag{1.3}$$

to the electrodes. This setup is called a Paul trap[7]. The Paul trap provides three dimensional confinement to charged particles without a magnetic field. The trapping potential U is more complex and contains a time dependent term leading to a so-called micro motion of the particles.

1.2.2 Mass measurements with Penning traps

The above mentioned motion of a trapped charged particle in an ideal Penning trap is a superposition of three independent harmonic oscillations[23].

- The reduced cyclotron motion, with a frequency of ω_+ is the circular movement of the particle around the magnetic field lines. Charged particles develop a cyclotron motion in a pure magnetic field with a frequency depending on their mass, charge and the strength of the magnetic field. If an electric field is added the frequency reduces to ω_+.

- The axial motion, with a frequency of ω_z is induced by the electric field. It is an axial motion of the particle around the field minimum.

- The magnetron motion is caused by the precession of the magnetic moment of the reduced cyclotron motion in the electric field. It leads to an oscillation frequency of ω_-.

The frequency of the particle's motion in the trap is called the cyclotron frequency and is given by [21]

$$\omega_c = \sqrt{\omega_+^2 + \omega_-^2 + \omega_z^2} = \frac{q}{m}B \ . \tag{1.4}$$

For an ideal electric quadrupole field the three eigenfrequencies are

$$\omega_z = \sqrt{\frac{qU_0}{md^2}} \ , \tag{1.5}$$

$$\omega_+ = \frac{\omega_c}{2} + \sqrt{\frac{\omega_c^2}{4} - \frac{\omega_z^2}{2}} \ , \tag{1.6}$$

$$\omega_- = \frac{\omega_c}{2} - \sqrt{\frac{\omega_c^2}{4} - \frac{\omega_z^2}{2}} \ , \tag{1.7}$$

where q is the particle's charge, m its mass, B the strength of the applied magnetic field, U_{dc} the trapping potential in proper polarity and d the half distance between the trapping electrodes. The particle's mass can therefore be

---

[7]Named after Wolfgang Paul (1913-1993) who shared the 1989 Nobel Prize in Physics for the development of the ion trap technique.
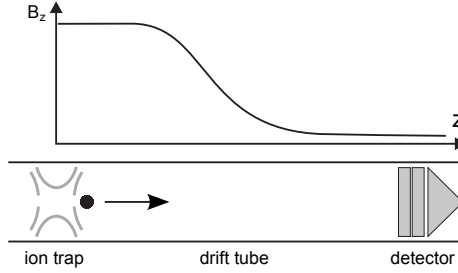
Figure 1.3: Sketch of the TOF extraction setup [19] including the ion trap, drifttube and detector. The axial component of the magnetic field along the axis z is shown.

derived if q, B and ω_c are known. Two methods are presented which can be used to measure the cyclotron frequency of a particle in a Penning trap.

As this thesis is concerned with an experimental setup which performs high-accuracy mass spectrometry on ions, the term "charged particle" is mainly used as a synonym and also to indicate, that some processes and techniques are valid for all charged particles.

Both hyperbolical Penning traps (e.g. TITAN) and cylindrical Penning traps (e.g. JYFLTRAP[24]) are used to carry out precision mass measurements using the follwoing method.

The Time of Flight (TOF) mass measurement method

The TOF method [25] (e.g. used by TITAN) determines the cyclotron frequency by measuring the flight time of an ion from the trap to a detector positioned at a apecific distance.

A quadrupole radio frequency (RF, e.g. $\omega_0 \approx 8.697056$ MHz for $^{85}\text{Rb}^{13+}$)[8] electric field is applied to the trap electrodes, with a frequency of $\omega_0 = \omega_c$. The RF field causes an oscillatory conversion of the ion's magnetron motion into pure reduced cyclotron motion. One complete oscillation is obtained after a time T_r. This process is called quadrupole excitation. After the excitation, the ions are extracted from the precision trap. A voltage pulse is therefore applied to the end cap electrodes and also used as a start signal for the particle time of flight measurement. During extraction, depending on its magnetic moment $\vec{\mu}$ the particle is pulled with a force [19]

$$\vec{F} = -\vec{\mu}\,(\vec{\nabla}\vec{B}) = \frac{E_\text{r}}{B}\hat{z}\,(\vec{\nabla}\vec{B}) = -\frac{E_\text{r}}{B}\,\frac{\partial B}{\partial z}\,\hat{z} \qquad (1.8)$$

through the magnetic field gradient $\vec{\nabla}\vec{B}$ along the trap axis z towards the detector. Its radial energy E_r is converted into axial kinetic energy. The particle then hits a multi channel plate (MCP) detector defining the end signal of the TOF. A sketch of the experimental setup including the magnetic strength is
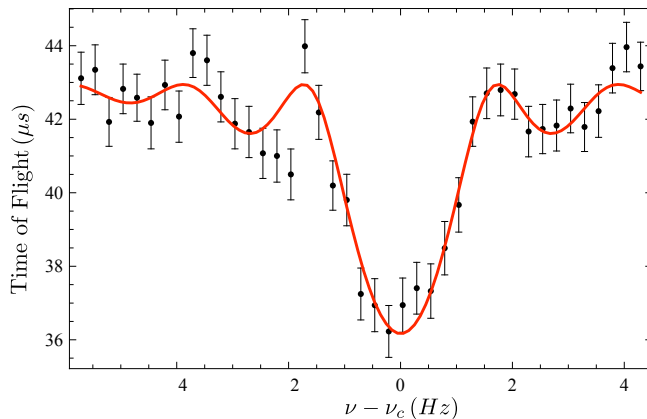
Figure 1.4: TOF measurement of ^{8}Li as a function of applied frequency including the theoretical curve as a fit [26]. A typical dataset taken at TITAN.

shown in Fig. 1.3.

This process is repeated for different frequencies ω_0 close to ω_c where the particles are always extracted after $T_r/2$ (having made exactly one full conversion for $\omega_0 = \omega_c$). The more ω_0 differs from ω_c, the more incomplete the motion conversion is. While extraction this results in less axial kinetic energy and a longer TOF. The resulting TOF spectrum then has a global minimum for $\omega_0 = \omega_c$. The time of flight as a function of applied frequency can be fitted in order to obtain the cyclotron frequency. A sample spectrum is shown in Fig. 1.4.

The fast Fourier Transform Ion Cyclotron Resonance (FT-ICR) mass measurement method

The FT-ICR method [27] (e.g. used by MIT ICR [28]) determines the frequencies of all motions of the charged particle in the trap. This method is non destructive.

The oscillating trapped particle induces image currents onto the segmented ring electrodes of the trap. A Fourier analysis of the induced current shows maxima at all three oscillation frequencies (ω_+, ω_-, ω_z). High-accuracy mass measurements are usually performed using single (or very few) ions [3] to avoid frequency shifts due to space charge effects. The radius of the circulating ion in the trap is kept as small as possible to minimize the impact of inhomogeneities of the trapping field. A major difficulty of this method therefore is noise suppression, as the signal of the oscillating particle is very weak.

---

[8]Inside the TITAN mass spectrometer with $B = 3.7$ T, $z_0 = 12.15$ mm and $\rho_0 = 15.00$ mm [Ph.D. Thesis Smith, M.: 26, p. 100]
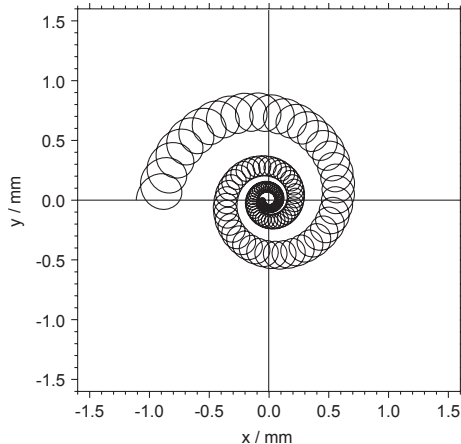
Figure 1.5: Sketch of the ion motions in a Penning trap undergoing a cooling process [19].

Dipole cleaning

Dipole cleaning [29] is used to clean unwanted ion species off the trap before starting the mass measurement procedure, so that only or mostly ions of interest remain. The reduced cyclotron frequency ω_+ of a trapped contaminant particle is applied to two trap electrodes. The dipole excitation increases the radius of the particle's cyclotron motion until the particle hits a trap electrode. In order for the dipole cleaning to work, the frequency has to be applied in a direction radial to the trap centre axis. In a Penning trap, this can be achieved by either splitting the ring electrode in two halves or by adding correction electrodes.

1.3   Cooling techniques

If the energy of a trapped ion bunch is decreased, the width of its energy distribution and respectively the energy spread of the ions decreases. This process is called cooling. The opposite case is called heating. Cooling results in decreasing the motional amplitudes of the stored ions as illustrated for the two radial motions in Fig. 1.5. Cooled ions can therefore be trapped in a smaller volume and are less affected by inhomogeneities of the electric and magnetic trapping fields [19].

Different techniques exist to cool particle bunches [3, 30]. These techniques either affect all three motional amplitudes individually or introduce a coupling of motions, where only one or two components are actively cooled, but kinetic energy is continuously converted between all degrees of freedom. The remaining motions are therefore passively cooled.

I our case the following requirements need to be fulfilled: fast, efficient and universally applicable (e.g. to a variety of ion species with different m/q).

1.3.1 Resistive cooling

Resistive cooling is used for example in g-factor experiments on simple systems in Penning traps [31]. As previously mentioned, trapped particles in a Penning trap induce image currents onto the trap electrodes. An external circuit resonant to the particle's oscillation frequency can be attached between two trap electrodes to successively absorb the current, transform it to thermal energy and dissipate it to the environment [19, 32]. The exponential energy loss of the particles has a time constant of

$$\tau = \left(\frac{2z_0}{q}\right)^2 \frac{m}{\omega L} \frac{1}{Q} \tag{1.9}$$

where z_0 is the half distance between the electrodes (see Fig. 1.1), q the ion charge, ω the particle's oscillation frequency, m the particle's mass, L the inductance of the circuit's inductor, and Q the quality factor of the circuit. The quality factor is a measure for the energy absorbency of the circuit, which depends on the temperature difference of the ion ensemble and the circuit electronics. Finally the ions and the circuit will be in a thermal equilibrium. The circuit is generally put in contact with a liquid helium bath at 4.2 K.

The narrow resonances of the circuit make it necessary to build different circuits for different values of q/m. With resistive cooling, cooling times in the order of 100 ms to seconds can be achieved, which makes this method inapplicable for short-lived isotopes.

1.3.2 Evaporative cooling

Evaporative cooling is used for example in Bose Einstein condensation (BEC) [33]. This method is implemented by lowering the trapping potential, so that it no longer provides confinement to the most energetic ions. The remaining ions remain in the shallower potential and re-establish a thermal equilibrium by collisions.

A certain loss of the distribution of particles of interest is a disadvantage of this method. The tail of the energy distribution is cut off, the amount of loss depends on the temperature that has to be achieved and the cooling time. The loss increases if the potential is lowered so fast that the ions don't have time to establish a thermal equilibrium. The process can be continued until only a few low energetic ions remain. If the goal of the cooling is to result in only one or very few cold ions and loss is therefore maximised, then the potentials can be lowered very fast making this approach the fastest cooling process.

This method can also be implemented in an environment where particles undergo a procedure that introduces heating (i.e. in an electron beam ion trap [34]). If a particle gains a sufficient amount of energy during this process the trap potential no longer provides confinement and it "boils" out of the trap. To minimize the loss of the particles of interest, particles with a lower charge state q can be added to the trap. Ions need an energy $E = q \cdot U_0$ to leave the trap. The potential trap wall is effectively lower to them leading to a higher probability

of evaporation during the process. The amount of energy they transport away lowers the temperature of the remaining particles, when they re-establish a thermal equilibrium.

1.3.3   Buffer gas cooling

Buffer gas cooling is used for example at TITAN to cool the ion beam prior to the precision mass measurement [35]. Neutral buffer gas is added to the trap. The particles then undergo energy exchanging collision with the gas molecules. The influence of the particle collisions with background gas can be described by a damping term in the particles' equations of motion which is proportional to the ions charge to mass ratio and the gas temperature and pressure [3]. Buffer gas cooling actively reduces the energy of all three oscillations. It also couples the motions.

As the ions axial amplitude decreases due to the damping axial energy is converted into radial energy. The amplitude of the radial magnetron motion therefore shows a slow net increase over time. A quadrupolar RF field with the true cyclotron frequency ω_0 has to be applied additionally in order to establish an additional coupling of the two radial motions. Magnetron motion can then be reduced over time by converting its energy into reduced cyclotron motion, which is actively cooled [36].

With buffer gas cooling cooling times in the order of 10 ms can be realised. It cannot be used for HCI, as the ionisation potential of the ion increases with its charge state. The HCI would capture electrons, ionize the gas, and change their charge state.

1.3.4   Laser cooling

Laser cooling is for example used in BEC as pre-cooling step before evaporative cooling [33]. Laser cooling is a very effective cooling technique for reaching very low temperatures $\ll 1$ K. The laser is tuned slightly below an electronic transition of the particle to be cooled. While the particle is moving towards the laser source it is Doppler-shifted into resonance. The probability of photon and thus momentum absorption is increased, slowing the particle down. De-excitation of the particle then occurs randomly into every direction, resulting in a zero average momentum gain [19].

This method is not optimal for use as a broadband cooler (i.e. for various HCI), as electronic transitions vary for different particles. This could be compensated by sympathetic laser cooling, which uses laser cooling to cool specific ions (e.g. Be^+, Mg^+, Ba^+, Hg^+, Yb^+, Sr^+, Ca^+, In^+) [30]. These ions are then used as a coolant for the ions of interest [33].

1.3.5   Sympathetic cooling

Sympathetic cooling is referred to [30] as cooling of ions with ions of a different species due to Coulomb collision. Other sources [37] refer to sympathetic cooling

as the cooling of protons with electrons. In this thesis sympathetic cooling will refer to cooling techniques implementing protons, ions and also electrons as a coolant. Hot ions will loose energy by undergoing energy-exchanging Coulomb collisions with the coolant. This process is discussed in greater depth in [15] Chapter 3.1.5, which presents simulations concerning cooling times and electron and proton densities required in order to cool bunches of hot ions.

This method can be applied for example in a cylindrical Penning trap with a sufficient number of electrodes. So called nested potentials have to be set up in the trap to confine particle with different charge, charge polarity and mass in the same trap volume. Nested potentials are potential wells formed by trap electrodes in different regions of the trap. This enables one to confine (different) particles at specific positions (see Fig. 1.6).

Electron cooling

Electron cooling is used for example to cool anti protons in the process of producing antihydrogen atoms [38]. The advantage of using electrons (over protons or ions) as a coolant is their ability to self cool in a magnetic field. A charged particle which is accelerated in a magnetic field emits energy in form of synchrotron radiation [15, 39]. The circular motion of the electron around the magnetic field lines is associated with the time dependent radial energy as

$$E(t) = E_0^{-\gamma t} \ , \tag{1.10}$$

where (in Si-units)

$$\gamma = \frac{e^2 \omega^2}{3\pi\epsilon_0 m_\mathrm{e} c^3} \ , \tag{1.11}$$

and

$$\omega = \frac{eB}{m_\mathrm{e}} \ , \tag{1.12}$$

and E_0 is the initial radial kinetic energy, ϵ_0 the electric constant, e the charge of the electron, m_e its mass, B the magnetic field strength and the time t. Synchrotron radiation therefore only cools the two radial components of the electron's movement. The axial energy of an electron in a Penning trap is reduced mainly due to collisions of the electrons with themselves, which couples the axial energy components with the radial components. Also the acceleration change at the turning points of the axial movement is causing synchrotron radiation and the reflection at the end caps of the trap also contributes to a mixing of degrees of freedom due to inhomogeneities of the trapping fields and non ideal axial alignment of the trap axis.

The cooling time constant $\tau = 1/\gamma$ depends on the field strength and is $\tau \approx 0.1$ s for $B = 7$ T.

As the amount of emitted energy scales inversely with the 3rd power of the mass (Eq. (1.10)), this effect is negligible for protons or heavier particles.

The disadvantage of electron cooling is the possibility of electron recombination, especially for HCI, as it alters the charge state q of the particles to be
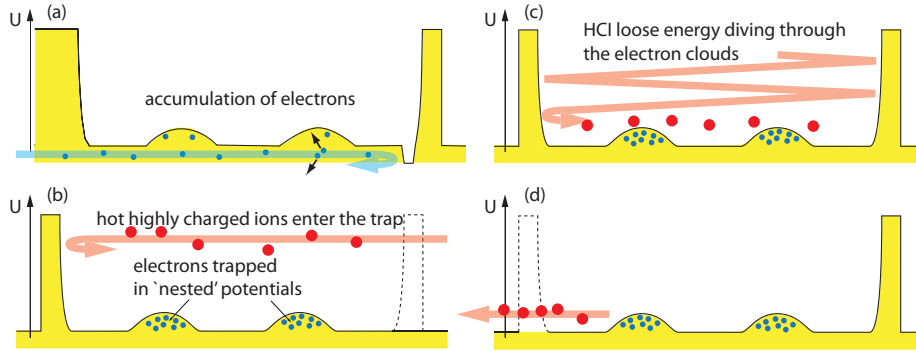
Figure 1.6: Schematic of the proposed electron cooling cycle for CPET in four steps[17]. a) Accumulation of electrons. b) Electrons have accumulated in nested potentials and cooled down via synchrotron radiation, hot HCI enter the trap. c) HCI loose energy by colliding with the electron clouds. d) cooled HCI are separated from the electrons and ejected from the trap.

cooled. Simulations ([15] Chapter 3.2) have shown, that HCI can be cooled down to an average energy of $E \approx 1$ eV allowing more than 95% of the HCI in the desired charge state to survive. A window of opportunity allows one extraction of the cooled particles before the recombination becomes dominant.

A schematic of the proposed electron cooling cycle for CPET is presented in Fig. 1.6. Electrons are first injected into the trap and lose energy due to synchrotron radiation. After the electrons cooled down, the HCI are loaded. As the ions fly through the nested electron wells they lose energy due to energy exchanging Coulomb collisions.

Proton cooling

Proton cooling [16] would avoid recombination of the electrons and hence preserve the charge state but the self cooling mechanism is strongly suppressed as compared to electrons. A larger amount of initially cold protons has to be available, which is challenging to realise and limited by the proton source. Calculations ([15] Chapter 3.1.5) have shown, that with an initial density of 10^7 electrons/cm^3 and 10^8 protons/cm^3, 10^3 HCI with initial energy of 500 eV/q can be cooled down to 1 eV/q within a fraction of a second.

Figure 1.7: Photograph of the TITAN setup at TRIUMF

1.4 Mass measurements at TITAN

1.4.1 General setup of the facility

TITAN[9] [1] is located at the Isotope Separator and Accelerator (ISAC[10] [40]) facility at TRIUMF[11], Canada's National Laboratory for Particle and Nuclear Physics.

The ISAC facility produces singly charged radioactive ion beams (RIB) for a variety of experiments using the isotope separator on-line (ISOL) method [41].

A continuous high intensity ($I \leq 100 \ \mu A$, $E = 500$ MeV) proton beam is produced by the TRIUMF cyclotron and directed onto a solid target. Nuclear reactions lead to a production of various isotopes lighter than the target material. They diffuse out of the target and are ionized using different techniques such as surface or laser ionization to a charge state of $q = 1$. Different targets are used to provide a large variety of different radioactive ion species.

The singly charged ions (SCI) are then electrostatically accelerated into the magnetic dipole separator which enables the selection of ions based on their charge to mass ratio.

---

[9] http://titan.triumf.ca/
[10] http://www.triumf.ca/research/research-facilities/ → ISAC
[11] http://www.triumf.ca/

After selection the SCI can be delivered to the low energy ($E \leq 60$ keV) experimental area or be further accelerated via a radio frequency linear accelerator (RFQ Linac) and a variable energy drift tube Linac (DTL). TITAN is located at the low energy experimental area.

1.4.2 TITAN setup

TITAN is a precision mass measurement setup which consists of three (later four) ion traps. The first two (three) ion traps are used to prepare the ion beam from ISAC in such a way, that the precision of the mass measurement in the fourth ion trap can be maximised.

The scientific goal of TITAN, are high precision mass measurements of short lived isotopes as a key to nuclear physics, nuclear astrophysics and weak interaction studies. These applications require the relative precision of atomic mass measurements between $\delta m/m \approx 1 \times 10^{-7}$ to 1×10^{-9}. TITAN implements the TOF method with a precision Penning trap to measure the masses of ions. The relative precision of the measurement method has the following dependencies [42]

$$\frac{\delta m}{m} \propto \frac{m}{T_r \, q \, B \, \sqrt{N}} \tag{1.13}$$

Due to the nature of the experiments performed, the precision is limited by the following factors:

1. The RF excitation time T_r cannot be arbitrarily increased, as the measurement time is limited by the life time of the short lived isotope (e.g. $t_{1/2} \approx 8.6$ ms of ^{11}Li).

2. The magnetic field strength of the precision trap magnet is $B \approx 3.7$ T and cannot be easily increased. 25 T magnets can be manufactured [43] but have lower field homogeneity. This option would also be an expensive major system change. The precision gain would still be limited to a factor of ≈ 8 for $B = 25$ T. The largest field for an operational Penning trap system is $B = 9.4$ T [44].

3. The number of ions N is defined by the ISAC beam intensity and cannot be increased. Higher statistics could be obtained by increasing the number of separate measurements, which is limited by the time window of availability of radioactive beam.

The remaining option of increasing the mass measurement precision is increasing the ion's charge state q. Equation (1.4) shows, that ω_c increases with increasing q, thus increasing the radial kinetic energy E_r of the ion. This leads to an increase of axial kinetic energy while extraction and to a higher resolution of the TOF method.

The TITAN setup therefore implements the unique combination of an electron beam ion trap (EBIT) [12] with a mass measurement Penning trap for the purpose of studying short lived isotopes. The ions are trapped in the EBIT [13]
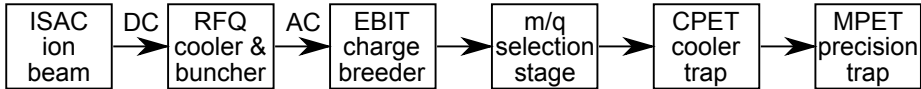
Figure 1.8: Scheme of the TITAN setup showing the path of the ions from the ISAC facility to the precision Penning trap MPET including the RFQ cooler and buncher, the EBIT charge breeder, the m/q selection stage and the future CPET cooler trap.

and with the use of an electron beam their charge state of initially $q = 1$ is raised. Electrons from the EBIT electron gun collide with the electrons from the ions. A large amount of kinetic energy is transferred as they have the same mass. This energy is sufficient to remove electrons up to a specific binding energy. To date, with an electron beam energy of up to 5 keV a mass measurement on ^{85}Rb with $q = 17$ has been successfully realized. With an envisioned electron beam energy of 40 keV the production of He-like Uranium[12] would be possible ($q = 90$). This would result in an idealized improvement of the measurement precision by almost two orders of magnitude.

The TRIUMF cyclotron produces a continuous proton beam and hence the RIB delivered by ISAC is also continuous (DC). In order for the charge breeding process in the EBIT to be fast and efficient, a cooled and bunched ion beam has to be injected. The TITAN facility therefore uses a radio frequency quadrupole (RFQ) cooler and buncher [35]. The RFQ accumulates ions from the continuous ISAC beam, cools them using buffer gas cooling, and ejects them as a bunch (AC). The path of the ions through the TITAN setup is shown in Fig. 1.8 and Fig. 1.9.

An unavoidable side effect of the charge breeding inside the EBIT is an increased energy spread of the ion beam, which counteracts the precision gain. The high intensity electron beam heats up the ion bunch. Based on data from [45, 46] spreads of tens of eV/q are expected. This effect can be cancelled out by cooling the ions prior to injecting them into the MPET. The cooler Penning trap CPET has been developed to serve this purpose.

The ions have a different velocity based on their m/q ratio. A selection stage allows the selection of ions of a specific m/q ratio by defining a time window. Ions that are travelling faster and thus arriving earlier at the gate will be cut out of the bunched beam. The same concept applies for ions slower than the selected window. The last step of the setup is the mass spectrometer, which is a hyperbolic precision Penning trap.

1.4.3 The cooler Penning trap (CPET)

The cooler Penning trap CPET is a cylindrical Penning trap. It will be used to cool HCI with an energy spread on the order of 10 eV to an energy spread

---

[12]He-like Uranium is taken as an example to show the charge breeding capabilities of the EBIT. Uranium ions cannot be produced at ISAC as no atoms heavier than Uranium can be used as a target material.
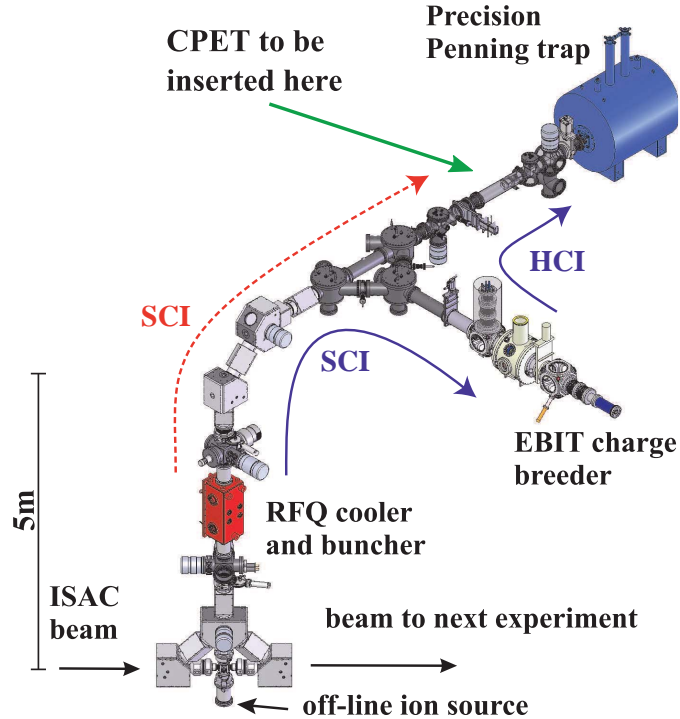
Figure 1.9: Sketch of the TITAN experimental setup at ISAC at TRIUMF [18]. Arrows indicate the direction of the ions with (blue, solid line) and without (red, dashed) being sent to the EBIT, as well as the future position of the cooler Penning trap. The setup is designed so that SCI (red, dotted line) can be injected directly into the MPET for singly charged measurements.

of 1 eV using various cooling techniques such as electron cooling. The cooling process will lead to an increased precision of the mass measurement performed in the subsequent Penning trap. A first setup aims at cooling times on the order of seconds. Future cooling times on the order of 100 ms are envisioned.

CPET consists of 29 inner trap electrodes and two longer electrodes which form the trap gates (or trap walls). The whole setup resides in a 7 T superconducting magnet. Different types of particles (e.g. HCI, SCI, electrons and protons) can be trapped in the same trap volume by formation of nested potentials [18]. A layout of the assembly is shown in Fig. 1.11 and Fig. 1.10. A photograph of the assembly is presented in Fig. 1.12.

Sympathetic cooling was chosen to be used with CPET because it is fast, efficient and universally applicable to different ion species (e.g. different m/q). Initially a stand alone test setup is planned which implements electron cooling with its own electron and ion source as shown in Fig. 1.10.

Based on the Eq. (1.10)-(1.12) the synchrotron radiation energy loss de-

pends on the strength B of the magnetic field. CPET resides in a $B = 7$ T superconducting solenoid. A field homogeneity of $\delta B/B = 10^{-5}$ is specified by the manufacturer to be provided in a cylindrical region of 100 mm length and 50 mm diameter in the centre of the magnet, where the electron self-cooling time constant is $\tau \approx 0.1$ s.

Besides electron and proton cooling, CPET can also be used to investigate m/q ion separation techniques and evaporative cooling. Two sections among the 29 trap electrodes consist of one 8-split electrode each which is surrounded by two half split electrodes (see Fig. 1.10). The 8-split electrodes can be used as quadrupoles to couple radial motions of trapped particles. They can also be used to investigate storage techniques like rotating wall electric fields [47], which create an additional centre force on the particles thus increasing their density. The four half split electrodes can be used for dipole cleaning. Arbitrarily programmable power supplies and an elaborate switching scheme are required to allow injection and extraction of different species and dynamic variation of the trapping potentials.

The CPET setup further consists of two long drift tubes on each side of the trap in order to transport the coolant and the HCI into the homogeneous region of the magnetic field. Various Einzel lenses and steerers will help facilitate the injection of the different particle types. Bi-polar high voltage (HV) switches enable the transmission of two different species (HCI and either electrons or protons). On the left side of Fig. 1.11 the feed through section of the setup is shown where 45 electrical connections to the trap electronics are guided out of the vacuum.

As the cooling process initially happens on a 1 s time-scale, the vacuum has to be sufficiently high in order to reduce the likelihood of collisions of coolant and the ions with background gas. Collisions with background gas could lead to particle loss or electron-ion recombination with electrons from gas molecules. Four 500 L/s turbo pumps will be aided by a specially coated vacuum pipe[13] to maintain a constant pressure of $p < 10^{-10}$ mbar [17].

After successful implementation of CPET, the cooling cycle will be optimised to work on a 100 ms timescale. Shorter cooling times are limited by the electron cooling process [15]. Shorter cooling times might be possible for protons if a sufficient proton density can be achieved. Protons can absorb more kinetic energy due to their higher mass, whereas electrons heat up very fast during the cooling process. In order for the electrons to further cool the ions, they need to radiate away their excess energy which is limited by the synchrotron radiation time constant of $\tau \approx 0.1$ s.

---

[13]The vacuum pipe has been coated on the inside using a non evaporative getter material (NEG) consisting of Zr, Ti and V. Under vacuum, the material acts as a pump. The accumulated material can be removed by heating the vacuum pipe while it is under vacuum.
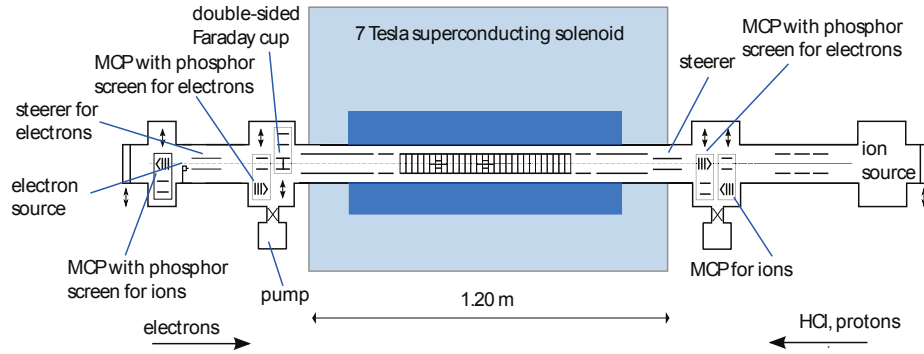
Figure 1.10: Sketch of planned CPET test setup including diagnostic electronics and vacuum setup.
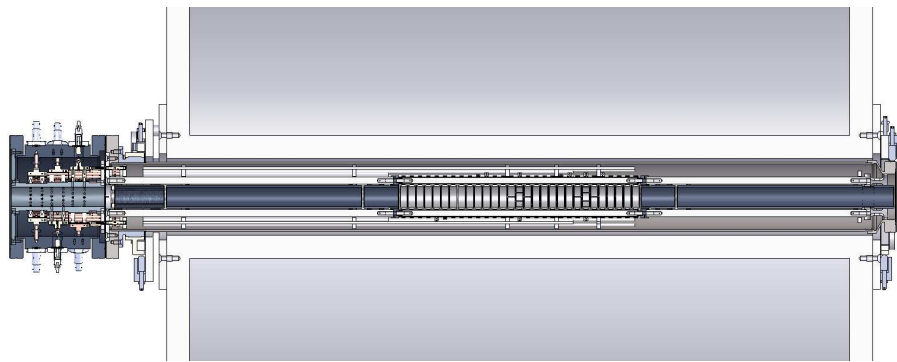
Figure 1.11: Vertical cut through the CPET SolidWorks assembly including the feed through section (left), the centre trap electrodes and the 7 T superconducting solenoid.
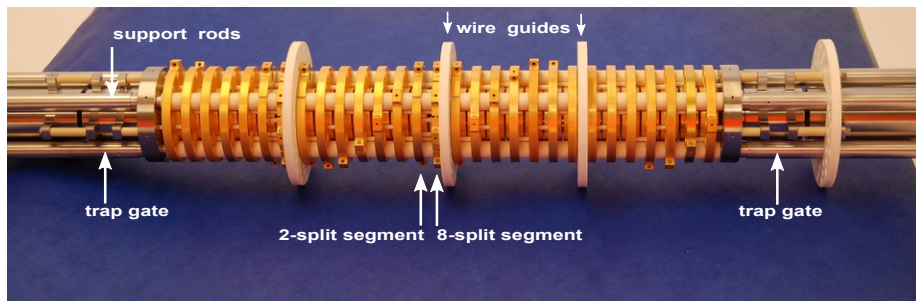
Figure 1.12: Photograph of CPET electrode structure containing the 29 gold plated trap electrodes. The longer gate electrodes and drift tubes on either side are labeled. The four white discs are ceramic wire guides.

Chapter 2

Electron manipulation with the cooler Penning trap

This chapter gives an overview of the cooler Penning trap operation cycle, as well as different electron injection or loading techniques. The concept of particle manipulation (axial transfer) in the cooler Penning trap is introduced and further investigated. Electrons are used as a sample species for this purpose in a 1D and 3D simulation of CPET. At last, the timescale of the synchrotron radiation cooling process of electrons in the 7 T magnetic field is determined.

2.1 The cooler Penning trap operation cycle

The previously mentioned electron cooling will be investigated with CPET. The electrons and the highly charged ions (HCI) will have to be injected, stored, separated, and ejected from the trap. These operations are called ion or electron manipulation and are performed using time dependent potentials, which are applied to the trap electrodes. The detailed cooling operation cycle is under development and will consist of the six following basic steps. Steps 1, 4, and 6 are also presented in Fig. 2.1.

1. Electron injection. (Duration: 100 ms to several seconds.)

2. Stop electron injection, electrons cool via synchrotron radiation. (Duration: 100 ms - several seconds.)

3. Prepare for HCI injection: raise potential on exit trap gate (Duration: few microseconds.)

4. Injection of HCI and switch of entrance trap gate. (Duration: 100 ns.)

5. HCI cooling. (Duration: 100 ms - seconds).
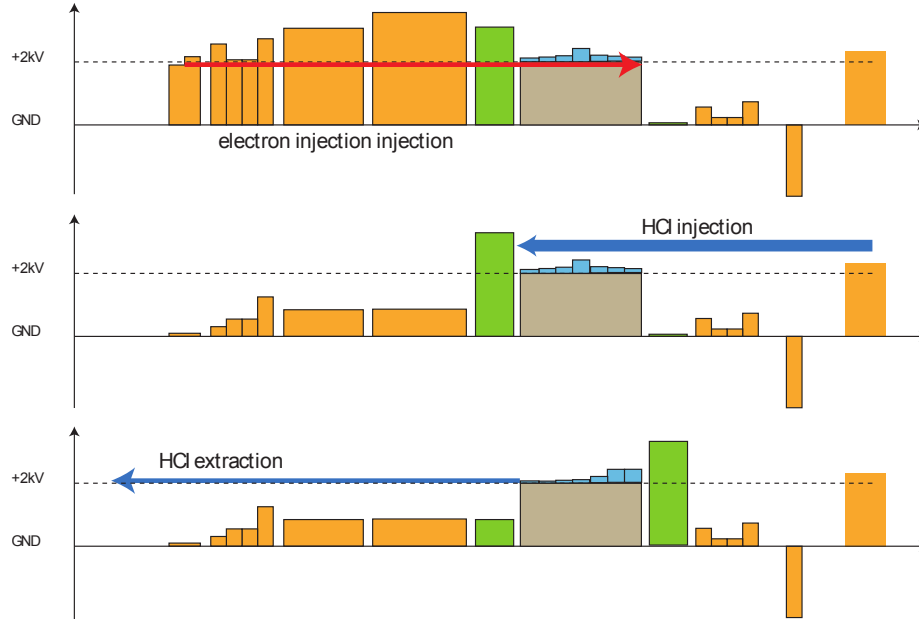
Figure 2.1: Schematic of the proposed operation cycle of CPET [18]. Electrons enter from the right, HCI from the left. Displayed are sample potentials of step 1 (top scheme) the injection of the electrons, step 4 (centre scheme) injection of the HCI and step 6 (bottom scheme) extraction of the HCI. The inner trap region is formed of individual (0 to 200 V) potentials (light blue) floated on a 2 kV platform (grey).

6. End of HCI cooling: HCI are now ready for extraction, waiting in the trap. (Duration: milliseconds.)

Two different electron injection methods planned to be tested with CPET.

The dynamic loading involves a static setting of the trap electrodes potentials and a continuous electron beam. The electrons enter the trap with a kinetic energy slightly higher than the trap gate potential. They lose axial energy inside the trap primarily due to collisions with electrons reflecting on the second gate. The electron beam density needs to maximised for this method work. The result is that the electrons do not have enough axial energy to leave the trap again via the entrance gate.

The multiple loading involves a bunched electron beam which is injected into the trap. The trap gate is open until an electron bunch enters the trap region. The trap gate is then closed before the reflected electron bunch leaves the trap region. By modifying trap electrode potentials, the electrons will be moved away from the entrance gate, towards the exit gate of the trap. They are confined there by lowering[1] electrode potentials in the centre of the trap. The trap now consists of two trapping sections. An electron storage section is

on the far side of the trap entrance and an empty section is close to the trap entrance, which is ready to receive a new bunch of electrons. The trap gate is reopened and the next electron bunch injected. After the trap gate is closed, the potential wall in the centre of the trap is lowered and all electrons are moved to the far side of the trap. This process is repeated until a sufficiently high electron density is achieved.

An electron density of 10^7 electrons per cm^3 has to be achieved in order for the electron cooling process to work on a sub-second timescale [15] for $\approx 10^3$ HCI at 500 eV/A. In order to achieve this density new storage techniques like rotating wall electric fields [47] will be tested. To date electrons densities of $1 \cdot 10^{11}$ cm^{-3} can be trapped and stored successfully [48].

2.2 Adiabatic Transfer of charged particles

Injecting the coolant (electrons or protons), initiating the cooling process, and ejecting the ions will involve a large number of potential switching operations of the trap electrodes, depending on the injection method. These switching operations introduce a change of potential energy into the system of trapped particles. The individual particle will gain a specific amount of energy depending on its current position in the potential well and the size of the potential shift Δx (see Fig. 2.2). As the energy of the trapped particles increases, their energy distribution broadens and respectively the particle bunch is heated. This effect is independent of the form of the potential well. A harmonic potential is chosen in the presented study, as it is simple to describe mathematically.

In the following text a "fast" process refers to an operation that happens within an infinitesimal small time step $\Delta t_{\rm rise}$. The particles do not change their position in the trap significantly during that period of time. A process being "slow" refers to an event stretching over a period of time in which the trapped particles have performed a large number of axial oscillations. It is first investigated how the particles are affected by fast potential changes. Section 3.3 (page 41) will then introduce the CPET electronics and describe how the switching process can be slowed down. Two non-realistic extreme switching modes are described next to illustrate the energetic impact of different stepsizes on the trapped particles. Both transfer a trapped particle bunch over the same distance Δx. The optimal switching mode lies in between.

The voltage of the electrodes which form the trapping potential is switched fast and in one step from one value to another. The average position of the particle bunch has shifted by Δx. The heating inflicted by this switching mode is maximal resulting in an unefficient cooling process. The switching might even result in a loss of coolant if particles gain enough energy that the potential barrier no longer provides confinement.

The second mode consists of an infinite number of infinitesimal small and fast potential changes. This mode is comparable to one slow potential change

---

[1]When confining electrons, the electrode potential has to be negative. Closing or raising a trap gate therefore also means lowering the applied potential.
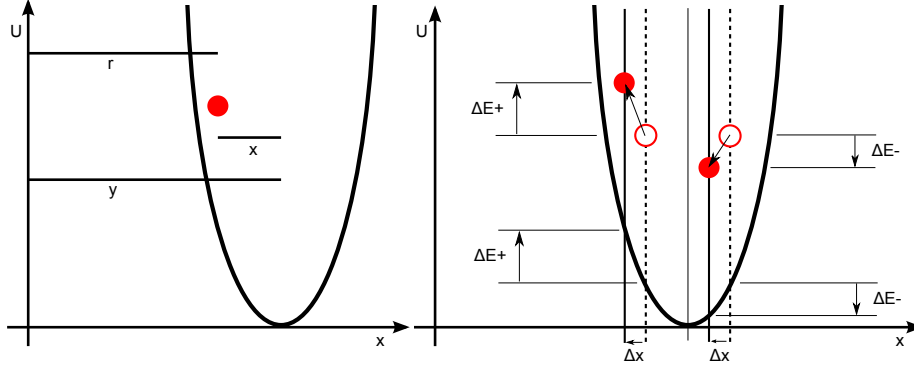
Figure 2.2: Sketch of a particle in a moving harmonic potential. The position of the centre of the potential is $y(t) = vt$, where v is the speed of the potential, leading to a position of the particle of $r(t) = y(t) - x(t)$ (left). The right figure shows the energy gain or loss for a particle being at position x and $-x$ in the potential, when the potential is undergoing a movement step of Δx.

and does not affect the energy of the trapped particles. This switching mode is called adiabatic switching. The process of shifting particles along the trap axis without introducing heat is called adiabatic transfer of particles. Although only an ideal switching process can be adiabatic, in the following the meaning of adiabatic switching behaviour will be minimized inflicted heating.

This chapter is concerned with establishing the values of timing and voltage step sizes causing the least amount of energy gain of the trapped particle bunch. First, a statistical approach is presented. This approach is based on an instantaneous movement ($\Delta t_{\text{rise}} = 0$), which is not physically possible but was chosen because it inflicts the theoretical maximum of energy gain.

No interaction between particles is assumed, which allows to investigate single particles of the particle bunch. The following calculations and simulations are based on a single particle trapped in a harmonic potential, as shown in Fig. 2.2. The probability distribution of a particle in a 1D potential is given by

$$\rho(x) = \frac{1}{\pi} \frac{1}{\sqrt{A^2 - x^2}} \tag{2.1}$$

with a standard deviation of

$$\sigma_x = \sqrt{<x^2> - <x>^2} = \sqrt{<x^2>} \tag{2.2}$$

with

$$<x^2> = \int_{-A}^{A} x^2 \rho(x) \, dx \tag{2.3}$$

and where A is the amplitude of the particle's oscillation, which is related to its initial energy (see Fig. 2.3).
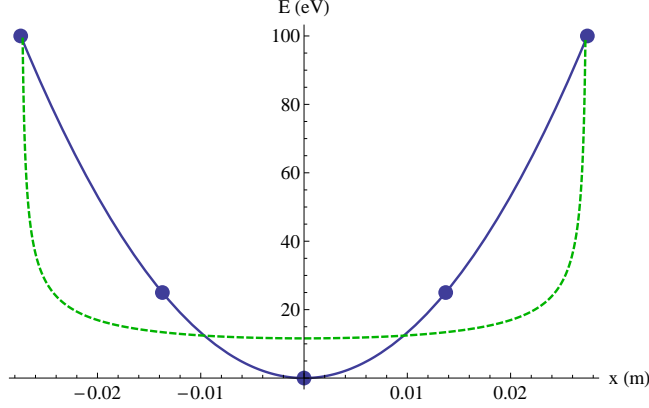
Figure 2.3: Harmonic potential (blue, solid line) and probability distribution (green, dashed) of a particle within it. The blue points are potential values which were used to interpolate the potential function.

Moving the potential $U(x)$ (and thus the particle's average position) by $\pm\Delta x$ (in one step) leads the particle to either gain energy ΔE_+:

$$\Delta E_+ = U(-(\sigma_x + \Delta x)) - U(-\sigma_x) \tag{2.4}$$

or lose energy ΔE_-:

$$\Delta E_- = U(\sigma_x - \Delta x) - U(\sigma_x) \ . \tag{2.5}$$

As an example the harmonic potential function

$$U(x) = \frac{1}{2e} \, k \, x^2 \tag{2.6}$$

is used with a spring constant of

$$k = \frac{2e100V}{(2d)^2} = 4.26 \times 10^{-32} \ \text{Nm}_\text{e} \tag{2.7}$$

and respectively

$$\omega^2 = \frac{k}{m_e} = 0.0468 \ \frac{\text{N}}{\text{m kg}} \ . \tag{2.8}$$

The values of Eq. (2.6) to (2.8) were derived from real CPET geometry data and will be discussed in detail in Section 2.3 (page 25).

As an example, an electron with a kinetic energy of 500 eV in the harmonic potential (2.6) is investigated. Based on the Eq. (2.4) and (2.5), the gain or loss of the particle's energy can be calculated. On average, if the movement of the potential is small compared to the amplitude, a particle on one side of the potential will gain potential energy, whereas a particle on the other side will lose

Table 2.1: Overview of the relation of amplitude A of electrons with an energy E_e in the harmonic potential (2.6), the number of potential switching operations N needed in order to shift the potential over a length of $L = 30$ cm and keep $\Delta x \leq A$, the resulting time between switching steps $\Delta t = T/N$ with $T = 100$ μs and the switching frequency $f = 1/\Delta t$.

E_e (eV)	A (cm)	N	Δt (ns)	f (kHz)
0.1	0.09	346	289.2	3458
1	0.27	109	914.4	1094
10	0.87	35	2891.6	346
100	2.74	11	9144	109

potential energy, depending on the direction in which the potential is moving. A fast movement (in this case it is instantaneous) of the potential by a distance equal to 10% of the particle's amplitude is compared with two jumps of 5%:

$$\Delta E_+(10\%) \;=\; 75.7\text{eV} \tag{2.9}$$
$$\Delta E_-(10\%) \;=\; -65.7\text{eV} \tag{2.10}$$
$$\Delta E_{++}(5\%) \;=\; 37.9\text{eV} \tag{2.11}$$
$$\Delta E_{--}(5\%) \;=\; -32.9\text{eV} \tag{2.12}$$

For a potential movement of 150% of the amplitude one gets:

$$\Delta E_+(150\%) \;=\; 2185.7\text{eV} \tag{2.13}$$
$$\Delta E_-(150\%) \;=\; 64.3\text{eV} \tag{2.14}$$

The above calculations show that when performing the movement, the energy gain of trapped particles is always larger than the energy loss, resulting in an average gain of kinetic energy for a large number of trapped particles. The energy gain introduced in the two 5%-jumps is less than in the single 10%-jump, leading to a statement that smaller switching steps are causing less energy gain. The potential movement of 150% of the particles amplitude shows an energy gain in both cases and an energy spread, which is two orders of magnitude larger than in the 10% case. It is assumed and further investigated in the next section, that the heating dramatically increases when the size of one movement step is equal to or larger than the amplitude.

Next, the desired electrode switching frequency for transferring electrons is derived. Electrons trapped in the harmonic potential are to be transferred from one side of the Penning trap to the other, which is taken to be a distance of $L = 30$ cm. The calculation is based on the operation cycle discussed in Section 2.1 (page 19). It presents a time-scale for switching processes of 100 ms to 1 s. The time for the shift of the potential over the entire 30 cm length is set to a much shorter value of $T = 100$ μs. This will allow for some hundreds of operations, which are required by some injection methods and give leeway for future improvements of the cooling process.

Table 2.1 shows the amplitude A of the particle in the harmonic potential (2.6), corresponding to the initial energy $E = U(A)$. As one potential movement step should not be larger than the length of A, the number of operations $N = L/A$ will be required to shift the potential over the whole length of L. As the entire operation should be performed in a time T and we assume equal time, one switching operation has to be performed every $\Delta t = T/N$. This leads to a switching frequency of $f = 1/\Delta t$.

For CPET, electrons with kinetic energy on the order of 10 eV will initially enter the trap. The statistical approach therefore suggests switching steps of $\Delta x \approx 0.9$ cm every $\Delta t \approx 3000$ ns, leading to a switching frequency of about $f \approx 300$ Hz.

2.3 1D Simulations

The magnetic field in CPET traps the electrons and ions radially, so the axial trapping (using potentials applied to the trap electrodes) can therefore be simplified to a one dimensional problem. In this Section a 1D simulation of different switching scenarios is presented. Mathematica [49] was used to solve the differential equation for a particle in a moving harmonic potential. A step function was used to simulate the switching of the electrodes from one potential set to another. Different step sizes and frequencies are tested with respect to their heating effect.

2.3.1 Electron motion in a switched potential

A simple harmonic potential

$$U(x) = \frac{1}{2e} k x^2 \tag{2.15}$$

is designed using five CPET electrodes at 100, 25, 0, 25, and 100 V (see Fig. 2.3). The length of a CPET electrode, including the distance to the neighbour electrode, is $d \approx 1.37$ cm. For simplicity it is assumed that the electric field in the centre of each electrode matches the electrode's potential and is not influenced by the potential of the neighbour electrodes. This simplification leads to an underestimation of the actual potential. The simplified potential is compared to the real potential in the 3D simulations chapter (see Fig. 2.10, page 33, discussed later). The potential dependent spring constant

$$k = \frac{2e \cdot 100V}{(2d)^2} = 4.26 \times 10^{-32} \ \mathrm{Nm_e} \tag{2.16}$$

can then be derived in SI units simply by using the $x = 2d$, $U = 100$ V data point (see Fig. 2.3). It follows that

$$\omega^2 = \frac{k}{m_e} = 0.0468 \ \frac{\mathrm{N}}{\mathrm{m \ kg}} \ . \tag{2.17}$$

The Lagrange equation of the particle in the moving potential is:

$$L \quad = \quad \frac{1}{2}m(\dot{y} - \dot{x})^2 - \frac{1}{2}kx^2 \tag{2.18}$$

$$y(t) \quad = \quad vt \tag{2.19}$$

$$r(t) \quad = \quad y(t) - x(t) \tag{2.20}$$

This leads to the equations of motion for the particle:

$$\frac{\partial L}{\partial \dot{x}} \quad = \quad -m(\dot{y} - \dot{x}) \tag{2.21}$$

$$\frac{\partial L}{\partial x} \quad = \quad -kx \tag{2.22}$$

$$0 \quad = \quad -kx + m(\ddot{y} - \ddot{x}) \tag{2.23}$$

$$\ddot{x} \quad = \quad -kx \tag{2.24}$$

$$\ddot{r} \quad = \quad -k(r - y) \tag{2.25}$$

The total energy of the particle is given by:

$$E \quad = \quad T + V \tag{2.26}$$

$$= \quad \frac{1}{2}m\dot{r}^2 + \frac{1}{2}kx^2 \tag{2.27}$$

$$= \quad \frac{1}{2}m\dot{r}^2 + \frac{1}{2}k(y(t) - r)^2 \tag{2.28}$$

For the movement of the potential, the step function

$$y(t) = \left\lfloor \frac{t}{\Delta t} \right\rfloor \Delta t \tag{2.29}$$

was used, where Δt is the time step size.

Mathematica was used to solve Eq. (2.25). A function was written which outputs the maximum energy of a trapped particle after a specific amount of switching steps. The initial energy of the particle E, the number of switching steps N and the total time T are input into the function. The same initial values as in the last section are used. The Mathematica code can be found in Section B.1 (page 74).

By performing this simulation, two different regions are investigated. As stated previously, it is tested if the potential movement steps should be smaller than the particles' amplitude. As the amplitude changes with every step, the initial amplitude A is used as a reference point. The energy gain of the particle was investigated in two different cases. First, the step size Δx was varied in relation to the initial amplitude of the particle in the potential. Second, the "speed" ($\Delta t/\Delta x$) of the potential was varied over a range close to the speed of the particle.
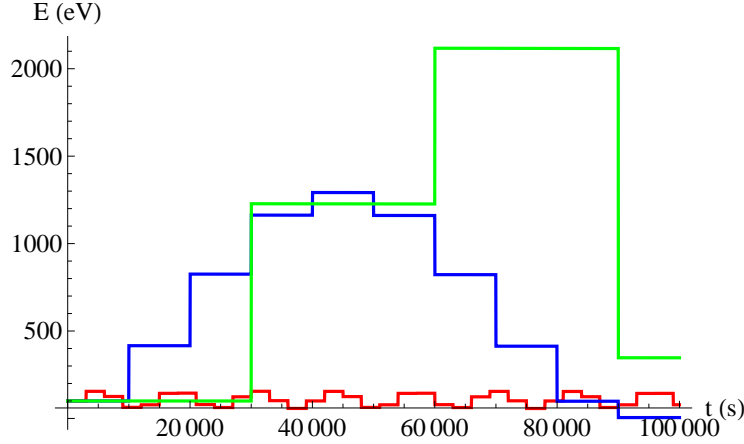
Figure 2.4: Simulated total energy as a function of time of a trapped electron in a harmonic potential undergoing potential jumps of $\Delta x = 0.9$ cm (red, 33 jumps), 3 cm (blue, 9), 9 cm (green, 3). The initial energy of the electron in all three cases is 100 eV.

2.3.2   Jump size and amplitude dependency of the energy gain

A result of how the particle's energy changes over time is shown in Fig. 2.4. An electron with 100 eV kinetic energy[2] is put into the harmonic potential.   The electron starts at a random position inside the potential with a random initial velocity[3].

The potential is shifted over the length of $L = 30$ cm in 100 μs, in three (green), nine (blue), and 33 (red) steps. The initial amplitude of every electron is $A \approx 2.7$ cm, based on the initial energy. The potential jump sizes are listed in Table 2.2. It can be seen that the maximum energy gain rises non linearly with $\Delta x/A$. This is further investigated.

From Fig. 2.4 it can be seen, that the energy does not rise infinitively. There is a potential, initial energy and step size dependent frequency, which makes the total energy oscillate over time. This frequency is due to the time dependence of the Lagrangian and can also be observed when the potential is moved linearly (Eq. (2.29) replaced by the linear function $y(t) = t$). In the linear case the amplitude of this frequency is on the order of A.

The dependence of the energy gain on $\Delta x/A$ is further investigated by running the described Mathematica function for different initial electron energies E, step sizes Δt and total shifting times T. Every result is derived from a mean over n = 2500 runs (see Fig. 2.5), where the initial electron (total) energy is fixed

---

[2]As the relation of step size and Amplitude is investigated, this Energy can be chosen arbitrarily for this example.

[3]The electrons position in the potential and its total energy specify the absolute value of the velocity but the orientation of the velocity vector is chosen randomly.

Table 2.2: Simulated maximum total energy E_{max} of an electron in the harmonic potential Eq. (2.15) after three different switching processes (see also Fig. 2.4). The initially electron energy is 100 eV, oscillating with an amplitude A. The switching processes consist each of N switching steps, shifting the potential over a length of Δx every Δt μs. The resulting potential jump to initial amplitude ratio is shown in column $\Delta x/A$.

Δt (μs)	N	Δx (cm)	A (cm)	$\Delta x/A$	E_{max} (eV)	graph color
30	3	9	2.7	333.33%	2100	green
10	9	3	2.7	111.11%	1300	blue
3	33	0.9	2.7	33.33%	150	red
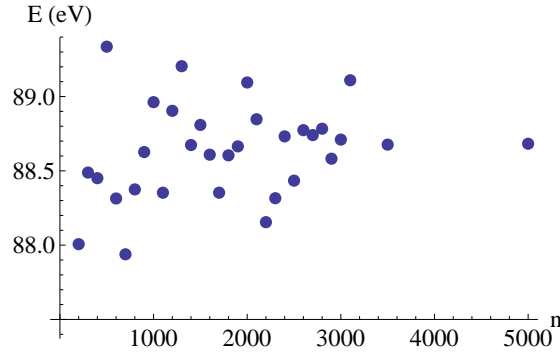
Figure 2.5: Simulated maximum energy E of an electron with 1 eV kinetic starting energy after $N = 10$ jumps in $T = 10$ μs. E is an average over n simulations. The value of E stabilizes at around $E = 88.6$ eV for a large number of runs and the deviation the results from this value decreases with increasing n.

and its position and velocity direction are chosen randomly. The magnitude of the velocity depends on the position of the particle in the harmonic potential. The number of n = 2500 was chosen to achieve a stable result with an adequate simulation time of about 40 min.

An example call of the Mathematica function looks like:

```
FindMaxEnergyAvg[stepsize, totaltime, starting energy, iterations]
FindMaxEnergyAvg[10, 2420, 100, 2500]
```

Fig. 2.6 shows the power dependence of the energy gain ΔE on the jump size divided by the amplitude $\Delta x/A$. The region with a ratio ≤ 1 shows energy gain limited to the order of the initial energy and is identified as adiabatic region. This meets the previous assumption that the size of the potential jump should be smaller than the amplitude of the particle. It can also be observed that electrons with a higher starting energy gain more energy for the same jump size to amplitude ratio. The data was fit using a power function.
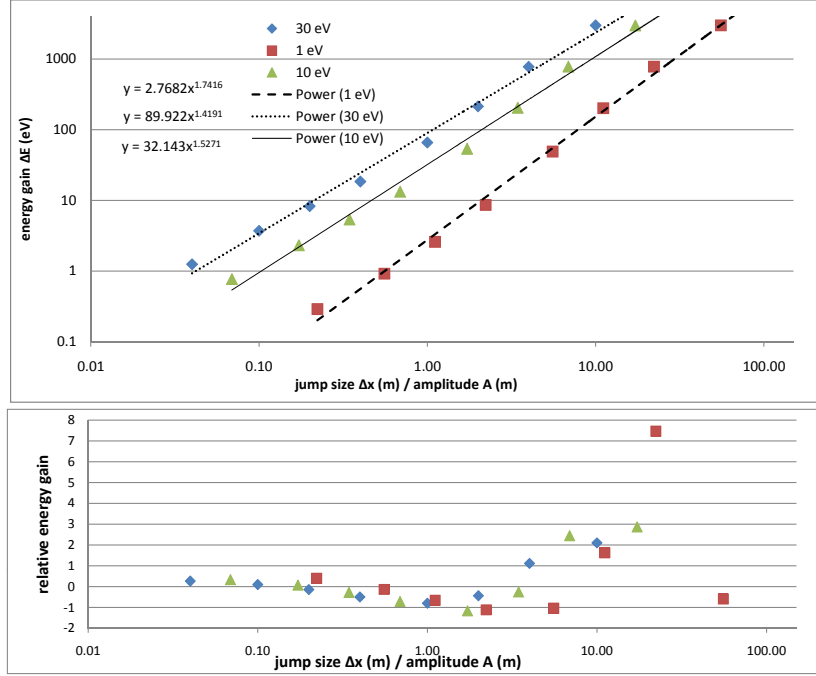
Figure 2.6: Simulated energy gain (ΔE) as a function of jump size divided by amplitude ($\Delta x/A$) plotted in a logarithmic scale (upper plot). The amplitude A is constant and determined by the starting energy of the electron E, the step size Δx is varied. The bottom plot shows the energy difference between the data and the fit, normalized by $\Delta x/A$ and E.

A systematic effect can be observed in the bottom plot, where the difference between the data and the fit is shown normalized by $\Delta x/A$ and E. The normalized energy gain shows a minimum for $\Delta x/A$ on the order of 1. For a lower starting energy E the minimum shifts towards a higher ratio. This leads to the conclusion that the energy gain does not solely depend on $\Delta x/A$, but also on Δx and A individually. It can be explained by the fact that the electron with $E = 1$ eV oscillates in a shallower region of the harmonic potential, where potential jumps in the order of its amplitude have a smaller effect. The probability distribution of the particle in the potential (see Fig. 2.3) suggests the highest probability for the electron's location to be close to the walls of the potential. A potential jump therefore has the highest probability of transferring the maximum amount of energy to the electron depending on its amplitude.

For a higher jump size to amplitude ratio (past the energy gain minimum) the gradient of the energy gain increases. The region of $\Delta x/A > 20$ was not investigated further as ΔE is on the order of keV in all three cases. Therefore this region is not relevant for the experiment. Also the ΔE results obtained from Mathematica for ratios > 20 were mostly faulty (in the order of eV),
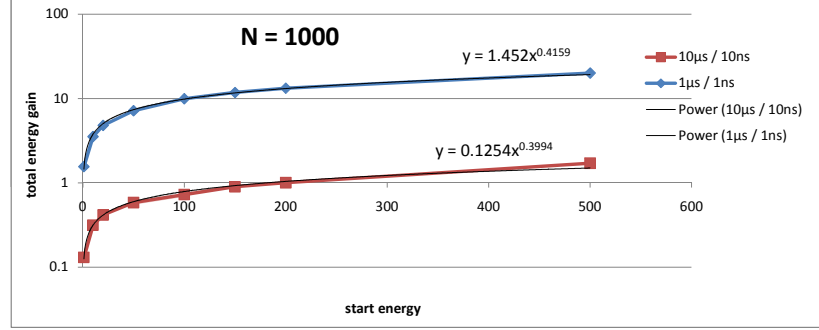
Figure 2.7: Simulated total energy gain as a function of start energy E for two different switching times T and Δt and a fixed number of switching steps of $N = 1000$.

which leads to the conclusion that the step size was too large for the internal numerical ODE[4]solver. The last point in the $E = 1$ eV series at $\Delta x/A = 55$ is therefore considered faulty as well.

In the following, different combinations of total time T, step size Δt, and initial electron energy E were simulated based on the number of switching steps $N = T/\Delta t$ and shown in Fig. 2.7. The energy gain is fitted using a power function and determined to rise approximately like a square root function of the starting energy. Higher starting energy leads to a larger amplitude of the electron in the harmonic potential. The ratio of the amplitude and the constant jump size therefore gets larger, leading to a smaller energy gain, as discussed before. A physical fit function could not be determined and was not found to be crucial for the interpretation of the results.

Fig. 2.8 shows simulation results for a total shifting time of $T = 10000$ ns. The region of $N > 100$ shows a total energy gain in the order of the initial energy. For $N < 100$ the energy gain shows a high increase. A number of $N = 100$ switching steps corresponds to a potential shift of 3 mm.

2.3.3 Velocity dependency of the energy gain

The oscillation frequency of the electron in this potential is:

$$\nu \approx 34.41 \text{ MHz} \tag{2.30}$$

leading to an oscillation period of

$$\frac{1}{\nu} \approx 29.06 \text{ ns} \tag{2.31}$$

When the switching time gets closer to, or even smaller than $1/\nu$, the adiabatic region is left and the energy gain increases dramatically. This behaviour is

---

[4]ordinary differential equation
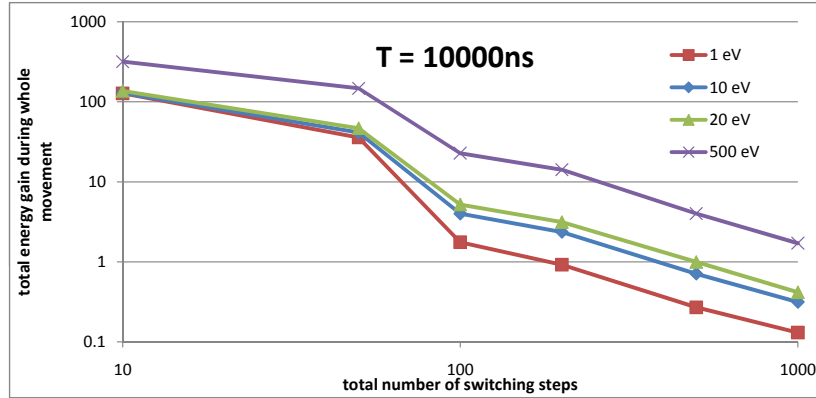
Figure 2.8: Simulated total energy gain over number of switching steps, with $T = 10\mu s$ total time.
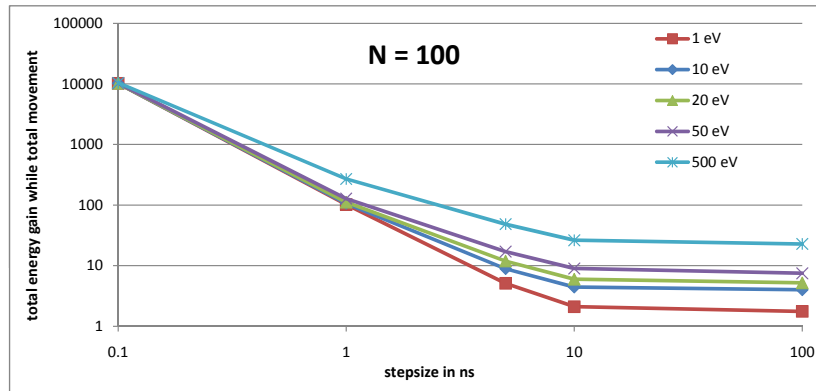
Figure 2.9: Simulated total energy gain over time step size, with $N = 100$ switching steps and $T = 10\ \mu s$ total time.

illustrated in Fig. 2.9, where the total energy gain as a function of switching time is plotted. The adiabatic region is determined to start at a minimum switching time of $\Delta t \approx 10$ ns. Below that value the potential movement gets "faster" than the electron and therefore keeping it on the "left" side of the harmonic potential (refer to Section 2.2, page 21) and a large amount of energy is transferred to it.

The energy gain as a function of step size for $N = 100$ (corresponding to a switch step size of $\Delta x \approx 3$ mm) is plotted in Fig. 2.9. For step sizes greater than 10 ns the energy gain for all starting energies is almost constant. The energy gain is significantly smaller than in the region where the step size is smaller than 10 ns. The same value for a minimal step size of 10 ns was determined for $N = 10$ and $N = 1000$.

Table 2.3 presents selected energy gain simulation results from this chapter.

Table 2.3: Mathematica simulation results. Shown are the times between each switching step Δt, the total switching time T, the number of switching operations N, the total starting energy of the electrons E_{start}, the maximum energy of the electrons obtained during the switching process E_{max}, and the maximum energy gain E_{diff}. All voltages are in (V), times in (μs), and energies in (eV).

Δt	T	N	E_{start}	E_{max}	E_{diff}
0.01	2.42	242	100	104.92	4.92
0.005	1.21	242	100	108.78	8.78
0.01	2.42	242	200	206.76	6.76
0.01	2.41	241	30	32.7	2.7
0.01	1.22	122	30	36.1	6.1
0.01	0.78	78	30	39.7	9.7
0.01	0.58	58	30	43.8	13.8
0.01	0.47	47	30	47.6	17.6
0.01	0.39	39	30	52.3	22.3
0.01	0.33	33	30	57.9	27.9

The same switching scenarios will be redone using a 3D simulation approach (see next Section 2.4).

2.4   3D simulations

A 3D SimIon [50] simulation is set up to investigate the energy gain of the electrodes by switching potentials. SimIon is a charged particle optics simulation software. It is used to simulate the particles trajectory in CPET's electric and magnetic fields. The approach is based on solving the Laplace equation using the Runge-Kutta method with variable-length dynamically adjusting and controllable time-steps. The real CPET SolidWorks [51] model and the magnet manufacturer specifications were imported into the simulation. The resolution of the 3D model after import into SimIon is 1 dot per cubic mm[5]. The resolution of the magnet field map is 1 dot per cubic cm. Mathematica has been used to interpolate the magnetic field map in order to match the resolution of the simulation.

The 1D simulations performed in Section 2.3 are now repeated by applying potentials to different simulated electrodes. As previously, the potential change happens immediately (from one simulation time step to the next). In order to compare the results, the same harmonic potential (see Section 2.3), built of potentials applied to five CPET electrodes, was used. The electrode voltages were 100, 25, 0, 25 and 100 V (compare Fig. 2.10 and Table 2.4). Every other electrode is set to the maximum value (100 V).

---

[5]A value of 1 dot per cubic mm has been chosen as a good trade off between simulation size and computer memory.
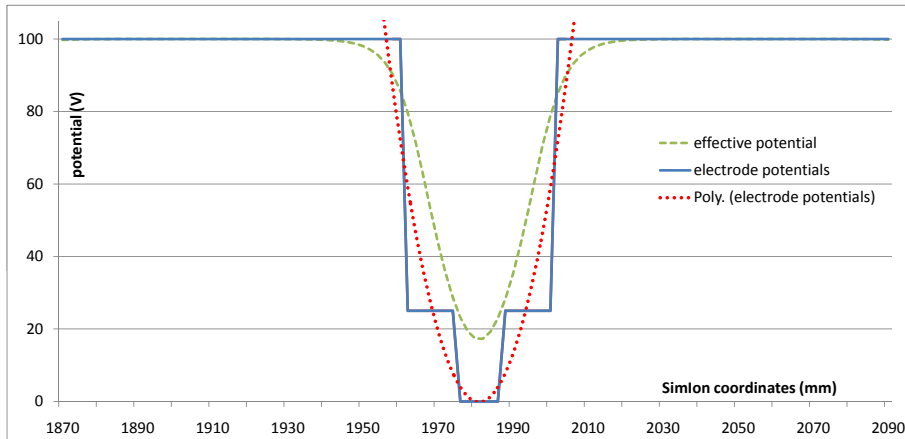
Figure 2.10: Overview of different potentials used in simulations. Potentials applied to CPET electrodes (stepped, blue curve), simple harmonic potential used in 1D simulations (dotted, red) and effective potential as calculated by SimIon (green, dashed curve). The horizontal axis shows simulation coordinates in mm. The vertical axis shows potential in units of V.

As every electrode contributes to the electric field at any point in the trap, the effective electric field at a given point in the trap is more complex than the simple interpolation between electrode potentials used in the 1D simulations chapter. SimIon calculates the effective field at any point in the trap internally. The difference between the harmonic potential used by SimIon and the one assumed previously is shown in Fig. 2.10. The straight blue graph shows the voltage applied to the electrodes. The dotted red graph shows the interpolation used in the 1D simulations. The dashed green graph shows the electric field used by SimIon. The effective potential along the trap axis as determined by SimIon was retrieved by sending a neutral[6] particle along the central trap axis as a probe.

Table 2.4 shows a part of a sample configuration file for the SimIon simulations, which is used to apply potentials to different electrodes at given times. The difference between two consecutive times is the time step size Δt and is always constant in each simulation. The sample dataset in the table shows how the harmonic potential is shifted over the length of one electrode (electrode numbers $28 \rightarrow 29$) in 60 ns and 5 steps (the first 6 lines of data).

The starting parameters of the simulation follow the approach of the 1D simulations. Electrons are randomly positioned in the harmonic potential, which is positioned at one end of the CPET trap. The potential is then moved to the other side of the trap by applying voltages listed in Table 2.4 at given times. Due to software limitations, the amount of electrons per simulation was set to

---

[6]A neutral particle was chosen as a probe since it is not affected by the electrical and magnetic fields of the simulation.

Table 2.4: Sample configuration file for the SimIon simulations. The first line indicates the SimIon internal electrode number. The first row is the time in μs at which the potential set in corresponding line is to be applied to the electrodes.

	22	21	35	36	34	30	29	28	27	26
0.00	100	100	100	100	100	100	25	0	25	100
0.01	100	100	100	100	100	81	16	1	36	100
0.02	100	100	100	100	100	64	9	4	49	100
0.03	100	100	100	100	100	49	4	9	64	100
0.04	100	100	100	100	100	36	1	16	81	100
0.05	100	100	100	100	100	25	0	25	100	100
0.06	100	100	100	100	81	16	1	36	100	100
0.07	100	100	100	100	64	9	4	49	100	100
0.08	100	100	100	100	49	4	9	64	100	100
0.09	100	100	100	100	36	1	16	81	100	100
0.10	100	100	100	100	25	0	25	100	100	100
0.11	100	100	100	81	16	1	36	100	100	100
0.12	100	100	100	64	9	4	49	100	100	100
0.13	100	100	100	49	4	9	64	100	100	100
0.14	100	100	100	36	1	16	81	100	100	100
0.15	100	100	100	25	0	25	100	100	100	100
0.16	100	100	81	16	1	36	100	100	100	100
0.17	100	100	64	9	4	49	100	100	100	100
0.18	100	100	49	4	9	64	100	100	100	100
0.19	100	100	36	1	16	81	100	100	100	100
0.20	100	100	25	0	25	100	100	100	100	100
0.21	100	81	16	1	36	100	100	100	100	100
0.22	100	64	9	4	49	100	100	100	100	100
0.23	100	49	4	9	64	100	100	100	100	100

be n = 35 instead of the previously determined value of n = 2500 .

An example data result of run #28 is plotted in Fig. 2.11 showing the average position of the electron bunch as a function of time. The oscillation of the electron bunch can be observed as well as the potential shift. Fig. 2.12 shows the average energy of the electrons as a function of time. Energy oscillations as discussed in the previous chapter can be observed as well as an overall energy gain. The average of the maximum total energy of the electrons during the run was determined and is presented in Table 2.5. It is compared with the results from the 1D simulations. The results are in the same order of magnitude. Also it is found, that the values for the 1D simulation the energy gains are between 35% and 55% of the energy gain values of the 3D simulation. The only exception being run #33, where the value is 1% larger. This seems to indicate a systematic error and that the previous approach of reducing the given problem to a 1D scenario is legitimate.

The difference of the results between the 1D and 3D simulations can be
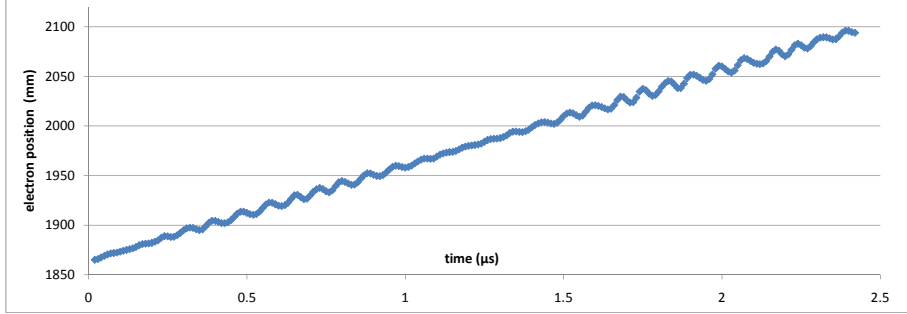
Figure 2.11: Simulation results for SimIon run #28. The plot displays the average position of a trapped electron bunch as a function of time. The vertical axis is defined by the SimIon coordinate system.
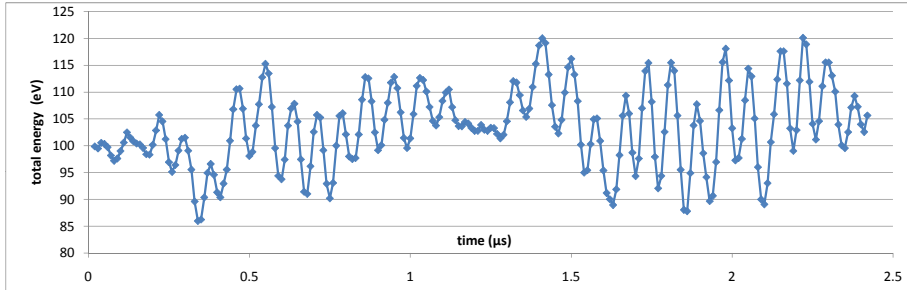
Figure 2.12: Simulation results for SimIon run #28. The plot displays the mean total energy of a trapped electron bunch as a function of time.

Table 2.5: SimIon (3D) simulation results and compares them with the Mathematica results (1D). All voltages are in (V), times in (μs) and energies in (eV).

run #	$V_{\max}$	Δt	T	N	E_{init}	$E_{\max}$	$E_{\mathrm{diff\_3D}}$	$E_{\mathrm{diff\_1D}}$
28	400	0.01	2.42	242	100	120.1	20.1	
29	400	0.005	1.21	242	100	109.3	9.3	
30	400	0.01	2.42	242	200	225.1	25.1	
32	100	0.01	2.41	241	30	34.1	4.1	2.7
31	100	0.01	1.22	122	30	34.0	4.0	6.1
33	100	0.01	0.78	78	30	39.6	9.6	9.7
34	100	0.01	0.58	58	30	61.6	31.6	13.8
35	100	0.01	0.47	47	30	59.2	29.2	17.6
36	100	0.01	0.39	39	30	66.6	36.6	22.3
37	100	0.01	0.33	33	30	80.6	50.6	27.9

attributed to a number of factors. The 3D simulation derives an average over only 35 random start positions instead of 2500, leading to a higher statistical error (compare Fig. 2.5, page 28 in the 1D simulation chapter).

As shown in Fig. 2.10, the potential function is derived differently for the 1D simulations, leading to a slightly broader and deeper potential and is therefore a source of systematic error.

In order for the SimIon simulation to run efficiently fast, the simulation time step size has been set to a rather large value (SimIon time step quality value = 0). Therefore, the electron "loses" energy over time, as the Runge-Kutta method becomes less precise. This effect becomes critical when simulating (long) switching processes of hundreds of milliseconds, where this type of "energy loss" was observed to be in the order of eV. This behavior is also observed in the Mathematica simulations, as it also solves the differential equations numerically. It does not have much of an effect when the total time T is on the order of μs, as was used in the simulations.

The theta-function like switching steps, which are used in both simulations, cause non adiabatic results by previous definition. The presented numbers are therefore assumed to present a maximum energy gain for the corresponding switching mode. Real power supplies that will drive the trap electrodes will not switch from one potential value to another instantaneously but have a specific slower rise time. The energy gain of the electrons is for this reason assumed to be less in a real environment. Therefore Table 2.5 does not contain any error values, but aims at providing only a qualitative overview of energy gains in different switching modes.

2.5   Simulation summary

It was found in simulations that a number of $N = 100$ switching steps (corresponding to a potential jump of $\Delta x = 3$ mm) limits the energy gain of the electrons to the order of eV, in the presented switching processes. For real CPET applications it will be possible to develop a programmable power supply, equipped with an internal memory large enough to store a few thousand data points. This would allow one to achieve roughly up to 50 switching processes similar to the ones presented to be realized. This makes potential jumps of $\Delta x = 3$ mm a good trade off between energy gain of the electrons and the number of data points to be stored in the amplifier.

The step size Δt should not be shorter than 10 ns to keep the energy gain within the adiabatic region. The programmable power supply should therefore allow potential changes on the order of 10 ns between two voltage settings. The capabilities of a prototype amplifier, similar to the one that will be built is tested in Chapter 3 (page 41).
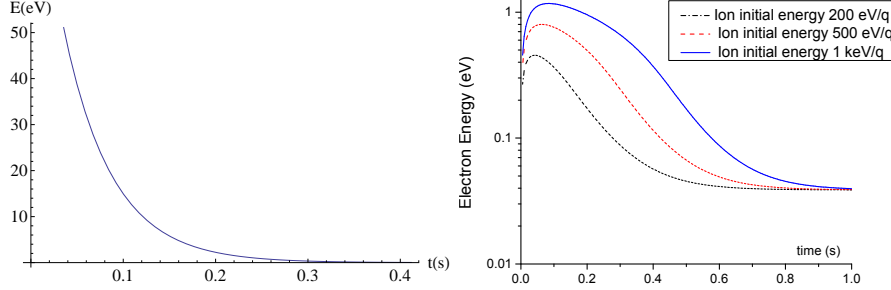
Figure 2.13: Calculated electron energy loss in B=7 T CPET magnetic field
as a function of time for an $E = 30$ eV electron (left). The energy loss has a
cooling effect, due to the exponential dependence of the radiation on the energy
of the particle. Energy evolution of electrons with different initial Kr^{36+} energy
during electron-Kr^{36+} cooling process (right) [15].

2.6 Timescale of synchrotron radiation for electrons in CPET

In this chapter it is investigated how synchrotron radiation plays a role on the
timescale of CPET operations. The CPET magnet provides a magnetic field
strength in the region of

$$B \approx 7 \ T \ . \tag{2.32}$$

The energy of electrons in this field can be calculated as a function of time as
[15, 39]

$$E = E_0^{-\gamma t} \tag{2.33}$$

with

$$\gamma = \frac{e^2 \omega^2}{3\pi\epsilon_0 m c^3} \tag{2.34}$$

and

$$\omega = \frac{eB}{m} \ . \tag{2.35}$$

Based on the previously determined switching parameters ($N = 100 \rightarrow \Delta x$
= 3 mm, $T = 10 \ \mu$s), the energy gain of the electrons during the described
switching process will be in the order of eV. A typical kinetic energy of electrons
entering CPET will be $E_{kin} \approx 10$ to 30 eV. As an example an electron with an
initial energy of 30 eV is taken, which gained 5 eV during the switching process.
It takes $\approx 8000 \ \mu$s to cool a 35 eV electron back down to 30 eV according
to Eq. (2.33)-(2.35). When increasing the number of switching steps to N
= 1000 (therefore doing $\Delta x = 0.3$ mm steps in $T = 10 \ \mu$s), the energy gain
due to switching would be on the order of 0.1 eV. The synchrotron radiation
cooling process would still take $\approx 800 \ \mu$s to cool a 30.5 eV electron down to
30 eV. It is clearly visible, that synchrotron radiation cannot compensate for
the switching energy gain immediately. Waiting periods of some hundreds of

μs can be introduced between steps of the cooling cycle in order to allow the electrons to cool. The timescale for the electron injection (see the point 1 and 2 in the proposed operation cycle in Section 2.1, page 19) has therefore be envisioned to be on the order of 100 ms to seconds.

The starting temperature of electrons for the HCI cooling process is taken to be 0.04 eV ($\approx$ 300 K) [15]. It is determined that an electron with a kinetic energy of 30 eV will need 0.4 s to cool down to 0.04 eV in a 7 T B-field (see also Fig. 2.13 (left). The second step in the operation cycle is therefore planned to last 100 ms to seconds. This enables the electrons to cool down sufficiently.

Electrons will also gain large amounts of energy due to collisions with HCI during the electron-HCI cooling process. This process of cooling down HCI from a few hundred eV to a few eV was investigated [15] to happen on a 100 ms to second timescale, so that collisional energy gain is compensated by synchrotron radiation cooling (see Fig. 2.13 (right)).

Chapter 3

Amplifier/ electrode driver tests

This chapter gives an overview of the cooler Penning trap electronics. An arbitrarily programmable power supply similar to the one to be used at CPET was investigated. The supply is referred to as an amplifier as it consists of a DAC[1] whose output voltage is further amplified[2]. The minimum (respectively the maximum) voltage output of the DAC results in a -200 V (200 V) output of the used amplifier. The performance of the amplifier was tested in stand alone mode as well as attached to the assembled CPET trap structure.

3.1   The cooler Penning trap electronics

The CPET electronics system will use fast bi-level HV switches and programmable amplifiers. The switches drive the drift tubes and the trap gate electrodes. The trap gates have to be switched fast to close the trap once the ions have entered to confine them inside. The drift tubes can be switched between two different voltage settings depending on the type of particles travelling through (e.g. the highly charged ions will exit the trap on the side where the electrons are injected).

The amplifiers will be arbitrarily programmable to supply 0 to 200 V. All amplifier channels will be floated together on a 2 kV platform, which matches the 2 kV potential energy that is given to the ions from the EBIT. This is as fluctuations of the platform voltage will affect every channel in the same way and will not cause potential fluctuations across channels.

In order to shape different potentials in the trap (e.g. for loading and extraction processes or to set up nested potentials) the amplifier has to be programmed to apply different potentials to the trap electrodes at given times (see also the

---

[1]A digital analogue converter. The DAC converts a digital signal (e.g. 16 bit) into and analogue signal (e.g. 0 - 5 V full scale)

[2]For the amplification process a unit like the Cirrus Logic Inc. PA78DK can be used.
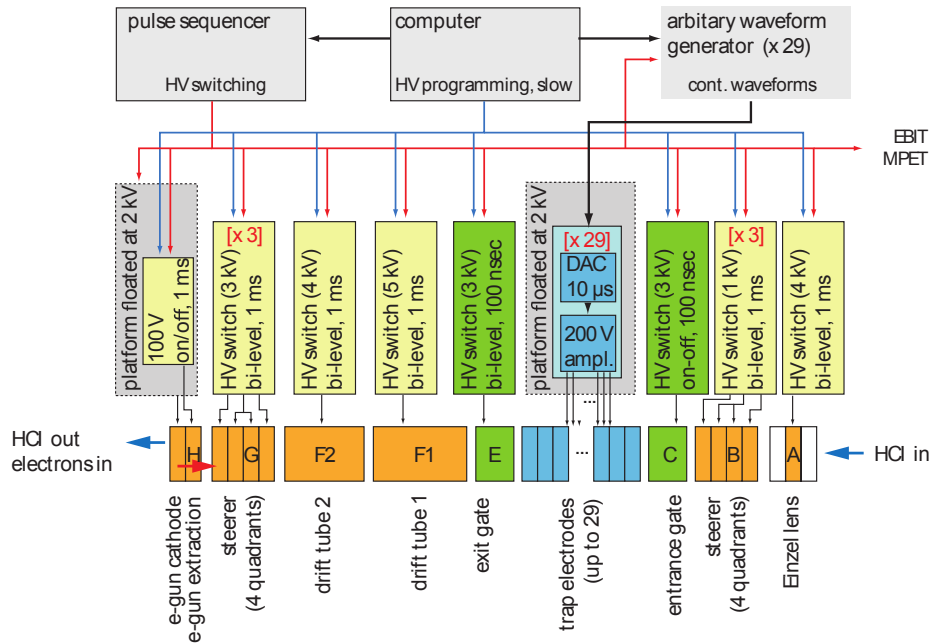
Figure 3.1: Sketch of CPET electrical layout taken from [18]. The figure shows the trap structure and the connected switches and amplifiers. The drift tubes will support two different voltage settings and are supplied by bi-level Behlke HV-switches. The trap electrodes will be floated on a 2 kV platform, additional 0 to 200 V are supplied by arbitrarily programmable switches. The switches and amplifiers are configured and triggered using AWG's and programmable pulse generators (PPG's).

schematic of the operation cycle shown in Fig. 2.1 (page 20)). A dataset to be uploaded into the amplifier can look like Table 2.4 (page 34). One column is applied to an amplifier channel and the timing is the first column is provided externally by a PPG. Based on previous simulations in Chapter 2 (page 36) it was determined that the amplifier should support storage of several thousand data points. It was also found that it should support signal rise times of 100 ns to several μs.

Switches and amplifiers will be controlled using the MIDAS [52] Data Acquisition Package.

3.2   Description of the measurement tools

In this section, the signal rise time of a prototype amplifier similar to the one planned to be used at CPET is investigated. The amplifier is first investigated in stand-alone mode with a dummy load and later connected to the CPET assembly, to investigate its behaviour with the attached capacity of the electrodes

and potential crosstalk of the trap.

The amplifier used for the tests is a GSI[3] bipolar amplifier[4] [53] similar to the ones used at HITRAP[5], which can deliver -200 V to 200 V in two operating modes. It can either be used as a switch, to switch between two preset voltages within the above mentioned range, or to switch sequentially between 40 preprogrammed voltage points. The configuration of the amplifier is done using LabVIEW [54] and the GSI CSframework [55]. The CS framework is a Lab-VIEW based control system framework for experiments. The GSI-HVSwitch2 class enables communication with the amplifier. User defined applications can be programmed in LabVIEW based on it.

The following equipment is used to perform the measurements:

- GSI amplifier box providing 6 individual amplifier units

- Agilent 33250A Arbitrary Waveform Generator (AWG) as external trigger for the amplifier

- Tektronix TDS2024C oscilloscope

- Signal cable length: 50 cm (All cables used in this chapter are RG59 [56] coaxial cables.)

- Tek P6134C - 10MΩ 10x probe with additional 50 cm of cable

3.3 Investigation of the signal shape and rise time

This subsection is determined to provide a qualitative overview of the amplifier signal output.

The experimental setup is shown in Fig. 3.2. An oscilloscope is connected to the output of an amplifier channel using a 10x probe. No additional serial resistor ($R_s = 0$ Ω) has been added to the output of the amplifier (but will be introduced later). The output of the amplifier is switched from a voltage U_{start} to a voltage U_{final}. These values are defined using the Labview interface and will be called setpoint values. The resulting output signal is investigated. Unless specified otherwise, the term "voltage difference" will refer to $U_{\mathrm{diff}} = |U_{\mathrm{final}} - U_{\mathrm{start}}|$.

Comments and definitions concerning the measurements in this section:

- Rise time - The time the signal needs to get from 0% (U_{start}) to 100% (U_{final}), determined on the fly on the scope screen by eye. Later, a different convention for rise time is used.

---

[3]GSI Helmholtzzentrum für Schwerionenforschung GmbH, Planckstr. 1, D-64291 Darmstadt, Germany

[4]Switchable programmable Powersupply (SPPS)/ HITRAP Fallenspannungsversorung (HFSV)

[5]http://www.gsi.de/forschung/ap/projects/hitrap/
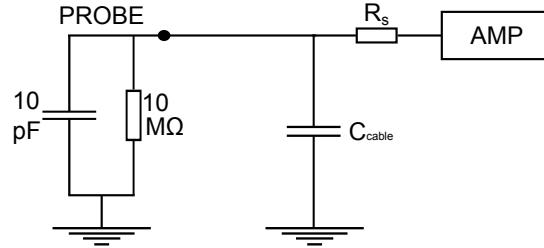
Figure 3.2: Schematic circuit diagram of a probe and oscilloscope (OSC) connected to the output of the amplifier (AMP) using a serial resistor and a cable. The serial resistor and the cable's capacity form an RC circuit.
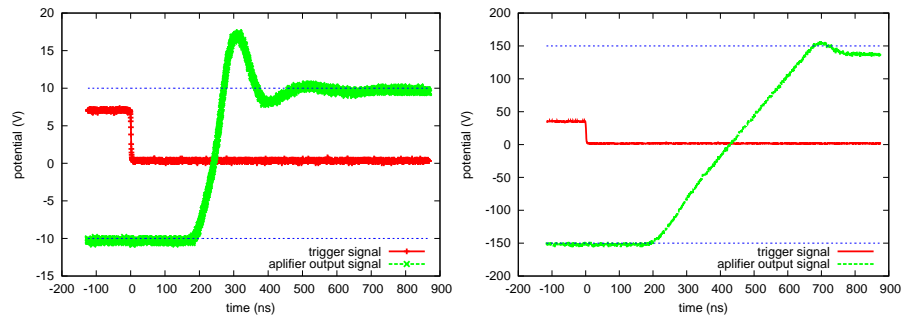
Figure 3.3: Measured amplifier signal rising slope from -10 V to 10 V (left) and -150 V to 150 V (right). CH1 (red) is the AWG signal at 5 Hz, CH2 (green) is the amplifier output signal. The blue dashed lines are the set values.

- Overshoot - The percentage of signal overshoot compared to the 100% signal (determined on the oscilloscope screen).

- Total time - Time between start of the rise and the signal hitting the 100% line for the 3rd time (after the second oscillation maximum).

Two sample output signals of the amplifier are presented in Fig. 3.3. It can be seen that the signal has a large overshoot for small voltage differences (left). The signal rises from -10 V to 10 V, then rises further up to about 17.4 V (7.4 V/20 V $\approx$ 37% overshoot) and starts to oscillate around its final value of 10 V until it eventually stabilizes. For the second signal it can also be observed that the setpoints are not satisfied. The signal rises from $U_{\text{start}} \approx$ -156 V to $U_{\text{final}} \approx$ 138 V with $U_{\text{diff}} \approx$ 294 V. This behaviour can be compensated by modifying the setpoint value, so that the output of the amplifier matches the desired voltage. The maximum signal is 158 V. The absolute signal overshoot is larger and the relative signal overshoot 20 V/294 V $\approx$ 7% is smaller.

The signal shows fluctuations (see Fig. 3.4) of $\approx$0.6 V for the -10 V (left) and $\approx$4 V for the -150 V signal (right).
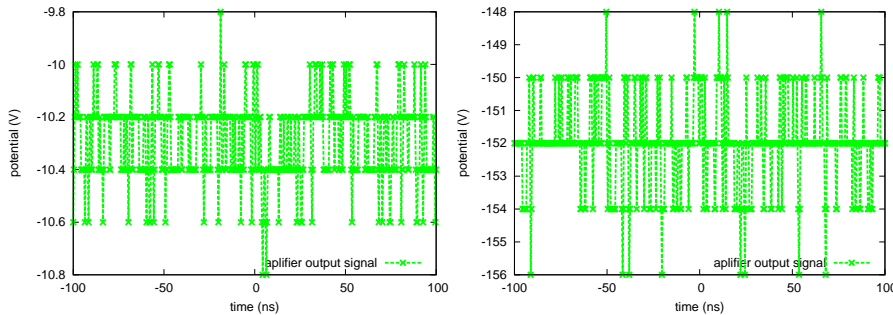
Figure 3.4: Measured amplifier voltage stability for -10 V (left) and -150 V (right). The lines are connected for better visibility only.

The delay between the AWG and amplifier output signal change is always ≈ 200 ns. Rising and falling slopes appear to be linear for higher voltage differences.

The following measurements were then performed next:

1. Switching from -10 to 10 V at 5 Hz, 50 Hz, 500 Hz, 5 kHz and 50 kHz determined the signal to be stable throughout the full range of frequencies needed for the switching process. No signal change could be observed on the oscilloscope while increasing the frequency.

2. Measurement (1) was redone for a larger voltage difference of -150 to 150 V. The signal also remained stable at higher frequencies.

3. Switch at a low rate of 5 Hz from $-x$ to x V with $x = 10, 20, 30, 50, 70, 100, 150$. The signal overshoot and the rise times were investigated for the listed negative to positive potential changes. It was sufficient to perform this measurement for a low frequency of 5 Hz, as the amplifier signal had already been determined to be stable at higher frequencies.

4. Redo (3) with the same voltage differences but only for positive voltages (switch from 0 V to 2x V). Compare the rise times to the results of (3).

5. Investigation of signal falling time.

Measurements (1) and (2) do not show any signal changes on the oscilloscope screen for applying switching frequencies from 5 Hz up to a few kHz. Results of the measurement series (3) and (4) are presented in Fig. 3.5 and determine the amplifier's rise time to be about 300 ns for small voltages and to have a signal overshoot of about 35% of the signal size. The rise time increased to 700 ns for large voltage jumps, where the overshoot almost disappears. The following difference is observed between measurements (3) and (4). For small voltage differences, the rise time is a bit shorter for unipolar positive jumps whereas for larger voltage differences the total time increases. It was also observed that the falling time is faster than the rise time. A 10 V to -10 V jump only took 70
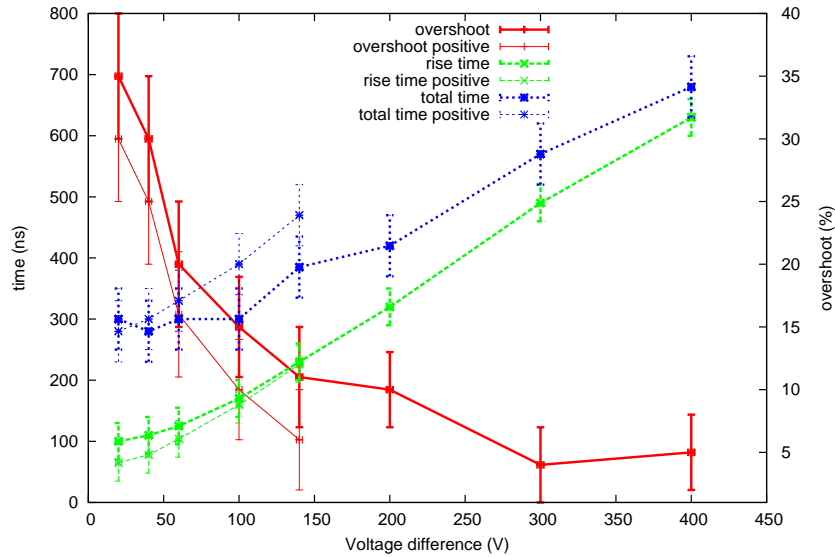
Figure 3.5: Measured signal rise times and overshoot as a function of voltage difference. Results of measurement (3) and (4). Shown is the overshoot (red, solid line), the rise time (green, dashed), and the total time (blue, dotted). The thick lines indicate measurements (3), potential jumps from negative to positive voltages. The thin lines (only possible to measure up to a voltage difference of 200 V) indicate measurements (4) with only positive potential jumps. The lines are connected for better visibility only.

ns for falling compared to 100 ns for rising. Errors are caused by the manual determination of the values from the oscilloscope screen. This method was chosen in order to get an qualitative overview of the amplifier signal output in a short time. Later on Gnuplot[6] will be used to analyse oscilloscope output data.

Being on the order of 100 ns the rise time of the amplifier signal meets the previously mentioned time requirements. The overshoot is considered problematic as it introduces additional energy into the system of trapped particles. In the next part a serial resistor will be added to the signal output of the amplifier in order to decrease back coupling and suppress the signal overshoot. The serial resistor increases the RC circuit oscillation time constant, therefore increases the rise time of the signal and suppresses the overshoot and the signal oscillation.

---

[6] http://www.gnuplot.info/
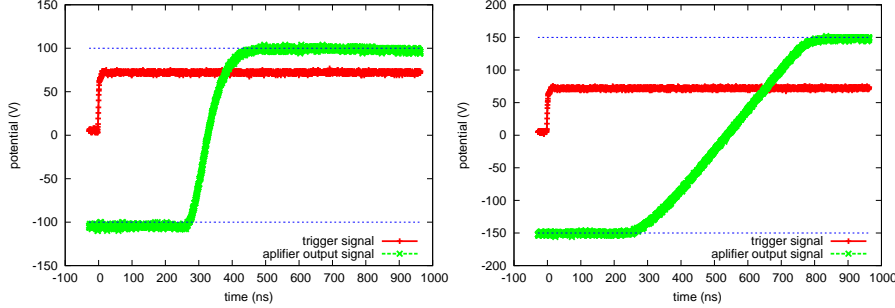
Figure 3.6: Measured amplifier signal rising slope with suppressed overshoot
for a -10 V to 10 V signal (left) and -150 V to 150 V (right) with serial resistance
of 561 Ω. CH1 (red) is the AWG signal at 5 Hz, CH2 (blue) is the amplifier
signal. An $l = 50$ cm coaxial cable was used.

Table 3.1: Measured amplifier signal overshoot (O) and rise time (t_{rise}) for a
5 Hz switching frequency, depending on serial resistance and voltage difference.
A 50 cm cable was used. The error of the voltage reading from the oscilloscope
is 0.1 V and therefore 0.14 V for V_{diff} based on Gaussian error propagation.

V_{start}	V_{final}	V_{diff}	R (Ω)	t_{rise}(ns)	O (%)	t_{total}(ns)	comment
-10V	10V	20V	none	60(5)	27(5)	275(10)	
-10V	10V	20V	50(1)	65(5)	23(5)	300(10)	
-10V	10V	20V	150(1)	80(5)	13(4)	325(10)	
-10V	10V	20V	561(1)	200(5)	0	200(10)	Fig. 3.6 L
-100V	100V	200V	561(1)	400(10)	0	400(10)	
-150V	150V	300V	561(1)	530(10)	0	530(10)	Fig. 3.6 R

3.4 Suppression of overshoot and determination of cable capacitance

A serial potentiometer was added to the output of the amplifier in order to
reduce the overshoot. The implementation of a serial resistor also increases the
rise time. As stated previously, this contributes to the adiabatic behavior of the
switching process, but also increases the overall minimal cooling time. Results
of the serial resistor measurements are presented in Fig. 3.6 and Table 3.1. It
was determined that the overshoot completely disappeared for the whole range
of voltage jumps for a serial resistor of at least $R = 561$ Ω, with the above
mentioned 50 cm BNC cable. The shortest cable among the ones that were
used was 40 cm, showing an overshoot for $R = 561$ Ω. The smallest resistance
used in the following measurements is therefore $R = 828$ Ω, which completely
suppressed the overshoot for all cables used and all switching operations.

For the following measurements the rise time was determined automatically
by the Tektronix oscilloscope using the standard convention (10% to 90%) and
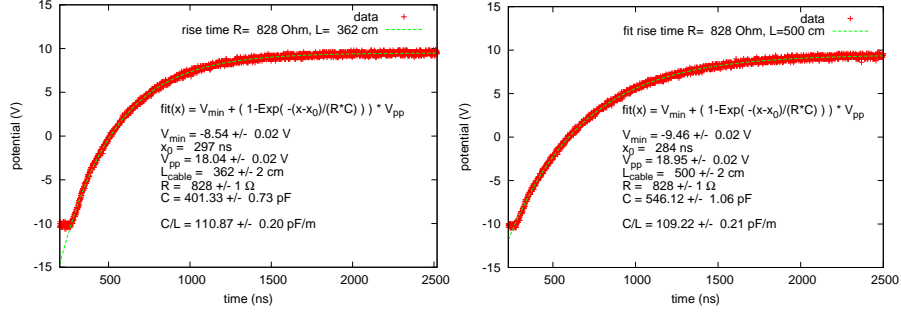
Figure 3.7: Measured and fitted rising slope for R=828 Ω and L=362 cm (left)/ 500cm (right) and cable capacity obtained from the fit.

Table 3.2: Measured capacity per meter (fit. C/l) of different coaxial RG59 cables using different cable lengths l and serial resistance R. The values are compared to the quoted value of "lit. C/l".

run	fit C/l (pF/m)	lit C/l (pF/m)	cable l (cm)	R (Ω)
37	102.7(0.4)	67.6	75(2)	828(1)
38	110.9(0.2)	67.6	362(2)	828(1)
39	109.2(0.2)	67.6	500(2)	828(1)
41	120.5(0.8)	67.6	362(2)	82(1)

therefore differs from the rise times determined in the first measurements. It was also found that the cable acts as a capacitor, affecting the rise time. It is first investigated how cable length and capacity relate to each other.

Fig. 3.2 shows the RC circuit consisting of the capacity of the cable and the added serial resistor. The inside of the probe is shown. Different signals were produced using various cable lengths and serial resistances and were recorded using the oscilloscope. Fig. 3.7 shows the signal output of an amplifier channel, which was switched from -10 V to 10 V using a cable length of $L = 362$ cm (left) and $L = 500$ cm (right) and a serial resistor of $R_s = 828$ Ω with no overshoot. The coaxial cables (standard RG59 [56]) have a quoted capacity of 68 pF per meter [56]. As every component of the circuit has not been taken into account (i.e. the internal resistance and capacity of the amplifier), the fit results in an effective capacity for the cable, which therefore has a potentially large systematic error. Nonetheless the result of $C \approx 110$ pF/m agrees approximately with the manufacturer specifications. All measurement results are shown in Table 3.2. The error for the cable length measurement is taken to be 1 cm on each end. The error of the resistance measurement is taken to be last digit of the multimeter. An error value for the quoted value of C was not specified in [56] and could not be found.
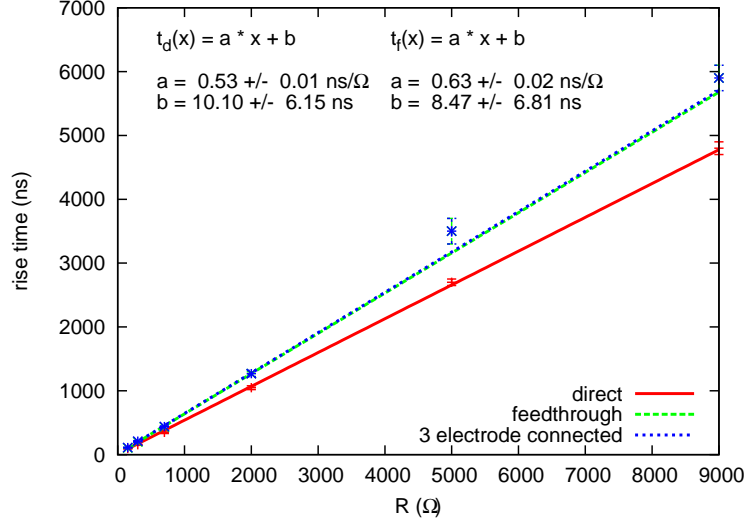
Figure 3.8: Measured and fitted rising slope of a -10 V to 10 V signal as a function of serial resistance for three different connection scenarios. First, the 3.50 m signal cable is directly connected to the oscilloscope probe. Second, the signal cable is connected to an electrode through CPET's feed through section, using CPET's internal wiring and the probe is connected directly to the electrode. Last, same setup as before and in addition, the neighbouring electrodes are set to 0 V and the trap is covered with grounded aluminium foil.

3.5   Rise time dependence on cable length and resistance

The effect of serial resistance R and cable length (i.e. cable capacity) L on a rise time t of the amplifier output was also investigated.

Fig. 3.8 shows that the rise time increases linearly with the added serial resistor, for a fixed cable length. The rise time errors originated from the rise time determination of the oscilloscope. The error for R is again taken as the last digit of the multimeter. For the actual experiment, a cable length of at least 3.50 m from the amplifiers to the CPET feed through section will be necessary. Another $\approx$ 50 cm has to be added for internal electrode wiring. Fig. 3.8 shows the difference in rise time for connecting the cable directly to the electrode (red, straight line) or additionally using the internal CPET wiring by feeding the signal through the feed through section of the trap (green, dashed line). As a next step, the neighbouring electrodes were connected to a 0 V output of the amplifier and the whole trap was wrapped in grounded aluminium foil, in order to simulate the vacuum tube (blue, dotted line). No significant difference in rise time could be determined in that case. It can be seen that with a 3.50 m cable rise times from 100 ns to 6 μs can be produced using 100 Ω to 10 kΩ resistors.
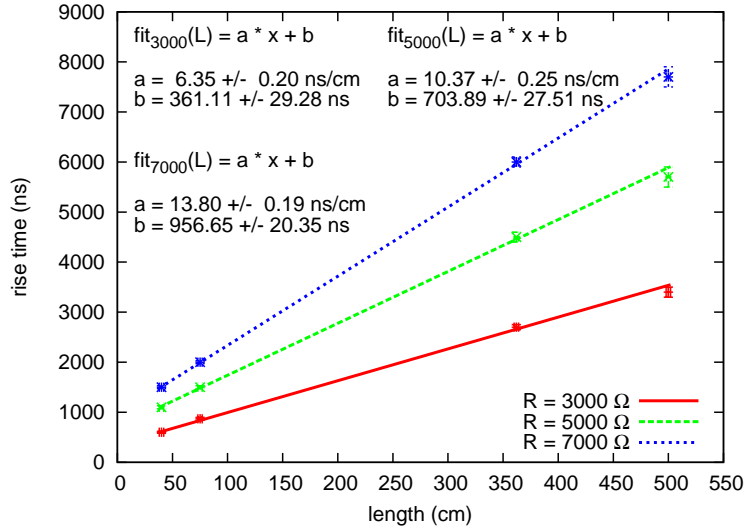
Figure 3.9: Measured and fitted rising slope of a -10V to 10V signal with specific serial resistance as a function of cable length. The oscilloscope probe is directly connected to the signal cable.

For longer rise times, it would be possible to increase the cable length or add an additional capacitor.

Fig. 3.9 shows how the rise time relates to the cable length (capacitance) for three different fixed serial resistors. As previously verified, each meter of cable exceeding the fixed 3.50 m determined for the real setup could be replaced by a capacitor of $C \approx 68$ pF.

3.5.1   Relation between resistance and cable length

Fig. 3.10 shows how cable length (capacitance) and serial resistance relate to each other resulting in three different fixed rise times. The errors were chosen to be the precision of the multimeter used to measure the resistance of the potentiometer and 2 cm per cable for the cable length. The used fit function is a power function which can be used to extrapolate the function towards longer cable lengths or resistances.

3.6   Investigation of induced peak potential

This section investigates the potential induced on neighbouring electrodes, while modifying the potential on another electrode. The amount of potential induced on the neighbour electrodes when performing a potential change should be minimized, as additional potential on trap electrodes will alter the energy of the trapped particles and can therefore have undesirable effects. The experimental
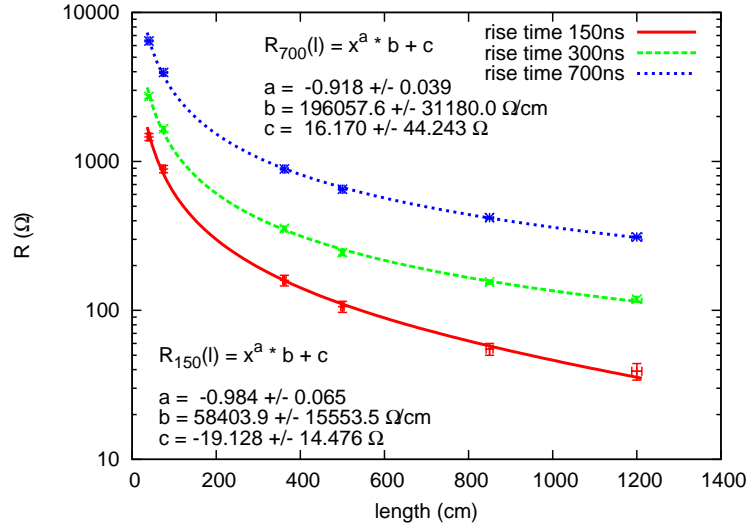
Figure 3.10: Measured and fitted resistance as a function of cable length with fixed rise time. The rise time of a -10 V to 10 V signal is kept constant by adjusting the serial resistance for different cable lengths.
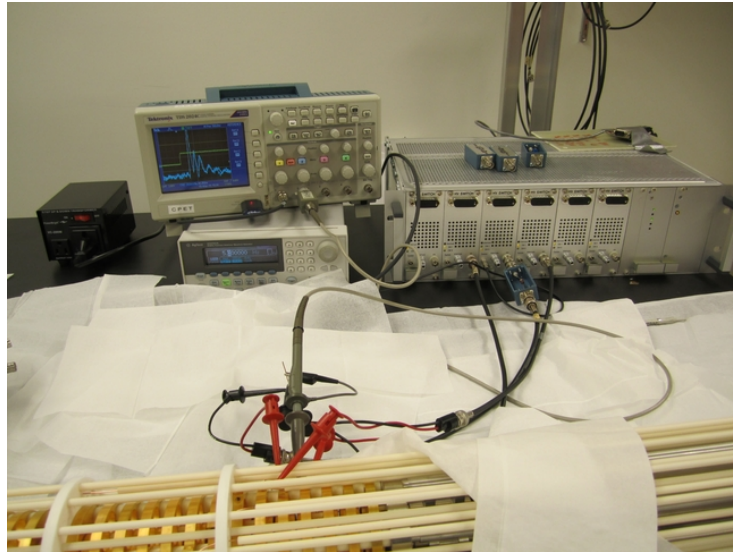
Figure 3.11: Photo of experimental setup. The oscilloscope and the AWG are placed on the far left side, the amplifier on is located on the right. In the front of the photograph resides the trap structure with connected probe and ground wires.
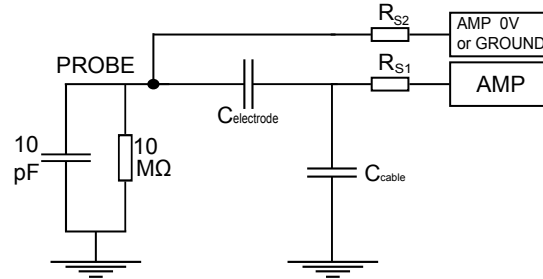
Figure 3.12: Schematic RC circuit diagram consisting of an amplifier channel (AMP) outputting a variable voltage and one amplifier channel at 0 V (alternatively this connection is grounded). Two serial resistors R_{S1} and R_{S2} are connected to the amplifier outputs. The two amplifier channels are connected to two (neighbouring) CPET electrodes, which form an additional capacitor ($C_{electrode}$). The capacity of the cable establishing the connection from AMP to the electrode has a value of C_{cable}. The oscilloscope probe is connected to the electrode which is set to 0 V or ground.

set-up is shown in Fig. 3.11 and the corresponding circuit diagram is shown in Fig. 3.12. The electrode on which the potential is applied is called the main electrode or just "electrode". The electrode which is used to measure the amount of induced potential is called the adjacent or the neighbour electrode. If a number is provided then the n-th distant electrode is meant (e.g. the second neighbouring electrode (or distance 2) is the one right after the direct neighbour).

A first measurement result is presented in Fig. 3.13. All cable lengths were 3.50 m and $R_{S1} = 1$ kΩ. The amplifier switched one electrode from 0 to 150 V. The neighbour electrode was grounded with a $R_{S2} = 5$ kΩ resistor. A peak voltage of $U_{peak} \approx 18.6$ V was induced on the neighbour electrode. The induced voltage signal has a rise time of ≈ 247 ns and decays within ≈ 1052 ns back to ground. This section investigates possibilities for decreasing U_{peak}. The term "induced potential" will further refer to U_{peak}. The rise and decay time, as well as the induced potential depend on the amplifier signal and R_{S2}. For $R_{S2} = 0$ Ω the induced potential $U_{peak} = 0$ V. In the later CPET setup every electrode will be connected to an amplifier channel with a defined internal resistance. Setting $R_{S2} = 0$ Ω is therefore not possible.

Another possibility of decreasing U_{peak} is increasing the signal rise time of the amplifier. Fig. 3.14 shows the measured induced potential as a function of the amplifier rise time. The signal is a 0 to 10 V potential change. It is applied to one electrode using a 5 m coaxial cable and varying serial resistance R_{S1} to vary the signal rise time. The neighbouring electrodes (two on each side) are connected to a stable 0 V output of the amplifier using a 40 cm cable and 7 kΩ serial resistance. It can be seen how different rise times of the signal affect the induced potential. As the influence should ideally be as small as possible, the suggested rise time for use in the actual experiment should be at least 6 µs,
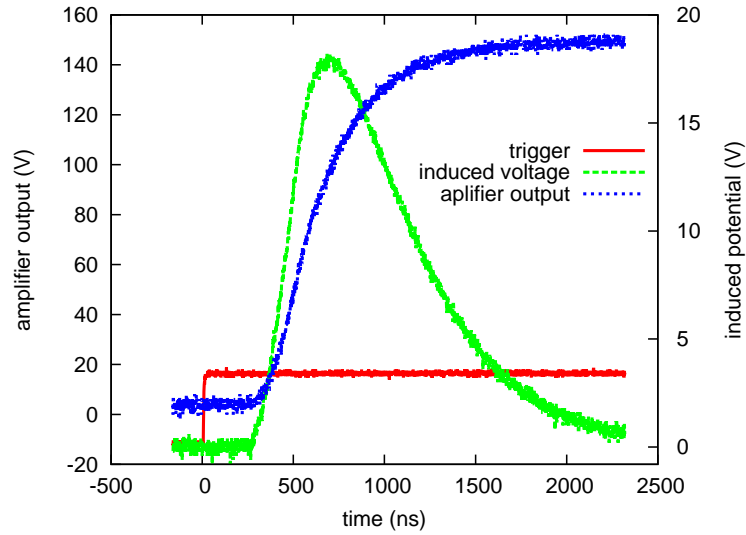
Figure 3.13: Measured amplifier output signal applied to an electrode and induced potential on the neighbour electrode as a function of time.
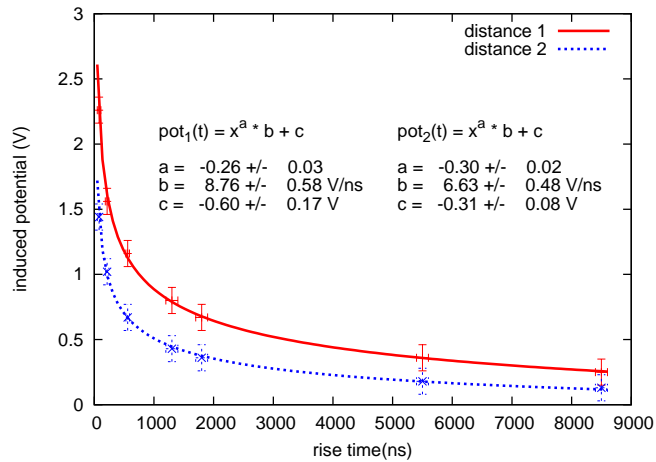
Figure 3.14: Measured induced maximum potential as a function of rise time. A 0 V to 10 V signal change is applied to the centre electrode. The measurement is performed on the neighbouring electrode. The red and solid line shows the induced voltage on the adjacent electrode, whereas the blue, dotted line shows the voltage on the second distant electrode.
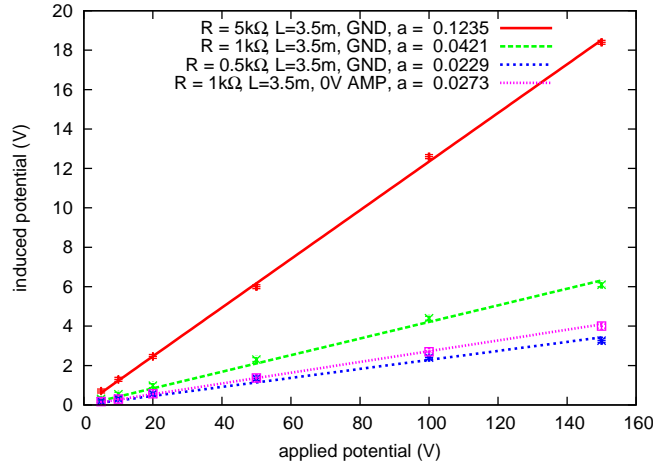
Figure 3.15: Measured induced maximum potential on neighbouring electrode as a function of applied potential. A potential change of 0 V to 10 V was applied to the centre electrode using a 3.5 m cable and 1 kΩ serial resistance. Two neighbouring electrodes were connected to a) ground using three different resistors or b) to a 0 V amplifier output using a 1 kΩ serial resistance.

which would contribute to maximize the adiabatic behaviour of the potential switching.

To theoretically determine the induced potential, the rising slope of the amplifier signal has to be analysed using a Fourier transform in order to identify the frequency which causes the major part of the potential induction. The used fit function is a power dependent function, which can be used to extrapolate the data. This is sufficient for the purpose of identifying the rise time which causes the least amount of induced potential.

Fig. 3.15 shows the induced potential on neighbouring electrodes as a function of applied voltage. The neighbour electrodes were either connected to a 0 V output of the amplifier or grounded using a serial resistor R_{S2} (Fig. 3.12). It can be seen that there is little difference between the case where the neighbour electrode is connected to a 0 V output using a $R_{S2} = 1$ kΩ resistor and the case where the electrode is connected to ground using the same resistance. The 0 V amplifier channel behaves approximately like a 1 $k\Omega$ connection to ground. It can be seen that the induced potential increases linearly with the applied potential. Therefore, only the y-axis in Fig. 3.14 would rescale for different applied potentials and the shape of the graph would remain invariant. A minimal rise time of 6 μs would globally apply for all different voltage changes.

It has also been determined that the induced potential on the neighbour electrode is independent of the potential applied to it. In Fig. 3.15, this would lead to an offset on the y-axis. On the other hand, it has been observed that the induced potential on the neighbouring electrode was significantly less when the neighbour electrode does not have a static potential applied, but is simulta-

Table 3.3: Measured induced maximum voltage on neighbour electrode for a 0 V to 100 V potential change on the main electrode. The potential U_i gets induced when the neighbour electrode is set to stable U_a V. The potential U_{is} is induced when the neighbour electrode is switched simultaneously from 0 V to U_a V. The error of U_i is 0.1 V. The error of U_{is} is dU_{is}.

U_a (V)	0	5	10	20	50	100	150
U_i (V)	2.7	2.7	2.7	2.7	2.7	2.7	2.7
U_{is} (V)	2.7	2.2	1.4	1.2	-	-	-
dU_{is} (V)	0.1	0.1	0.2	0.5	-	-	-

neously switched between two voltages as well. The larger the potential change on the neighbour, the lower the induced voltage on it. This phenomena could not be investigated in greater depth, because the resolution of the scope was not high enough to distinguish small voltage differences on top of large applied voltages.

The experimental set-up is similar to the one shown in Fig. 3.12, except that various voltages U_a are applied to the channel marked as grounded, which is connected to the neighbour electrode. The main electrode (connected to the amplifier channel AMP) is switched from 0 V to 100 V. All cable lengths are l = 3.5 m, the serial resistor are set to $R_{S1} = R_{S2} = 1$ $k\Omega$. The measurements that were taken are presented in Table 3.3. If the neighbour electrode is set to a static value of U_a, the induced voltage U_i is invariantly 2.7 V. If the voltage of the neighbour electrode is switched from 0 V to U_a simultaneously as the main electrode, the induced voltage U_{is} decreases with increasing U_a. The error dU_{is} increases with increasing U_a, as the resolution of the oscilloscope made it more and more difficult to identify the induced voltage U_{is} out of the applied voltage U_a. For values of $U_a > 20$ V identification of the signal was impossible.

The used oscilloscope digitized the full signal. When zooming in, the resolution decreases. This measurement could be redone with an oscilloscope which allows analogue pre-shifting of the signal before digitalization, so that the full ADC (analogue digital converter) range is available for a specific voltage range (for parts of the signal).

3.7 Rise times with added low pass filter

As discussed previously, the combination of different capacity and serial resistance enables control of the rise time. As these are the components of a low pass filter, such a filter could be used to suppress noise and control the rise time at once. The proposed set-up is shown in Fig. 3.16 and consists of an initial serial resistor of 1 kΩ directly after the output of the amplifier to suppress the signal overshoot, then the 3.50 m signal cable and lastly, directly at the feed through section connectors of the trap, the low pass filter. The filter in this set-up consists of a $C = 470$ pF capacitor (which corresponds to $l \approx 7$ m of
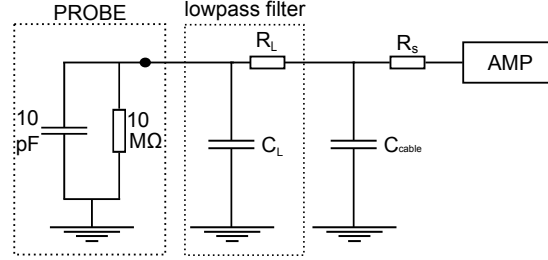
Figure 3.16: Schematic RC cirquit consisting of a serial resistor, cable capacity and a low pass filter.
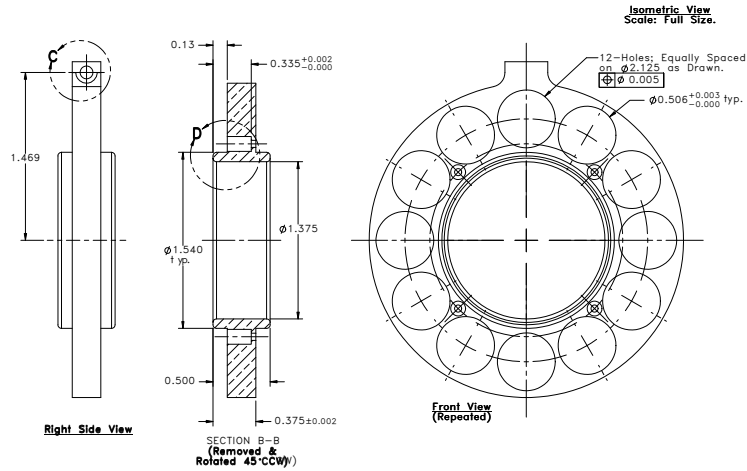
Figure 3.17: SolidWorks drawing of a single CPET electrode.

RG59 cable) and a 0 to 10 kΩ potentiometer. By modifying the potentiometer from 0 to 10 kΩ, the rise time could be manipulated linearly from 2 to 10 μs, which makes this set-up a suitable choice for the actual experiment. To achieve even larger rise times, the capacitance could be increased but should be at least $C = 470$ pF.

3.8 Capacity measurement of two electrodes

A SolidWorks drawing of a single electrode is shown in Fig. 3.17 and its dimensions are listed in Table 3.4. The values are provided in the original unit of inch as used in the drawing. Based on these numbers, the capacity of two CPET electrodes was determined to be

$$C_{\text{geo}} = \frac{A}{d} = 6.8 \pm 0.6 \text{ pF} \tag{3.1}$$

Table 3.4: Diameters of all holes in a CPET electrode and the electrode as a whole (in units of inch), as shown in Fig. 3.17. The third column identifies the number of corresponding holes.

	diameter (in)	#
electrode	2.75	1
holes	0.506	12
spacer holes	0.063	4
centre hole	1.375	1
inner ring	1.54	1
electrode distance	0.29	-
inner ring distance	0.04	-

using the SolidWorks measurement tool. The tool does not provide errors for the measurement. The electrodes have been manufactured using a tolerance of 0.005 in for the diameters and distances specified. The error for C_{geo} has been determined using Gaussian error propagation. The electrodes do furthermore not have a flat surface. Electric fringe fields are caused by the edges of the 19 holes and the inner ring. This causes an additional systematic error.

The capacity of two electrodes was also measured using the capacity setting of a Wavetech Meterman CR50 multimeter [57]. While assembled, the value is determined to be $C_{asse} = 38.2$ pF. Two electrodes are extracted from the trap set-up and put onto the wooden table. Their distance is maintained using four ceramic spacers which also maintain the electrode distances in the set-up. The capacity of the electrodes is now determined to:

$$C_{meas} = 8.8 \pm 1.0 \text{ pF} . \tag{3.2}$$

The value of C_{asse} is much higher than C_{meas} as it was obtained while the trap was fully assembled including all neighbour electrodes. Also the trap wiring adds to the measured capacity as the two electrode connection wires face each other along the trap structure. The multimeter applies a known frequency of 820 Hz and a voltage < 3.5 V and measures the resulting voltage across the capacitor. The manufacturer specifies the error for this type of measurement as 5% of the measured value plus 1 digit uncertainty plus 0.5 pF which was taken as the error of C_{meas}.

3.9 Summary of the amplifier measurements

The cooler Penning trap operation cycle currently aims at cooling times on the order of seconds, but faster cooling cycles are envisioned and increase the requirements on the electronics hardware. Rise time can then be increased "on the fly" by adding serial resistance and additional capacity to the output of the amplifier (e.g. with a low pass filter). The rise time of the amplifier should be set to at least 6 μs in order to reduce the amount of potential conferred

to neighbouring electrodes while switching. Lowpass filter with a $C = 470$ pF capacitor and a $R = 10$ kΩ resistor were found to be suitable for this purpose.

Two investigations are proposed to be performed in the future, when the correspondent equipment will be available. The influence of the very short ($\approx$ 60 ns) and high (≈ 3 kV) switching of the trap gates on the whole trap region should be investigated. This is crucial to investigate as this switching step happens after the HCI injection, with already cooled electrons stored in the trap. It should also be tested how a potential change on one electrode affects all the other electrodes of the trap, especially further distant ones than already investigated.

Chapter 4

Summary and Outlook

The main goal of the study was to investigate the effect of switching the potential of the cooler Penning trap electrodes on trapped electrons. Two different simulation approaches were chosen in the first part and produced similar results. Based on the simulations it was found that the proposed operation cycle of the cooler Penning trap operates on a timescale which lies well in the so-defined adiabatic regime. The simulations also showed that the axial manipulation of electrons should be on the same order of magnitude as their axial amplitude in the trapping potential. Furthermore, some requirements on the amplifier which is to be built were determined (e.g. the number of potential settings to be stored in memory). These information will contribute to the development of a detailed operation cycle including ion and electron injection, the cooling process, and ion ejection.

In the second part of the thesis a programmable amplifier and its influence on the trap was investigated. It was found that the amplifier signal should be fed into the trap using a 3.50 m coaxial cable combined with a specific lowpass filter. The filter reduces noise picked up from the cable and should also be tuned to increase the rise time of the amplifier signal to at least 6 μs in order to minimize the potential crosstalk between the electrodes. The performed investigation provides input for the development process of the cooler Penning trap electronics equipment and its setup in the experiment.

As a next step for the simulations, protons and HCI should be investigated. The programs presented in this thesis are easily adaptable to simulate particles with different charges and masses, which was not possible within the scope of this work. Multi particle effects like space charge and plasma effects should be taken into account to prove the validity of the single particle results or improve the simulation results. For this purpose the simulations could be redone using the particle-in-cell approach [58–61] which reaches a very high accuracy in particle trajectory calculations in electric fields and reasonable simulation times for a large number of simulated particles.

When the electronics equipment for the cooler Penning trap are fully available, the present measurements should be extended using all 29 amplifier chan-

nels and the trap gate switches.

All parts of the cooler Penning trap have undergone an extensive UHV cleaning and the assembly is to be completed within the next days. Once completed the trap structure will be ready to be placed into the magnet. A test setup including an electron and an ion source is planned and should be operational within the year. After successful tests, the cooler Penning trap will be inserted into the main TITAN beamline.

Bibliography

[1] J. Dilling, P. Bricault, M. Smith, and H. Kluge "The proposed TITAN facility at ISAC for very precise mass measurements on highly charged short-lived isotopes" *Nuclear Instruments and Methods in Physics Research Section B* vol. **204**, pp. 492–496 (2003). DOI: 10.1016/S0168-583X(02)02118-3 (cit. on pp. 1, 13).

[2] M. Smith et al. "First Penning-Trap Mass Measurement of the Exotic Halo Nucleus ^{11}Li" *Physical Review Letters* vol. **101** no. 20, p. 202 501 (2008). DOI: 10.1103/PhysRevLett.101.202501 (cit. on p. 1).

[3] K. Blaum "High-accuracy mass spectrometry with stored ions" *Physics Reports* vol. **425** no. 1, pp. 1–78 (2006). DOI: 10.1016/j.physrep.2005.10.011 (cit. on pp. 1, 7, 8, 10).

[4] P. Schury et al. "Precision mass measurements of rare isotopes near N= Z= 33 produced by fast beam fragmentation" *Physical Review C* vol. **75** no. 5, p. 055 801 (May 2007). DOI: 10.1103/PhysRevC.75.055801 (cit. on p. 1).

[5] B. Povh et al. "The Baryons" in *Particles and nuclei: an introduction to the physical concepts* springer, 2008, pp. 201–227 ISBN: 978-3-540-79368-7. DOI: 10.1007/978-3-540-79368-7_15 (cit. on p. 1).

[6] B. Povh et al. "Phenomenology of the Weak Interaction" in *Particles and Nuclei* springer, 2008, pp. 127–150 ISBN: 978-3-540-79368-7. DOI: 10.1007/978-3-540-79368-7_10 (cit. on p. 1).

[7] G. Savard et al. "Q Value of the Superallowed Decay of ^{46}V and Its Influence on V_{ud} and the Unitarity of the Cabibbo-Kobayashi-Maskawa Matrix" *Physical Review Letters* vol. **95** no. 10, p. 102 501 (Aug. 2005). DOI: 10.1103/PhysRevLett.95.102501 (cit. on p. 1).

[8] B. Povh et al. "Global Properties of Nuclei" in *Particles and Nuclei* springer, 2008, pp. 11–23 ISBN: 978-3-540-79368-7. DOI: 10.1007/978-3-540-79368-7_2 (cit. on p. 1).

[9] S. Naimi et al. "Critical-Point Boundary for the Nuclear Quantum Phase Transition Near A= 100 from Mass Measurements of ^{96,97}Kr" *Physical Review Letters* vol. **105** no. 3, p. 32 502 (Jul. 2010). DOI: 10.1103/PhysRevLett.105.032502 (cit. on p. 1).

[10]   B. Povh et al. "Nuclear Stability" in *Particles and Nuclei* springer, 2008,
       pp. 25–40 ISBN: 978-3-540-79368-7. DOI: 10.1007/978-3-540-79368-7_3
       (cit. on p. 1).

[11]   J. C. Hardy and I. S. Towner "Superallowed $0^+ \to 0^+$ nuclear β decays: A
       new survey with precision tests of the conserved vector current hypothesis
       and the standard model" *Phys. Rev. C* vol. **79** no. 5, p. 055 502 (May
       2009). DOI: 10.1103/PhysRevC.79.055502 (cit. on p. 1).

[12]   A. Lapierre et al. "The TITAN EBIT charge breeder for mass measure-
       ments on highly charged short-lived isotopes–First online operation" *Nu-
       clear Instruments and Methods in Physics Research Section A* (2010). DOI:
       10.1016/j.nima.2010.09.030 (cit. on pp. 2, 14).

[13]   F. Currell and G. Fussmann "Physics of electron beam ion traps and
       sources" *Plasma Science, IEEE Transactions on* vol. **33** no. 6, pp. 1763–
       1777 (2005). DOI: 10.1109/TPS.2005.860072 (cit. on pp. 2, 14).

[14]   Z. Ke et al. "A cooler ion trap for the TITAN on-line trapping facility at
       TRIUMF" *Hyperfine Interactions* vol. **173** no. 1, pp. 103–111 (2006). DOI:
       10.1007/s10751-007-9548-x (cit. on p. 2).

[15]   Z. Ke "A cooler ion trap for the TITAN on-line trapping facility at
       TRIUMF" PhD thesis University of Manitoba, Department of Physics
       and Astronomy (2008). [Online]. Available: http://titan.triumf.ca/
       research/publications/ke_CPET_thesis_2008.pdf (cit. on pp. 2, 11,
       12, 17, 21, 37, 38).

[16]   V. L. Ryjkov et al. "TITAN project status report and a proposal for a new
       cooling method of highly charged ions" in *The 4th International Confer-
       ence on Exotic Nuclei and Atomic Masses* C. J. Gross, W. Nazarewicz,
       and K. P. Rykaczewski, Eds. Springer, 2005, pp. 53–56 ISBN: 978-3-540-
       37642-2. DOI: 10.1007/3-540-37642-9_14 (cit. on pp. 2, 12).

[17]   V. V. Simon, P. Delheij, J. Dilling, Z. Ke, W. Shi, and G. Gwinner "Cool-
       ing of short-lived, radioactive, highly charged ions with the TITAN cooler
       Penning trap" in *to be published in: Hyperfine Interactions* Springer 2011.
       DOI: 10.1007/s10751-011-0309-5 (cit. on pp. 2, 12, 17).

[18]   V. V. Simon, U. Chowdhury, P. Delheij, J. Dilling, B. Eberhardt, and G.
       Gwinner "A cooler Penning trap for the TITAN on-line trapping facility"
       in *to be published in: JPCS* IOP Publishing 2011 (cit. on pp. 2, 16, 20,
       40).

[19]   K. Blaum and F. Herfurth *Trapped charged particles and fundamental
       interactions* ser. Lecture Notes in Physics. Springer, 2008 vol. **749** ISBN:
       3540778160. DOI: 10.1007/978-3-540-77817-2 (cit. on pp. 3, 6, 8–10).

[20]   H. Dehmelt "Experiments with an isolated single particle at rest" *Rev.
       Mod. Phys* vol. **62** no. 3, pp. 525–530 (Jul. 1990). DOI: 10.1103/RevModPhy
       s.62.525 (cit. on p. 2).

[21] L. S. Brown and G. Gabrielse "Geonium theory: Physics of a single electron or ion in a Penning trap" *Reviews of Modern Physics* vol. **58** no. 1, pp. 233–311 (Jan. 1986). DOI: 10.1103/RevModPhys.58.233 (cit. on pp. 2, 3, 5).

[22] M. Brodeur "First direct mass measurement of the two and four neutron halos 6He and 8He using the TITAN Penning trap mass spectrometer" PhD thesis University of British Columbia (Apr. 2010). [Online]. Available: http://titan.triumf.ca/research/publications/ubc_2010_fall_brodeur_maxime.pdf (cit. on p. 3).

[23] M. König, G. Bollen, H. J. Kluge, T. Otto, and J. Szerypo "Quadrupole excitation of stored ion motion at the true cyclotron frequency" *International Journal of Mass Spectrometry and Ion Processes* vol. **142** no. 1-2, pp. 95–116 (1995). DOI: 10.1016/0168-1176(95)04146-C (cit. on p. 5).

[24] V. S. Kolhinen et al. "JYFLTRAP: a cylindrical Penning trap for isobaric beam purification at IGISOL" *Nuclear Instruments and Methods in Physics Research Section A* vol. **528** no. 3, pp. 776–787 (2004). DOI: 10.1016/j.nima.2004.05.029 (cit. on p. 6).

[25] G. Gräff, H. Kalinowsky, and J. Traut "A direct determination of the proton electron mass ratio" *Zeitschrift für Physik A Hadrons and Nuclei* vol. **297** no. 1, pp. 35–39 (1980). DOI: 10.1007/BF01414243 (cit. on p. 6).

[26] M. Smith "A Mass Measurement of the Short-lived Halo Nucleus ^{1}1Li with the TITAN Penning Trap Spectrometer" PhD thesis University of British Columbia (Apr. 2008). [Online]. Available: http://titan.triumf.ca/research/publications/ubc_2008_spring_smith_mathew.pdf (cit. on p. 7).

[27] A. G. Marshall, C. L. Hendrickson, and G. S. Jackson "Fourier transform ion cyclotron resonance mass spectrometry: A primer" *Mass spectrometry reviews* vol. **17** no. 1, pp. 1–35 (1998). DOI: 10.1002/(SICI)1098-2787(1998)17:1<1::AID-MAS1>3.0.CO;2-K (cit. on p. 7).

[28] S. Rainville, J. K. Thompson, and D. E. Pritchard "An ion balance for ultra-high-precision atomic mass measurements" *Science* vol. **303** no. 5656, p. 334 (2004). DOI: 10.1126/science.1092320 (cit. on p. 7).

[29] G. Savard et al. "A new cooling technique for heavy ions in a Penning trap" *Physics Letters A* vol. **158** no. 5, pp. 247–252 (1991). DOI: 10.1016/0375-9601(91)91008-2 (cit. on p. 8).

[30] W. M. Itano, J. C. Bergquist, J. J. Bollinger, and D. J. Wineland "Cooling methods in ion traps" *Physica Scripta* vol. **1995** no. T59, p. 106 (1995). DOI: 10.1088/0031-8949/1995/T59/013 (cit. on pp. 8, 10).

[31] K. Blaum et al. "g-factor experiments on simple systems in Penning traps" *Journal of Physics B: Atomic, Molecular and Optical Physics* vol. **42**, p. 154 021 (2009). DOI: 10.1088/0953-4075/42/15/154021 (cit. on p. 9).

[32] D. A. Church and H. G. Dehmelt "Radiative cooling of an electrodynam-
      ically contained proton gas" *Journal of Applied Physics* vol. **40** no. 9,
      pp. 3421–3424 (1969). DOI: 10.1063/1.1658214 (cit. on p. 9).

[33] K. B. Davis et al. "Bose-Einstein Condensation in a Gas of Sodium Atoms"
      Phys. Rev. Lett. vol. **75** no. 22, pp. 3969–3973 (Nov. 1995). DOI: 10.1103/
      PhysRevLett.75.3969 (cit. on pp. 9, 10).

[34] M. B. Schneider, M. A. Levine, C. L. Bennett, J. R. Henderson, D. A.
      Knapp, and R. E. Marrs "Evaporative cooling of highly charged ions in
      ebit: an experimental realization" *AIP Conference Proceedings* vol. **188**
      no. 1, pp. 158–165 (1989). DOI: 10.1063/1.38414 (cit. on p. 9).

[35] M. Smith, L. Blomeley, P. Delheij, and J. Dilling "First tests of the titan
      digital rfq beam cooler and buncher" *Hyperfine Interactions* vol. **173**,
      pp. 171–180 1 (2006). DOI: 10.1007/s10751-007-9554-z (cit. on pp. 10,
      15).

[36] G. Bollen "Traps for Rare Isotopes" in *The Euroschool Lectures on Physics
      with Exotic Beams, Vol. I* J. Al-Khalili and E. Roeckl, Eds. vol. 651 ser.
      Lecture Notes in Physics Springer, 2004, pp. 169–210. DOI: 10.1007/978-
      3-540-44490-9_6 (cit. on p. 10).

[37] D. S. Hall and G. Gabrielse "Electron cooling of protons in a nested Pen-
      ning trap" *Physical Review Letters* vol. **77** no. 10, pp. 1962–1965 (Sep.
      1996). DOI: 10.1103/PhysRevLett.77.1962 (cit. on p. 10).

[38] M. Amoretti et al. "Production and detection of cold antihydrogen atoms"
      Nature vol. **419** no. 6906, pp. 456–459 (2002). DOI: 10.1038/nature01096
      (cit. on p. 11).

[39] G. Z. Li, H. S. Kim, S. Guan, and A. G. Marshall "Radiatively Self-Cooled
      Penning-Trapped Electrons: A New Way To Make Gas-Phase Negative
      Ions from Neutrals of Low Electron Affinity" *Journal of the American
      Chemical Society* vol. **119** no. 9, pp. 2267–2272 (1997). DOI: 10.1021/
      ja962350k (cit. on pp. 11, 37).

[40] M. Dombsky et al. "Commissioning and initial operation of a radioactive
      beam ion source at ISAC" *Review of Scientific Instruments* vol. **71** no. 2,
      pp. 978–980 (2000). DOI: 10.1063/1.1150364 (cit. on p. 13).

[41] M. Dombsky, P. Bricault, T. Hodges, A. Hurst, and P. Schmor "Online
      isotope separation at ISAC with a 10 [mu] A proton driver beam" *Nuclear
      Physics A* vol. **701** no. 1-4, pp. 486–490 (2002). DOI: 10.1016/S0375-
      9474(01)01632-3 (cit. on p. 13).

[42] G. Bollen "Mass measurements of short-lived nuclides with ion traps"
      Nuclear Physics A vol. **693** no. 1-2, pp. 3–18 (2001). DOI: 10.1016/S0375-
      9474(01)00353-0 (cit. on p. 14).

[43] Cryogenic Ltd. Company Profile [Online]. Available: http://www.cry
      ogenic.co.uk/company/profile.asp (visited on 30/04/2011) (cit. on
      p. 14).

[44] G. Bollen and S. Schwarz "Penning trap mass measurements on rare isotopes—status and new developments" *Journal of Physics B* vol. **36** no. 5, p. 941 (2003). DOI: `10.1088/0953-4075/36/5/313` (cit. on p. 14).

[45] R. E. Marrs "Self-cooling of highly charged ions during extraction from electron beam ion sources and traps" *Nuclear Instruments and Methods in Physics Research Section B: Beam Interactions with Materials and Atoms* vol. **149** no. 1-2, pp. 182–194 (1999). DOI: `10.1016/S0168-583X(98) 00624-7` (cit. on p. 15).

[46] N. Oshima et al. "Project to produce cold highly charged ions using positron and electron cooling techniques" in *Journal of Physics: Conference Series* IOP Publishing vol. **2** 2004, p. 127. DOI: `10.1088/1742-6596/2/1/016` (cit. on p. 15).

[47] E. M. Hollmann, F. Anderegg, and C. F. Driscoll "Confinement and manipulation of non-neutral plasmas using rotating wall electric fields" *Physics of Plasmas* vol. **7** no. 7, pp. 2776–2789 (2000). DOI: `10.1063/1. 874128` (cit. on pp. 17, 21).

[48] T. Mohamed "Successful production of non-neutral electron plasma of high density in the multi-ring trap" *Plasma Devices and Operations* vol. **16** no. 3, pp. 181–188 (2008). DOI: `10.1080/10519990802259460` (cit. on p. 21).

[49] Wolfram Research, Inc. Wolfram Mathematica: Technical Computing Software [Online]. Available: `http://www.wolfram.com/mathematica` (cit. on p. 25).

[50] Scientific Instrument Services Inc. (SIS). SIMION - Ion and Electron Optics Simulator [Online]. Available: `http://simion.com/` (visited on 28/04/2011) (cit. on p. 32).

[51] SolidWorks Corp. 3D CAD Design Software SolidWorks [Online]. Available: `http://www.solidworks.com/` (visited on 28/04/2011) (cit. on p. 32).

[52] S. Ritt. Maximum Integration Data Acquisition System MIDAS [Online]. Available: `http://midas.psi.ch/` (visited on 28/04/2011) (cit. on p. 40).

[53] GSI Helmholtzzentrum für Schwerionenforschung GmbH. (Jul. 2010). Switchable Programmable Powersupply - Technical Documentation [Online]. Available: `http://www.gsi.de/documents/DOC-2011-Apr-50-1.pdf` (visited on 28/04/2011) (cit. on p. 41).

[54] National Instruments. LabVIEW a graphical programming environment to develop sophisticated measurement, test, and control systems. [Online]. Available: `http://www.ni.com/labview/` (visited on 28/04/2011) (cit. on p. 41).

[55] GSI Helmholtzzentrum für Schwerionenforschung. CS - A Control System Framework for Experiments - HVSwitch2 [Online]. Available: `http:// wiki.gsi.de/cgi-bin/view/CSframework/CsGSI-HVSwitch2` (visited on 28/04/2011) (cit. on p. 41).

[56]   Thomas Jefferson Lab National Accelerator Facility. Typical RG59 Coax-
       ial Cable Specifications [Online]. Available: `http://hallaweb.jlab.org/`
       `tech/Detectors/public_html/cables/rg59.htm` (visited on 28/04/2011)
       (cit. on pp. 41, 46).

[57]   Wavetech Meterman. (Mar. 2005). CR50 Resistance Meter Datasheet [On-
       line]. Available: `http://www.testequipmentdepot.com/meterman/pdf/`
       `cr50.pdf` (visited on 28/04/2011) (cit. on p. 55).

[58]   E. N. Nikolaev, R. Heeren, A. M. Popov, A. V. Pozdneev, and K. S. Chin-
       gin "Realistic modeling of ion cloud motion in a Fourier transform ion
       cyclotron resonance cell by use of a particle-in-cell approach" *Rapid Com-
       munications in Mass Spectrometry* vol. **21** no. 22, pp. 3527–3546 (2007).
       DOI: `10.1002/rcm.3234` (cit. on p. 57).

[59]   M. C. Lai, W. W. Lin, and W. Wang "A fast spectral/difference method
       without pole conditions for Poisson-type equations in cylindrical and spher-
       ical geometries" *IMA Journal of Numerical Analysis* vol. **22** no. 4, pp. 537–
       548 (2002). DOI: `10.1093/imanum/22.4.537` (cit. on p. 57).

[60]   C. K. Birdsall and A. B. Langdon *Plasma physics via computer simulation.*
       Mc Graw-Hill Book Co., New York, NY, Dec. 1985 ISBN: 0070053715 (cit.
       on p. 57).

[61]   J. W. Eastwood and R. W. Hockney *Computer Simulation using particles.*
       A. Hilger, Bristol [England] ; Philadelphia, Jan. 1988 ISBN: 9780852743928
       (cit. on p. 57).

[62]   Scientific Instrument Services Inc. (SIS). SL Tools Tutorial: Importing/-
       Exporting PA Files [Online]. Available: `http://simion.com/sl/tools_`
       `tut.html#v2pa` (visited on 01/04/2011) (cit. on pp. 78, 80).

Appendix A

Cooler Penning trap assembly logbook

In this chapter, the first assembly of the cooler Penning trap is documented, including progress pictures and notes about difficulties and problems.

A.1   Assembly

In order to run first tests, to check that no parts are missing, to insure that all the parts are fitting together as planned in SolidWorks and to get familiar with difficulties during the assembly, a so-called "dirty assembly" is performed.

For a dirty assembly every part and every screw is cleaned with soap water and acetone. This simple cleaning procedure does not meet the UHV specifications of the TITAN group. Every part is therefore still considered "dirty" and needs another extensive cleaning (which will be explained later) in order to perform the clean assembly, which is then put into the vacuum tube and subsequently into the magnet.

The assembly is started at the proton injection side of the trap, which is
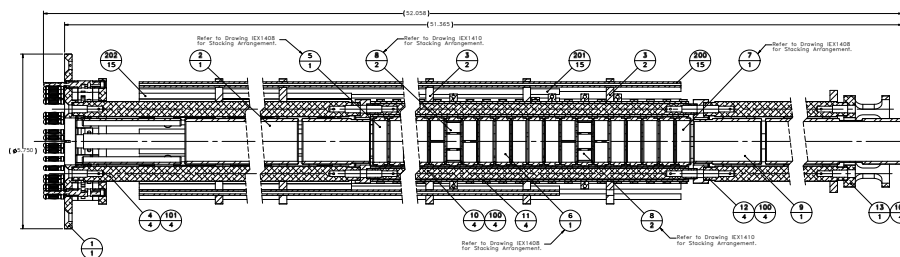
Figure A.1: SolidWorks drawing of the CPET trap structure. Similar drawings were used for the assembly.
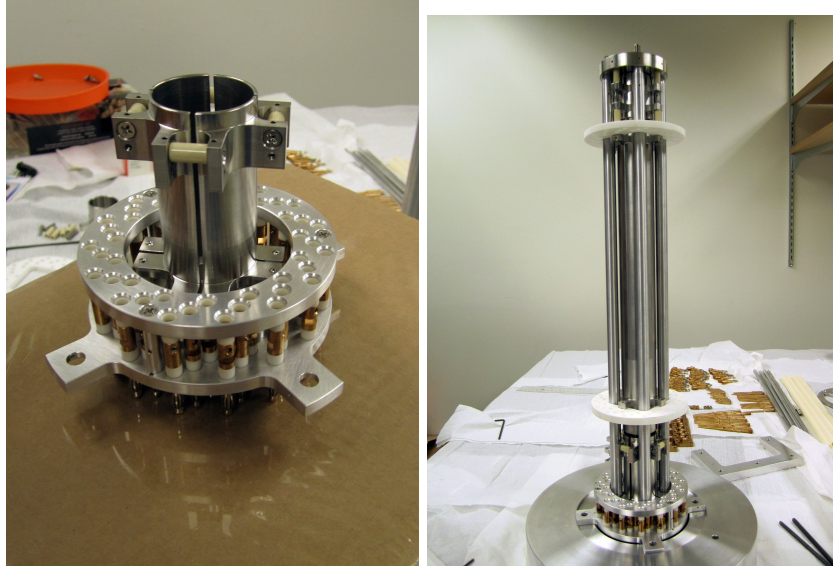
Figure A.2: Photo of CPET Bananaplug-Assembly and first 4-split steerer (left) and proton injection side of the trap including steerer, long drifttude und first wall electrode on the upper end (right).

on the left side on the drawings in Fig. 1.11 and Fig. A.1. The "banana-plug section" is assembled first. A feedthrough section, which will be assembled later, will then be plugged into it using banana connectors, to guide the electrical contacts out of the vacuum.

First, all banana plugs including ceramics and set-screws are put into the upper ring (see Fig. A.2). The second ring and a solid surface are put on top. The assembly is then turned around and all the plugs fall into the lower holes (and hopefully remain in the upper ones).

Four metals rods, a long drifttube, to guide the protons into the homogeneous magnet field region and the proton wall electrode are installed (right picture Fig. A.2). The holes in the white wire-guiding ceramics (the white discs) have to match and be in the same orientation each. A good reference point is the hole marked with a green arrow in Fig. A.5, as it is the hole, which is closest to one of the four metal rods.

First, 13 whole electrodes, then one half split electrode, one eight split, half, five whole electrodes, half, eight split, half and five whole electrodes again are stacked on top of the wall electrode and form the cylindrical penning trap, which will later reside in the homogeneous region of the 7 T CPET magnet (the electrode stacking is shown in Fig. A.3).

The distance between the electrodes is maintained by ceramic spacers. The holes that hold the spacers, are vented to the other side of the electrode. Special care needs to be taken about these vent holes, so that they are never covered
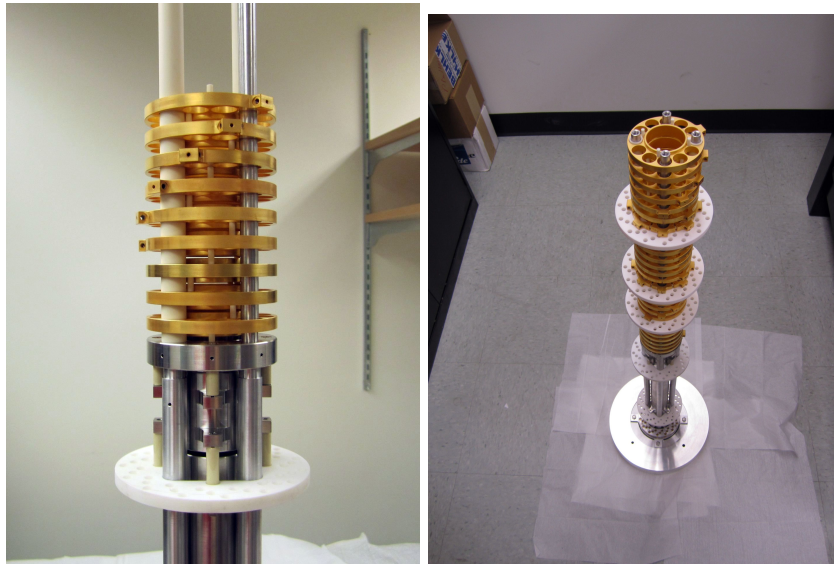
Figure A.3: Photo of the first nine gold plated whole electrodes stacked above the stainless steel gate electrode (left) and the cylindrical penning trap with all electrodes assembled (right).

by the spacers of the adjacent electrode. Every electrode has 12 large holes, as can be seen on Fig. A.4. The holes reduce the amount of material that gets introduced into the trap and also allows the electrodes to be rotated into 12 unique orientations to prevent the vent hole covering. As the electrode connectors in Fig. A.3 show, every electrode that is added to the stack is rotated further clockwise by one hole. The 8-split electrodes are symmetric under this rotation, their vent holes therefore have extra venting slits, so they are allowed to match the spacers on the previous electrodes.

Four metal rods, insulated with ceramic tubes, are used to hold the electrodes (Fig. A.3 left). At this point, two ceramic tubes are currently re-done. They turned out to be slightly oval shaped and the holes in the electrodes were too small to fit them. Therefore two of the white ceramic wire guide discs were positioned right under the 8-split electrodes to increase their stability (Fig. A.3 right).

The 8-split electrode is best assembled on the table and then put as a whole onto the stack (see Fig. A.4).

As a last step of the inner trap region assembly, the last golden whole electrode is put onto the steel support (Fig. A.4), which is then turned around and put onto the electrode stack (Fig. A.3 right). Special care has to be taken, that the ceramic spacers only enter the holes in the steel part and not in the trap electrode.

The complete wiring is performed in the dirty assembly as well. Wires and
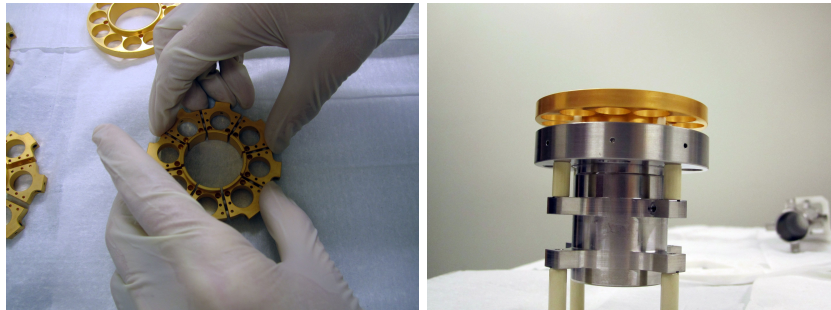
Figure A.4: Photo of the assembly of an 8-split electrode (left) and preparation of the top wall electrode to be mounted on the electrode stack (right).
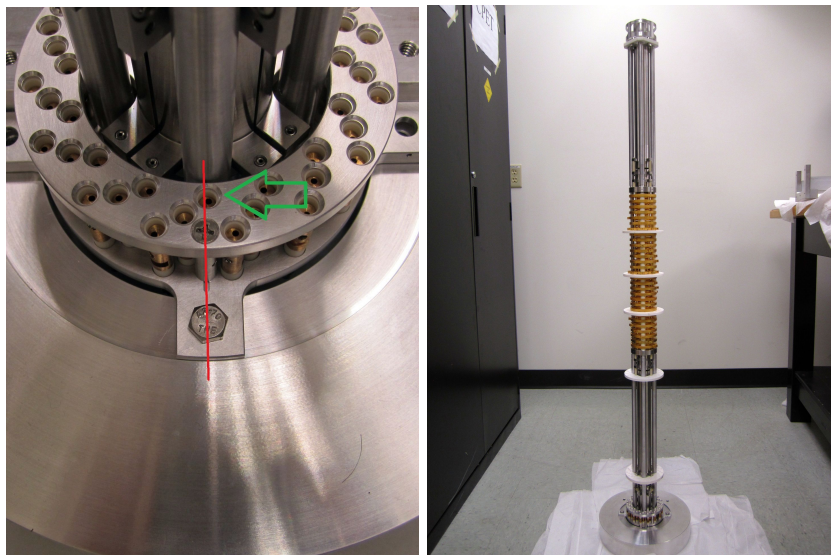
Figure A.5: Photo of the wire plug section defining the circled point as *up* for reference on the orientation in which the electrodes are mounted (left) and the complete trap assembly without wires (right).

wire insulating ceramics will be cut accordingly. Therefore, the orientation of the electrodes must not be changed between now and the final clean assembly. As every electrode can be assembled in 12 different orientations, the current electrode configuration is written down in a clock-like format. A specific point in the bananaplug-assembly, where two screws match up as shown in Fig. A.5, is used as 12 o'clock reference point.

The orientation of the electrodes, determined by the electrodes connector, and the position of the wire guide discs (*wgd*) are as follows. Half split electrodes have two connectors, which sit at half hour positions and the 8-split electrodes

Figure A.6: Photo of the completely assembled cooler Penning trap without electrode wiring.

are invariant under rotation.

- 7 o'clock, 8, 9, 10, 11, 12, 1, wgd, 2, 3, 4, 5, 6, 7

- nested section 1) $4\frac{1}{2}$ & $10\frac{1}{2}$, wgd, 8-split, $4\frac{1}{2}$ & $10\frac{1}{2}$

- 6, 7, 8, 9, 10

- nested section 2) same as (1)

- 12, 1, 2, 3, 4

A problem occurred at this point. There is not enough slack for the electrode stack. The short ceramic spacers in between the electrodes are slightly too long (e.g. cut with an angle). Every ceramic spacer is slightly grinded for compensation. A fotograph of the completly assembled cooler Penning trap without electrode wiring is shown in Fig. A.6. The wiring process is described next.

Wiring

In the first setup the second section of splitted electrodes will not be used. They were therefore shortened. The following electrode wiring process is performed in order to connect every electrode with a connector in the feedthrough section. Every wire is covered by a ceramic tube that matches its length to prevent shorts. These tubes will be referred to as "ceramics". The following wiring process has been performed.

1. Short the second dipole/octupole/dipole combo (before ceramics are inserted, or at least before the long ones are).

2. Wire the steerer and the first drift tube at the bottom, again before ceramics are placed.
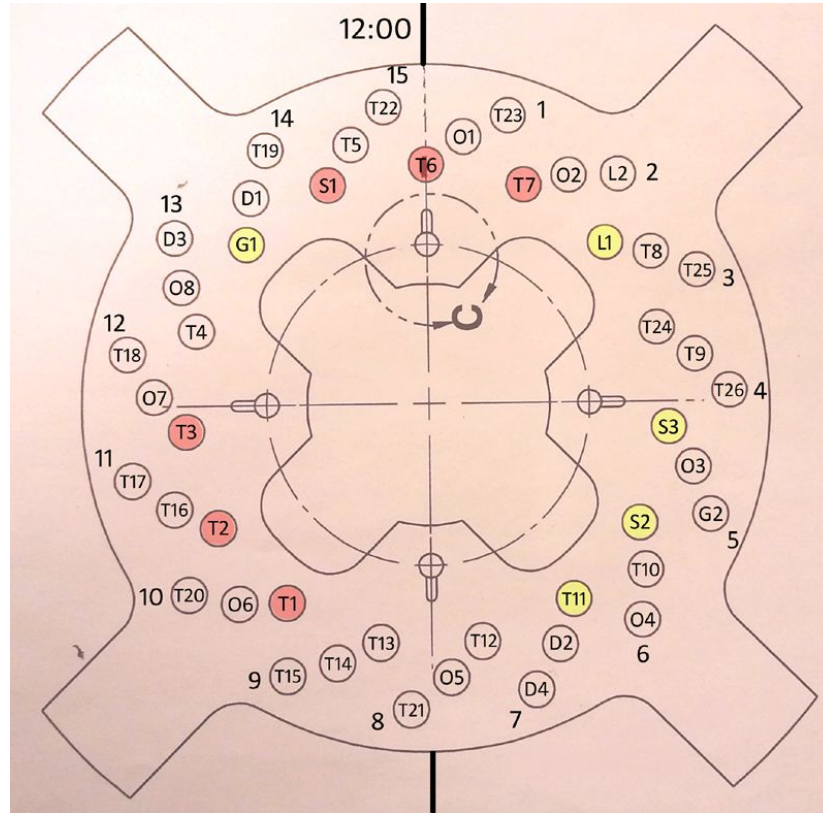
Figure A.7: Schematic of the initial CPET wiring plan including the 12'o clock reference point. Holes that are shaded red are only accessible in the first lens stack (i.e. the first seven single lenses below the first ceramic spacer), and holes that are shaded yellow are only accessible below the second ceramic spacer.

3. Insert ceramics and remaining wires, in order from bottom (first single lens at the side of the feedthrough section) to top (second drift tube).

Figure A.7 shows a ceramic wire guide disk (also referred to as "ceramic spacer"). Four of these disks are placed along the trap in order to guide wires to the electrodes. Shown is a wiring diagram of the first disc which shows the corresponding electrode to be wired through every whole. The connections shown are labelled as follows (numbers are electrode numbers, increasing with distance from the feedthrough section):

- trap electrodes (single lenses): T1 - T26 (this includes the second dipole/ octupole/ dipole combo which will be shorted to form three single lenses),

- dipole electrodes ("2-split"): D1 - D4 (D1 and D2 form the fist pair, D3 and D4 the second),
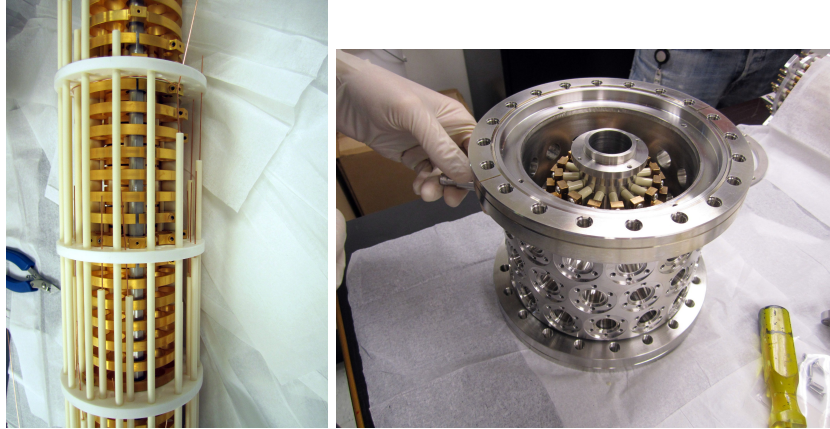
Figure A.8: Photo of electrode wiring in place (left) and of the assembled trap feed through section (right).

- octupole electrodes ("8-split"): O1 - O8,

- drift tubes: L1 and L2,

- gates (or "walls"): G1 and G2,

- Lorentz steerer: S1 - S3 (S1 is two of the steerer quadrants shorted to the same voltage)

The 3-hole groups are numbered 1 through 15, with group 1 corresponding to the pre-designated 12:00 reference point (and moving CW from there). The inner, middle, and outer radii holes in each group are further labelled as -1, -2, and -3, respectively. For example, lens T7 is wired through hole 2-1, T8 through 3-2, etc.

The guiding idea behind the wiring scheme is to minimize the need for wire running horizontally around the stack.

The gate electrodes (G1 and G2) are high voltage/fast-switching, and should therefore be placed in ceramic guides for shielding. As well, the inner radius of holes do not have a lot of clearance above the outer surface of the electrodes, and should probably be housed in guides. Ultimately, only a fraction of the wires will be enclosed in ceramics, but for now all 45 tubes (plus extras) are cut to give us maximum flexibility. The ceramic tubes are cut two inch shorter than the distance from the plug section to the electrode to be wired. All ceramic tubes are then installed on the trap (see Fig. A.8 (left)).

In a last step, the feed through section is assembled without complications as shown on Fig. A.8 (right). It can then be plugged onto the banana plug section on the lower end of the trap assembly. The right orientation of the plug can be determined by positioning the trap's banana plug section shifted 45 degrees relative to the equally shaped ceramics cover of the feed through section.

The assembly is checked for shorts and then disassembled for UHV cleaning.

Figure A.9: Photo of disassembled CPET showing all the parts to be cleaned.

A.2   Clean assembly

In order to achieve a UHV in CPET of down to 10^{-11} mBar, a very extensive and strict cleaning procedure has to be applied to all the parts being assembled. The procedure itself is described as follows:

1. Inspect the components first to ensure that all required venting holes and slots are in place. If components are excessively greasy or dirty, use a solvent bath to remove the grease. Pay special attention to any holes and tapped threads. Air guns can also be used to ensure that machining chips are removed from any holes or tapped threads.

2. Wash all components with soapy water (20% simple green/water mix). Again pay special attention to any holes and tapped threads. Rinse with hot city water. The purpose of this step is to ensure that all the grease, light oils and machining chips are completely removed from the part. Use clean gloves onward from this step and post process.

3. Put the component in a clean container and submerge with soapy water mix (same mix ratio as in step (2) above). Immerse container into an ultrasonic cleaner and agitate for 30 min. Ensure that the transfer medium in the ultrasonic cleaner does not contaminate the cleaning solution used.

4. Transfer the component to another clean container and rinse with hot city water.

5. Leaving the component in the same container, rinse with distilled or de-ionized water.

6. After rinsing, fill container to a level sufficient to submerge the part. Immerse the container into an ultrasonic cleaner and agitate for 30 min.

7. Do a final rinse of the component in the container with distilled or deionized water.

8. Transfer the component to a clean container and allow it to air dry in a dust free environment.

It is a requirement that two people work together when assembling or disassembling UHV components. All components used in a UHV system MUST first be cleaned to the UHV standards described in the procedure listed above.

1. Person #1 is to wear clean gloves. Care must be taken when placing gloves on one's hands. It is vital to keep the working surfaces of the gloves free from contaminants such as dirt, grease or skin oils. Person #1's role is to handle and assemble the various UHV cleaned components used in the UHV system.

2. Person #2 is not required to wear gloves as their role is as a "dirty" helper for person #1. Person #2's major responsibility is to ensure that person #1 remains clean. If a component requires tightening, then person #2 gets the tool required, cleans the working end of the tool with acetone and a clean tissue and then tightens the component while person #1 holds the clean assembly. Under no circumstance does person #1 handle tools and person #2 handle clean components.

3. For components are contained in clean bags or storage containers; the outside surfaces of the bags or storage containers MUST be considered contaminated. In this instance person #2 opens the storage container or bag and places the bag or container in such a way that person #1 can remove the item from the container or bag without touching anything but the component.

Appendix B

Simulation setup and code

B.1 Mathematica simulation code

- **initialize some constants**

```
SetOptions[Plot, BaseStyle → {FontFamily → "Times", FontSize → 16}];
SetOptions[ListPlot, BaseStyle → {FontFamily → "Times", FontSize → 16}];
$MaxExtraPrecision = 200;
e = 1.602176487 * 10^-19; (* elementary charge in C from nist.gov *)
m = 9.10938215 * 10^-31; (* mass of electron in kg from nist.gov *)
h = 6.62606896*^-34; (* planck constant in Js from nist.gov *)
hb = h / (2 Pi);
c = 299 792 485; (* speed of light in m/s from nist.gov *)
α = 7.2973525376*^-3;
eps0 = 8.854187817*^-12; (* electric constant nist.gov *)
nuLength = hb c / e; (* 1eV^-1 of length in m *)
nuMass = e / c^2; (* 1ev of mass in kg *)
nuTime = hb / e; (* 1eV^-1 of time in s *)
nuCharge = Sqrt[4 Pi α]; (* 1 unit of charge in C (Lorentz-Heaviside/ rationalized) *)
nuVelocity = c; (* 1 unit of speed in m/s *)
nuk = hb^2 / (e c^2); (* 1eV^-1 of k in Nm *)
```

- **trap related constants from harmonic oscillator.nb**

```
In[17]:=  k = 4.2581936241547395`*^-32
          km = k / m
          d = 0.0127 + 0.001016; (* length of one electrode + distance to next electrode in m *)
          CPETLength = 0.3 ; (* 30cm *)
```

Out[17]= 4.25819×10^{-32}

Out[18]= 0.0467451

■ **functions**

```
(* Probability function that electron is at position pFx in a trap with size pFd (only pos vals) *)

ProbFunc[pFx_, pFd_] := 1/(π√(pFd² - pFx²));

PotentialFunc[x_] := 1/2 k*10^18 x^2 / e; (* calc potential based on k *)

ShowConst[] := Module[{},
  Print["StepsizeT=" <> ToString[StepsizeT] <> ", Tp=" <> ToString[Tp] <> ", StepsizeX=" <>
    ToString[StepsizeX] <> ", Plotfrom=" <> ToString[Plotfrom] <> ", Plotto=" <>
    ToString[Plotto] <> ", KEp=" <> ToString[KEp]];
];

FindMaxAmpOld[fmaKEp_] := Module[{fmaTmpSolve, fmaAmp},
  fmaTmpSolve = Solve[PotentialFunc[x] == fmaKEp, x][[2]][[1]]; (*determine maxAmp based on total E*)
  fmaAmp = x /. fmaTmpSolve;
  Return[fmaAmp];
];

FindMaxAmp[fmaKEp_] := Sqrt[2 e fmaKEp /k 10^-18];

FindStartPos[fspMaxAmp_] := Module[{fspTmpCount, fspHighNumMax, fspStartPosRand, fspHighNumRand},
  fspTmpCount = 0; (*monte carlo reject method,returns pos of electron based on ProbFunc dist*)
  fspHighNumMax = 10000; (*high number for y cutoff of scatterplot (probdist goes up to inf) *)
  While[True,
    fspTmpCount++;
    fspStartPosRand = Random[] * fspMaxAmp ; (*rand startpos of el based on maxAmp at given energy*)
    fspHighNumRand = Random[] * fspHighNumMax;
    If[({fspHighNumRand < ProbFunc[fspStartPosRand, fspMaxAmp]) || (fspTmpCount > 500),
      Return[{fspStartPosRand, fspTmpCount}]; (* return count for curiosity *)
      Break[]; (* break when function value > random y value *)
    ];
  ]
];
```

```mathematica
FindStartPosAlt[fsp2MaxAmp_] := Module[{},
   Return[{fsp2MaxAmp Sin[π Random[]], 1}];
   ];

(* speed of electron in m/ns based on kinetic energy in eV *)
SpeedEV2MNS[ev2mnsEnergy_] := Sqrt[2 * ev2mnsEnergy * e/m]/10^9;

sign[] := Random[Integer] * 2 - 1; (* randomly returns +1 or -1 *)

ShowVelocities[svStepsizeT_, svTp_, svTp_, svKEp_] := Module[{svStepsizeX, svVPot, svVElec},
   svStepsizeX = CPETLength / svTp svStepsizeT; (* determine stepsizeX by cpet length and Tp *)
   svVPot = svStepsizeX / svStepsizeT ; (* speed of potential is length-/timestepsize m/ns*)
   svVElec = SpeedEV2MNS[svKEp];
   svStepsizeP = PotentialFunc[svStepsizeX];
   Print["v particle: " <> ToString[svVElec] <> " m/ns, v trap: " <>
   ToString[svVPot] <> " m/ns, v trap/ v part = " <>
   ToString[svVPot / svVElec * 100] <> "%, Pot Jump=" <> ToString[svStepsizeP] <> "V"];
   ];

FindMaxEnergy[fmeStepsizeT_, fmeTp_, fmeKEp_, fmePlotfrom_, fmePlotto_] := Module[{
   fmeStepsizeX, fmeVPot, fmeVElec, fmeTfuncs, fmeTfunc, fmeY, fmeAmp,
   fmeTmpRet, fmeStartPosRand, fmeTmpCount, fmeStartPosRandPot, fmeVElecRand,
   fmeEqsho, fmeIn1, fmeIn2, fmeSho, fmeR, fmeDR, fmeKin, fmeRet1, fmeRet2, fmeRet3, r, t},

   fmeStepsizeX = CPETLength / fmeTp fmeStepsizeT ; (* determine stepsizeX by cpet length and Tp *)
   fmeVPot = fmeStepsizeX / fmeStepsizeT ; (* speed of potential is length-/timestepsize m/ns*)
   fmeVElec = SpeedEV2MNS[fmeKEp];
   fmeTfuncs = t; (* smooth function *)
   fmeTfunc = fmeTfuncs /. t -> Floor[t / fmeStepsizeT] fmeStepsizeT; (* stepfunction *)

   fmeY[t_] = fmeVPot * fmeTfunc; (* pos of harmonic potential in dependency of t - incl steps *)
   fmeAmp = FindMaxAmp[fmeKEp];

   fmeTmpRet = FindStartPosAlt[fmeAmp];
   fmeStartPosRand = fmeTmpRet[[1]];
```

```mathematica
fmeTmpCount = fmeTmpRet[[2]]; (* return the number of iters of monte carlo reject run *)
fmeStartPosRandPot = PotentialFunc[fmeStartPosRand];
fmeVElecRand = SpeedEV2MNS[fmeKEp - fmeStartPosRandPot];

fmeStartPosRand = sign[] * fmeStartPosRand;
fmeVElecRand = sign[] * fmeVElecRand;

fmeEqsho = D[r[t], {t, 2}] == -km * (r[t] - fmeY[t]); (* diff eqn for electron in pot (stepfunc move *)
fmeIn1 = r[0] == fmeStartPosRand; (* initial position of electron *)
fmeIn2 = r'[0] == fmeVElecRand; (* initial velocity of electron *)

(*,AccuracyGoal->2*) (* solve the DGL (step) *)
fmeSho = NDSolve[{fmeEqsho, fmeIn1, fmeIn2}, r[t], {t, fmePlotfrom, fmePlotto}, MaxSteps -> 50 000 000];
fmeR = r[t] /. fmeSho; (* upperscale r is used to store the solution of the dgl *)
fmeDR = ∂t fmeR;

fmeKin = (1/2 m fmeDR^2 / e * 10^18)[[1]]; (* calc kin energy of electron, divide by e to display in eV *)

fmeRet1 = fmeStartPosRand;

(*fmeRet2=Check[MaxValue[{fmeKin,t>0,t<fmeStepsizeT},t],fmeKin];*)
fmeRet2 = Quiet[MaxValue[{fmeKin, t > 0, t < fmeStepsizeT}, t]]; (* max kin energy during first step *)
(*fmeRet3=Quiet[MaxValue[{fmeKin,t<fmePlotto,t>fmePlotto-fmeStepsizeT},t]];*)
fmeRet3 = Quiet[MaxValue[{fmeKin, t > 0, t < fmePlotto}, t]]; (* max kin energy during last step *)
Return[{fmeRet1, fmeRet2, fmeRet3, fmeTmpCount}];
];

FindMaxEnergyAvg[fmeaStepsizeT_, fmeaTp_, fmeaKEp_, fmeaIterations_] := Module[{fmeaTmparr},
fmeaTmparr = Table[FindMaxEnergy[fmeaStepsizeT, fmeaTp, fmeaKEp, 0, fmeaTp], {i, 1, fmeaIterations}];
Return[Mean[Table[fmeaTmparr[[i]][[3]], {i, 1, fmeaIterations}]]];
];

EnergList = {1, 10, 20, 50, 100, 150, 200, 500};

Table[FindMaxEnergyAvg[5, 500, EnergList[[i]], 2500], {i, 1, 8}]

{6.10981, 18.9224, 31.912, 67.0564, 122.491, 178.005, 230.65, 548.396}
```

B.2   SimIon setup and LUA code

This section describes the setup of the SimIon 3D simulations and presents the corresponding LUA[1]sourcecode.

Converting CAD files from SolidWorks to SimIon

The 3D model of CPET, which was used to design and build the trap is available as a SolidWorks 2006 assembly (see Fig. 1.11 page 18). Using SolidWorks, all structural parts and insulation material are removed from the assembly. The split electrodes are replaced by single electrodes in order to reduce the total electrode number in the simulation. This becomes important when running the simulation, as every electrode consumes an equal amount of computer memory. The remaining assembly consists of single CPET electrodes, drift tubes, steerers and the vacuum tube as shown in Fig. B.1). This assembly is exported from SolidWorks into the STL format. It has to be specified that the data of every electrode is written into separate .stl files.

Using the SimIon stl tools, the resulting 38 stl files are converted into one SimIon .pa# (potential array) file, following instructions from the SimIon web-site[2] [62]. The settings for the CPET stl import are shown in Fig. B.2.

The .pa# file is then loaded using the SimIon main interface and "fast adjusted". During this process a .pa file is created for every electrode. The .pa files contain a rasterized field map (coordinates and values) of the spatial simulation volume listing the electric field strength produced by the electrode. If the potential of an electrode is changed, the field map is adjusted. During runtime, all electrodes (all .pa files) are loaded into computer memory, making it possible to perform these adjustments in a short time. The scale factor shown in Fig. B.2 needs to be adjusted so that the sum of the size of the pa files does not exceed 2 GB, which is the maximum amount of memory that SimIon is designed to use. SimIon assigns an internal number to every electrode. In order to change the potential of a specific electrode during runtime, all the electrodes and their corresponding internal number have to be identified using the "Fast adjust voltages..." button in the "PA's" tab in the workbench view.

SimIon, Lua and Excel

In order to simulate electron manipulation with the cooler Penning trap, a large number of different potential values need to be applied to the trap electrodes over time. An example of different potentials to be applied at given times during the simulation is shown in Table B.1 (and Table 2.4, page 34). A clear way of implementing this table into the simulation is needed, so that it is convenient

---

[1]LUA (from Portuguese: lua meaning "moon") is a programming scripting language which is used by SimIon. The LUA interface enables the user to write his own subroutines to modify the simulation according to his needs.

[2]http://simion.com/sl/tools_tut.html#v2pa
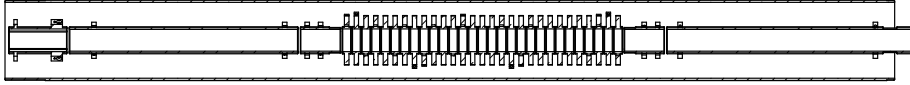
Figure B.1: SolidWorks drawing of CPET. Contains only single electrodes, drift tubes and steerers for SimIon export and therefore consists of exactly 38 parts that will be recognized as electrodes in SimIon. Electrons will be injected from the right side, ions from the left.
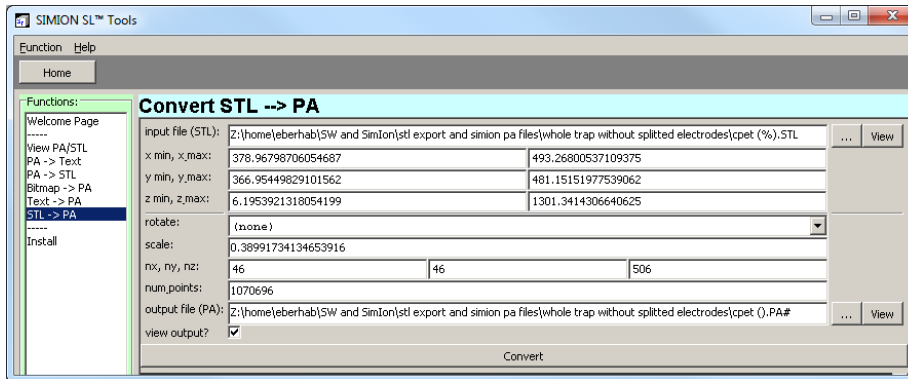
Figure B.2: Screenshot of SimIon STL tools. Settings for converting the 38 CPET SolidWorks STL files into one SimIon PA# file.

and fast for the user to change potential values and rerun the simulation based on a new list.

SimIon comes with LuaCOM[3], an add-on library to the Lua language that allows Lua scripts to use and implement objects that follow Microsoft's Component Object Model (COM) specifications and use the ActiveX technology for property access and method calls. LuaCOM therefore provides an interface to access Excel from SimIon. Excel provides the capability of storage and easy manipulation of large lists of values. The combination of LuaCOM and Excel is used to hold the table of potential values and to access it during the simulation.

The electron's position and velocity during the simulation are written back to Excel at given time intervals. They can be immediately displayed in a pre arranged excel scatter plot.

Integrating the CPET magnetic field into SimIon

This subsection describes how the the manufacturer specifications of the magnetic field strength are imported into the simulation.

The resolution of the 3D trap model in SimIon is 1 dot per cubic mm. The resolution of the magnet field map provided by the manufacturer is 1 dot per cm

---

[3]http://www.tecgraf.puc-rio.br/~rcerq/luacom/

Table B.1: Example of three potential sets to be applied to the CPET electrodes during the simulation run. The first line contains the internal electrode number, the first row contains the time in (ns) at which the voltage set in the corresponding line should be applied. Only electrodes 17-28 of 38 electrodes are shown. Potential values are displayed in (V).

	17	18	19	20	21	22	23	24	25	26	27	28
0.0	0	0	0	-2000	200	200	200	200	200	0	0	0
0.2	0	0	0	-2000	200	200	200	200	200	-2000	0	0
1.0	0	0	0	0	200	200	200	200	200	-2000	0	0

along the positive centre trap axis (z-axis, the centre of the coordinate system being at the centre of the magnet). Mathematica is used to extrapolate the field towards the negative z-axis and to interpolate the magnetic field along the z-axis in order to match the resolution of the simulation. the field strength is also extrapolated in along a second axis (e.g. the y-axis).

A Mathematica function is used to export the resulting half plane into an ASCII text-file with a format that can then be converted into a .pa# for use with SimIon. The ASCII file contains a list of lines specifying a point on the half plane (coordinates y and z) and the field strength (field_y, field_z). The conversion into the .pa# file format is done using the SimIon SL-tools[4] [62]. The SL-tools *Text* ⟶ *PA* function rotates the half plane around the z-axis and generates the full 3D field map.

Comments on the the Lua program code

The Lua program code consists of nine predefined, so-called user program segments. These segments are program functions which are called by SimIon before or after specific actions. Depending on the segment, read and/ or write access is granted to different simulation parameters. For example the *Tstep_Adjust* segment is called before performing an integration time step and gives the user control over the time step size throughout the simulation. The *Initialize* segment is called before the simulation is started. A more detailed explanation can be found in the user manual which comes with the software.

Some new functions have been defined in order to facilitate reading rows and columns from Excel and writing array values to Excel. The *Tstep_Adjust* segment keeps track of the current simulation time (t) and of the next time index (see Table B.1 first column) where a potential change is defined (t_p). When performing the next time step (Δt) would exceed the time index for the next potential (if $t + \Delta t > t_p$), the size of the next time step is redefined to $\Delta t = t_p - t$, so that after performing the time step t would be equal to t_p. The *Other_Actions* segment, which is called after each time step, checks if $t == t_p$. If true, the corresponding potential values of t_p are applied to the electrodes

---

[4]http://simion.com/sl/tools_tut.html#t2pa
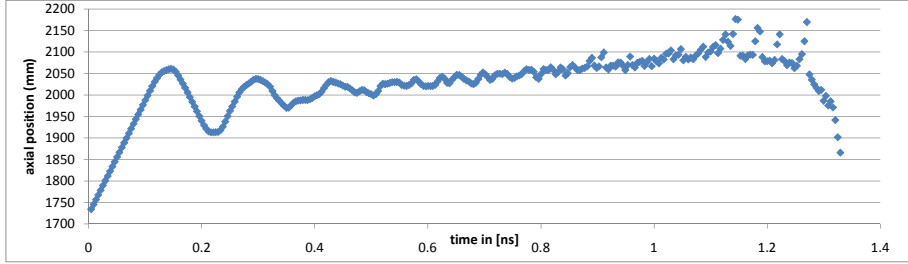
Figure B.3: Plot of position of one electron on the axis along the trap as a function of time.
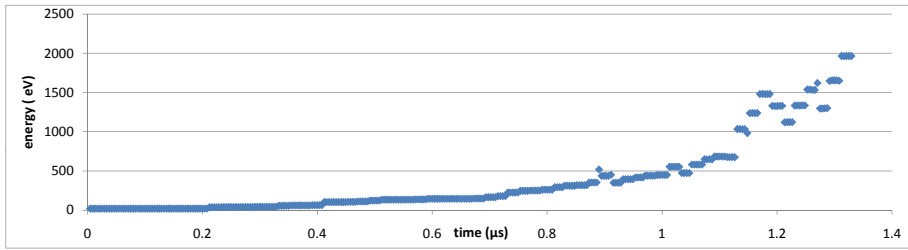
Figure B.4: Plot of velocity of one electron in the trap as a function of time.

and the next potential set is loaded into memory. A similar technique is applied to facilitate logging at specific logging time steps.

Running the simulation and the Lua program

As a first try, a bunch of 20 electrons is started simultaneously outside the inner trap region (coming from the side left in Fig. B.1), with a small Gaussian distribution in both axial position and velocity. The potential values from Table B.1 are used to change the voltages of the electrodes during the simulation. Electrode number 26 is the first electrode of the inner trap region at the injection side (referred to as the entrance electrode), and electrode number 20 is the last (exit electrode).

At first, all electrodes are set to the potential values in the first line (time index 0.0 μs). The electrons then start to travel and after they have all reached the inside of the trap at ≈ 0.2 μs, electrode 26 is set from 0 V to -2000 V. This prevents the electrons from leaving the trap at the entrance side. Electrode 20 is already set to -2000 V from the beginning. The electrons will then oscillate in the trap for 0.8 μs and are ejected by lowering the potential on electrode 20 to 0 V.

Next, a more complex scenario is implemented by modifying the values in the table. Again, a bunch of 20 electrons is injected using the method described above. The electrons then oscillate in the potential well formed by the outer

electrodes 26 and 20. Subsequently, every 0.02 μs the potential of the inner electrodes is raised, starting with the second electrode (number 27) on the injection side. The order of the first electrode numbers is 26, 27, 28, 29, 30, etc. The potential change is applied using the following scheme:

1. 0.22 μs Electrode 27 is set to -1000 V.

2. 0.24 μs Electrode 27 is set to -2000 V and Electrode 28 is set to -1000 V.

3. 0.26 μs Electrode 28 is set to -2000 V and Electrode 29 is set to -1000 V.

4. 0.28 μs etc.

The presented switching behaviour decreases the size of the potential well over time. The axial position of the electrons and their total energy can be investigated in two different output tables during and after the simulation. Figure B.3 shows a plot of the mean position of the electron bunch. The injection is started at 0.00 μs. The reflection of the electron bunch on the "closed" exit electrode can be observed, as well as the reflection on the entrance electrode right after its closure at 0.20 μs. The plot further shows how the axial region narrows down over time giving the electrons less space to oscillate, as well as the shift of their mean position towards the exit electrode. At $\approx$ 1.20 μs, electrons start to escape the trapping potential via the exit electrode as they gain enough energy to jump over the potential barrier. This causes the plotted average to show "escape peaks", as the position of the escaping electron increases until it leaves the spatial simulation volume. Figure B.4 shows the mean total energy of the electron bunch over time. A decrease of mean energy is caused when an escaping electron with a relatively high energy leaves the simulation and stops contributing to the average.

SimIon LUA code

```lua
1: simion.workbench_program()
2:
3: -- ##### INITIAL USER VARIABLES #####
4: local filename = "W:\\SW and SimIon\\stl export and simion pa files\\whole trap without splitted electrodes\\times.xlsx"
5: local filename = "C:\\Users\\eberhab\\desktop\\whole trap without splitted electrodes\\times.xlsx"
6:
7: adjustable synchr = 0                          -- electron cooling via synchrotron rad on/ off
8: adjustable xls_log_step = 1000                 -- log to simionlog every n timesteps
9: adjustable max_ions = 40                       -- maximum number of ions to log into excel file
10: adjustable verbose = 1                        -- increase logging
11: local timestep_factor = 1                     -- increase the size of timesteps by this factor (results in
    errors)
12: adjustable log_every_step = 0.01              -- log every x micro seconds to excel
13: adjustable log_next_step = log_every_step     -- next timestep to print out log to excel, initial value
14: local continued_run = 0                       -- set to 1 if sim is continued. (default = 0) (doesnt work
    yet!)
15:
16:
17: -- ##### FUNCTIONS & CONSTANTS #####
18: local logrow = 1                              -- last excel row of kinetic energy, from where to continue
    the log of the simulation (default = 1)
19: local ctnr = 1                                -- current timestep index, from where to cont the simulation
    (excel row - 1) (default = 1)
20: local excel = luacom.GetObject("Excel.Application")  -- Gets a running instance of Excel
21: local count = 0                               -- counts from 1 to xls_log_step. everytime it hits
    xls_log_step, write log is triggered and count gets reset to 0
22: local first = 1                               -- used in other_actions, is set to 0 after the very first
    call of the function
23: local first_round = 1                         -- used in other_actions, is set to 0 after other_actions
    has been called for all ions for the first time
24: local first_in_round = 1                      -- used in other_actions, is 1 only for the first ion that
    other_actions is called with each timestep
25: local last_in_round = 0                       -- used in other_actions, is 1 only for the last ion that
    other_actions is called with each timestep
26: local Ion_number_tmp = 0                      -- used in other_actions, to memorize the previous ion_number
27: local electron_mass = 9.1 * math.pow(10,-31)  -- electron mass in [kg]
28: local element_charge = 1.602 * math.pow(10,-19)  -- elementary charge in [As]
29: local mm_us2m_s = 1000                        -- 1 mm/us = 1000 m/s
30: local trigger_log_to_excel = 0               -- trigger log to excel from tstep_adjust -> other_actions
31: local fly_time_offset = 0                     -- if this is a continued run, then this will be set to the
    ions
32: local maxTotEnergy = 30                       -- maximum total energy of electron is now set here, not in
    fly file
33:
```

```lua
34: function my_ion_time_of_flight()
35:   return ion_time_of_flight + fly_time_offset          -- in case the simulation was aborted, this sums up to the
      total ion tof
36: end
37:
38: function log(log_nr)
39:   if log_nr == 1 then                                  -- write electrode potential to log everytime the potential
      is changed
40:     -- print(cur_switch_time .. "ms, 20:" .. adj_elect[20] .. ", 26:" .. adj_elect[26])
41:     print("Current time: " .. cur_switch_time .. "ns. switching to next potential set.")
42:   end
43:
44:   if log_nr == 2 then                                  -- check increase of radial energy and timestep size
45:     if verbose == 1 then
46:       -- print(my_ion_time_of_flight() .. " " .. ion_time_step .. " " .. log_next_step .. " " ..
vel2kin(Ion_Vy_mm)+vel2kin(Ion_Vz_mm))
47:       -- print(Ion_Px_mm .. " " .. Ion_Volts)
48:       print(my_ion_time_of_flight() .. " " .. log_next_step .. " " .. vel2kin(Ion_Vx_mm)-Ion_Volts .. " " ..
log_next_step)
49:     end
50:   end
51: end
52:
53: function kin2vel(k2v_kin)
54:   return math.sqrt( 2 * element_charge / electron_mass * k2v_kin) / mm_us2m_s
55: end
56:
57: function vel2kin(v2k_vel)                              -- ions velocity in kinetic energy (mm/us -> eV)
58:   --Ion_V_m_sqr = ((Ion_Vx_mm * Ion_Vx_mm) + (Ion_Vy_mm * Ion_Vy_mm) + (Ion_Vz_mm * Ion_Vz_mm)) * math.pow(1000,2)
59:   return 0.5 * electron_mass / element_charge * v2k_vel * v2k_vel * mm_us2m_s * mm_us2m_s
60: end
61:
62: function dv()                                          -- adjust electron velocity (synchrotron radiation)
63:   local dv_tau = 1/10                                  -- radiation time constant
64:   local dv_kin = vel2kin(Ion_Vx_mm)
65:   dv_kin = (1- math.exp(- my_ion_time_step_sec() / dv_tau)) * dv_kin
66:   local dv_vel = kin2vel(dv_kin)
67:   if Ion_Vx_mm > 0 then                               --
68:     dv_vel = -dv_vel
69:   end
70:   return dv_vel
71: end
72:
73: function my_ion_time_step_sec()                        -- get ions timestep size in seconds (microsecond in second)
```

```lua
74:        return ion_time_step * math.pow(10,-6)
75:    end
76:
77: function load_next_voltage_set()                                    -- load next voltage set and set update flag for fast_adjust
    function
78:        cur_switch_time = switch_time                                -- save current switch time for log output only!
79:        switch_time = times[ctnr + 1]                                -- switch time needs to be one step ahead to know about when
    to switch to the next step
80:        voltages = read_xls(2,ctnr+1,1)                              -- read next voltage sets (numbering is 1 row plus compared
    to times-array index)
81:        if switch_time == nil then                                   -- after last timestep the switch_time variable is set back
82:            switch_time = 0
    to zero to avoid future calling load_next_voltage_set() in segment.other_actions()
83:        end
84:        ctnr = ctnr + 1                                              -- incr current-timestep-number
85:    end
86:
87: function apply_voltages(switch)                                     -- apply current voltages to electrodes, if switch = 0 then
    even deactivated electrodes get fast adjusted (just for initial FA)...
88:        if switch == 1 then                                         -- ... switch = 1 means respect the xls setting wether an
89:            for index,value in ipairs(electrodes) do
    electrode should be FA or not
90:                if value ~= 0 then                                  -- do nothing when electrode is numbered as 0 (fast adjust
    deactivated) in excel sheet
91:                    adj_elect[value] = -voltages[value]             -- fast adjust the electrode
92:                end
93:            end
94:        elseif switch == 0 then                                     -- if switch == 0 then FA every electrode
95:            for index,value in ipairs(electrodes) do                -- index is the electrode number, value is the electrode
    number if it should get FA during the run, otherwise its 0
96:                adj_elect[index] = -voltages[index]
97:            end
98:        end
99:    end
100:
101: function load_sim_values()
102:        logrow = ws6.Cells(3,3).Value2 - 1
103:        ctnr = ws6.Cells(4,3).Value2
104:        fly_time_offset = ws6.Cells(2,3).Value2
105:
106:        load_next_voltage_set()
107:        positions = read_xls(4,logrow,1,2)                          -- read positions from cell(4,logrow). read as row (1). read
    from sheet (2)
108:        kins = read_xls(4,logrow,1,4)                               -- read kinetic energy from cell(4,logrow). read as row (1).
    read from sheet (4)
```

```lua
109:     totals = read_xls(4,logrow,1,3)            -- read total energy from cell(4,logrow). read as row (1).
                                                    read from sheet (3)
110:     vel = read_xls(4,1,1,5)                    -- read velocity from cell(1,4). read as row (1). read from
                                                    sheet (5)
111:     accel = read_xls(4,2,1,5)                  -- read acceleration from cell(1,4). read as row (1). read
                                                    from sheet (5)
112:
113:     logrow = logrow + 1                        -- jump one row further for next log entry
114:   end
115:
116:   -- ##### EXCEL FUNCTIONS #####
117:   function open_excel_wb(fname)
118:     excel = luacom.CreateObject("Excel.Application")  -- create new excel instance ...
119:     excel.Visible = true
120:     local wb = excel.Workbooks:open(filename)  -- ..: and open cpet times xlsx file
121:     ws1 = wb.Worksheets(1)                     -- this sheet contains the voltage sets
122:     ws2 = wb.Worksheets(2)                     -- this sheet contains the output of the x_position of the
                                                    electrons
123:     ws3 = wb.Worksheets(3)                     -- this sheet contains the output of the whole energy of the
                                                    electrons
124:     ws4 = wb.Worksheets(4)                     -- this sheet contains the output of the kinetic energy of
                                                    the electrons 1D
125:     ws5 = wb.Worksheets(5)                     -- this sheet contains the output of the kinetic energy of
                                                    the electrons 3D
126:     ws6 = wb.Worksheets(6)                     -- this sheet contains data for a run to continue
127:   end
128:
129:   function init_excel()
130:     if excel == nil then                       -- if excel is not running then we need to open a new
                                                    instance and open cpet times file
131:       open_excel_wb(filename)
132:     else
133:       sheets = excel.Worksheets                -- Gets the set of worksheets from open excel workbook (will
                                                    crash if excel is open without any open WB)
134:       ws1 = sheets:Item(1)                     -- this sheet contains the voltage sets
135:       ws2 = sheets:Item(2)                     -- this sheet contains the output of the x_position of the
                                                    electrons
136:       ws3 = sheets:Item(3)                     -- this sheet contains the output of the whole energy of the
                                                    electrons
137:       ws4 = sheets:Item(4)                     -- this sheet contains the output of the kinetic energy of
                                                    the electrons 1D
138:       ws5 = sheets:Item(5)                     -- this sheet contains the output of the kinetic energy of
                                                    the electrons 3D
139:       ws6 = sheets:Item(6)                     -- this sheet contains data for a run to continue
```

```lua
140:          tmpval = ws1.Cells(1,1).Value2    -- our worksheet is identified by having the string "CPET"
        in cell (1,1)
141:          if tmpval ~= "CPET" then          -- is the right WB opened?
142:             open_excel_wb(filename)
143:          end
144:       end
145:       osclock = os.clock()
146:       --ostime = os.time()
147:       ws = {ws1,ws2,ws3,ws4,ws5,ws6}        -- array with all worksheets
148:       print(excel.Sheets.Count)
149:    end
150:
151:    function clear_xls_plot()                -- clear all the cells in the excel sheet, so that the plot
        is empty when the run is started
        print("clear xlsx file...")
152:       local i,j
153:       local wsheets = {ws2,ws3,ws4,ws5}     -- which sheets to clear?
154:       for _,w in pairs(wsheets) do          -- loop over every worksheet
155:          i = 3                              -- column (start is 3rd column as the first two are reserved
156:                                             for mean & misc)
157:          j = 1                              -- row
158:          while i <= max_ions do             -- as long as there are values along the current column ...
159:             while w.Cells(j,i).Value2 ~= nil do  -- ...set them to empty, so that it does not affect excel
160:                w.Cells(j,i).Value2 = x
        average value function.
161:                j = j + 1                    -- jump down to next row
162:             end
163:             i = i + 1                        -- jump right to next column
164:             j = 1                            -- jump back to first line
165:          end
166:       end
167:    end
168:    i = 1
169:    while ws1.Cells(i,41).Value2 ~= nil do    -- delete keep track of simulation time over realtime (set
170:       ws1.Cells(i,41).Value2 = x
        in read_xls())
171:       i = i + 1
172:    end
173:
174:    i = 1
175:    while ws3.Cells(i,2).Value2 ~= nil do     -- delete keep track of simulation time over realtime (set
176:       ws3.Cells(i,2).Value2 = x
        in segment.other_actions())
177:       i = i + 1
```

```lua
178:      end
179:    end
180:
181:  function read_xls(startcolumn,startrow,row,sheetnr)          -- read numbers from excel row (row=1) or column (row=0),
      sheetnumber
182:    local array = {}
183:    local mode = "*n"                                          -- read numbers
184:    local x = startcolumn
185:    local y = startrow
186:    local sheet = ws[1]
187:    if sheetnr ~= nil then
188:      sheet = ws[sheetnr]
189:    end
190:
191:    if row == 0 then                                           -- read values in a column (timings)
192:      while true do
193:        local v = sheet.Cells(y,x).Value2
194:        y = y + 1
195:        if not v then break end
196:        --print(v)
197:        table.insert(array, v)
198:      end
199:    elseif row == 1 then                                       -- read values in a row (potentials)
200:      while true do
201:        local v = sheet.Cells(y,x).Value2
202:        sheet.Cells(y,41).Value2 = os.clock() - osclock        -- keep track of simulation time over realtime
203:
204:        x = x + 1
205:        if not v then break end
206:        --print(v)
207:        table.insert(array, v)
208:      end
209:    end
210:    return array
211:  end
212:
213:  function log_to_excel()                                      -- once per ion, called from other actions
214:    --print(logrow)
215:    ws2.Cells(logrow,3).Value2 = my_ion_time_of_flight()
216:    ws2.Cells(logrow,Ion_number + 3).Value2 = Ion_Px_mm
217:
218:    ws3.Cells(logrow,3).Value2 = my_ion_time_of_flight()
219:    ws3.Cells(logrow,Ion_number + 3).Value2 = kin - pot
220:    ws3.Cells(logrow,2).Value2 = os.clock() - osclock          -- keep track of simulation time over realtime
```

```lua
221:
222:        ws4.Cells(logrow,3).Value2 = my_ion_time_of_flight()
223:        ws4.Cells(logrow,Ion_number + 3).Value2 = kin
224:
225:        ws5.Cells(logrow,3).Value2 = my_ion_time_of_flight()
226:        ws5.Cells(logrow,Ion_number + 3).Value2 = kin3D - pot
227:
228:        ws6.Cells(1,3).Value2 = my_ion_time_of_flight()    -- save latest ions velocity and acceleration in a tmp
                                                               worksheet
229:        ws6.Cells(1,Ion_number + 3).Value2 = Ion_Vx_mm
230:        ws6.Cells(2,3).Value2 = my_ion_time_of_flight()
231:        ws6.Cells(2,Ion_number + 3).Value2 = Ion_Ax_mm
232:        ws6.Cells(3,3).Value2 = logrow
233:        ws6.Cells(4,3).Value2 = ctnr
234:
235:        --print(Ion_Vx_mm .. " " .. dv)
236:    end
237:
238:    -- ##### SIMION LUA SEGMENTS #####
239:    init_excel()
240:
241: function segment.initialize()    -- simion segment (1) initialize the ions conditions (gets
                                       called for every ion)
242:    end
243:
244: function segment.init_p_values()    -- simion segment (2) initialize electrodes (TODO:
     fastadjust, set electrode potentials to xls row 1)
245:        times = read_xls(1,2,0)    -- read timesteps from excel column
246:
247:        cur_switch_time = 0    -- save current switch time for log output only!
248:        switch_time = times[ctnr + 1]    -- we need to know about when to switch to the next set
249:
250:        voltages = read_xls(2,2,1)    -- read initial voltage set from first excel row (gets
     applied automatically in fast_adjust until other_actions loads a new set at switch_time)
251:        electrodes = read_xls(2,1,1)    -- read complete set of electrode numbers (zero if not to
     adjust during flight)
252:
253:        update_pe = 1    -- initially flag update of PE surface display
        (other_actions)
254:
255:        if continued_run == 0 then
256:            print("initial fast adjust. this may take a while ...")
257:            apply_voltages(0)    -- initially fast adjust EVERY electrode (this actually
     happens on disk, not in ram!) ...
```

```
258:          ctnr = ctnr + 1                                          -- ... but only if its a new run and not a continued run
259:       end
260:    end
261:
262: function segment.tstep_adjust()                                    -- simion segment (3) adjust the timestep
263:    --ion_time_step = 0.00001                                       -- manually set time step. needs to be small enough to see
     the electrons cyclotron motion
264:    --print(my_ion_time_of_flight() .. " " .. switch_time)
265:
266:    --ion_time_step = ion_time_step * timestep_factor               -- boost the simualtion speed
267:
268:    if log_next_step < my_ion_time_of_flight() then
269:       log_next_step = log_next_step + log_every_step
270:       trigger_log_to_excel = 1
271:    end
272:
273:    --local ion_time_step_tmp = min(ion_time_step, log_next_step - my_ion_time_of_flight())
274:    --if ion_time_step ~= ion_time_step_tmp then
275:    --  ion_time_step = ion_time_step_tmp
276:    --  log_next_step = log_next_step + log_every_step
277:    --end
278:
279:    if switch_time ~= 0 then
280:       if my_ion_time_of_flight() < switch_time then                -- Let's make sure the time step ends right on the switch
     time
281:          ion_time_step = min(ion_time_step, switch_time - my_ion_time_of_flight())
282:       end
283:    end
284: end
285:
286: function segment.other_actions()                                   -- simion segment (8) - Handle display updates & write ion
     position to excel - initialize excel table
287:
288:    -- ### handle running variables initial ###
289:    if first == 1 then                                              -- manage the "first" variable and perform all the
     "first"/onetime-actions
290:       if continued_run == 0 then                                   -- clear excel plot if this is not a continued run
291:          clear_xls_plot()
292:       end
293:    end
294:    if Ion_number_tmp >= Ion_number then                            -- this keeps the variables first_round and first_in_round
     up to date
295:       first_round = 0                                             -- first round is over the first time that Ion_number_tmp is
     bigger than Ion_number ...
```

```
296:              first_in_round = 1                    -- ... this is only true for the first ion in round
297:              count = count + 1                     -- only increase count for first ion (once a timestep),
       otherwise the more electrons we had the more often in time we would log
298:              last_ion = Ion_number_tmp             -- save the number of the ion before the first ion in round
       (must be the last ion then)
299:              --trigger_log_to_excel = 0
300:           else                                     -- otherwise its not the first ion
301:              first_in_round = 0
302:           end
303:           Ion_number_tmp = Ion_number
304:           last_in_round = 0
305:           if Ion_number == last_ion then
306:              last_in_round = 1
307:           end
308:
309:           -- ### do stuff ###
310:           if continued_run > 0 then               -- continue aborted run. restore ions conditions. do not
       clear xls file
311:              if first_round == 1 then
312:                 if first == 1 then
313:                    print("loading previous sim values...")
314:                    load_sim_values()              -- load sim values is a one time thing (first)
315:                 end
316:                 Ion_Px_mm = positions[Ion_number]   -- restoring ion position and energy has to be performed
       once for every ion (first_round)
317:                 Ion_Vx_mm = vel[Ion_number]
318:                 --Ion_Ax_mm = accel[Ion_number]
319:                 print(kins[Ion_number] .. " " .. vel2kin(Ion_Vx_mm) .. " " .. Ion_number)
320:              end
321:           end
322:
323:           if synchr == 1 then                     -- activate synchrotron rad
324:              Ion_Vx_mm = Ion_Vx_mm + dv()
325:           end
326:           kin = vel2kin(Ion_Vx_mm)                -- kinetic energy of the particle
327:           kin3D = kin + vel2kin(Ion_Vy_mm) + vel2kin(Ion_Vz_mm)  -- all kinetic energy components
328:           pot = Ion_Volts                         -- potential energy of the particle
329:
330:           if first_round == 1 then                -- set kinetic energy of electron, depending of the position,
       so that the total equals maxTotEnergy
331:              print("energy and velocity for ion " .. Ion_number .. " is " .. kin - pot .. " and " .. Ion_Vx_mm)
332:              kin = (maxTotEnergy + pot)
333:              Ion_Vx_mm = kin2vel(kin) * math.pow(-1,Ion_number)
334:              print("energy and velocity for ion " .. Ion_number .. " is " .. kin - pot .. " and " .. Ion_Vx_mm)
```

```
335:        end
336:
337:        if my_ion_time_of_flight() == switch_time then   -- transition point (timestep was adjusted, so that these
            two double values can actually be compared)
338:            ion_color = ctnr + 1                          -- change ion color every timestep (better visibility in gui)
339:            mark()                                        -- Mark ion location.
340:            update_pe = 1                                 -- trigger pot lines update in gui
341:            trigger_log_to_excel = 1
342:            load_next_voltage_set()                       -- this whole section is only executed once because this
            line sets switch_time to the next value
343:        elseif update_pe == 1 then                        -- trigger display update one timestep later, when new
            voltage set has been applied by fast_adjust()
344:            update_pe = 0
345:            sim_update_pe_surface = 1                      -- Mark PE display for update.
346:            update_log = 1                                -- trigger log output in fast_adjust
347:        end
348:
349:        if count == xls_log_step then                     -- if count matches the specified log_step, then write
            current electron position to excel and plot it
350:            if first_in_round == 1 then                   -- only when excel logging takes places and only for first
            ion ...
351:                log(2)                                    -- check increase of radial energy and timestep size
352:            end
353:
354:            if trigger_log_to_excel == 1 then
355:                if Ion_number < max_ions then             -- limit the number of ions that will be logged to excel, so
            that experimenting with higher numbers wont kill the xlsx file
356:                    log_to_excel()
357:                    --print(Ion_number .. " " ..max_ions)
358:                end
359:            end
360:
361:
362:            -- ## handle running variables final ###
363:            if count > xls_log_step then                  -- reset count once it gets bigger than log_step. I cant
            really put it into the if-condition above,
364:                count = 0                                 -- ... because then we would only be able to log the first
            ions position
365:            end
366:            if first == 1 then                            -- set first to 1, so this is never performed again
367:                first = 0
368:            end
369:            if last_in_round == 1 then
370:                if trigger_log_to_excel == 1 then
```

```lua
371:                     trigger_log_to_excel = 0    -- turn excel logging of when the last ion in round has been
         logged
372:         logrow = logrow + 1                     -- logrow is used to enumerate excel rows, it gets increased
      everytime a logrow has been written
373:       end
374:     end
375: end
376:
377: function segment.fast_adjust()                  -- simion segment (4) fast adjust the electrodes in ram
     while flying
378:     apply_voltages(1)                           -- voltages have to be adjusted EVERY timestep (no if
     condition), with respect to activation or deactivation of the electrode in xls
379:     if update_log == 1 then                     -- write log when pot change just happened
380:       log(1)
381:       update_log = 0
382:     end
383:   end
384:
385: function segment.terminate()                    -- simion segment (9)
386:     sim_retain_changed_potentials = 1           -- dont restore changed potentials at end of flight
387:     --excel.Quit()
388:   end
```

Index